COBALT, NICKEL AND ZINC-DNA INTERACTIONS:

A STRUCTURAL STUDY

A Thesis Submitted to the College of Graduate Studies and Research

in Partial Fulfillment of the Requirements for the

Degree of Doctor of Philosophy

in the Department of Biochemistry

University of Saskatchewan, Saskatoon

by

Shaunivan Lee Labiuk

PERMISSION TO USE

In presenting this thesis in partial fulfillment of the requirements for a postgraduate degree from the University of Saskatchewan, I agree that the Libraries of this University may make it freely available for inspection. I further agree that permission for copying of this thesis in any manner, in whole or in part, for scholarly purposes may be granted by the professors who supervised my thesis work, or in their absence, by the Head of the Department or the Dean of the College in which my thesis work was done. It is understood that any copying or publication or use of this thesis or parts thereof for financial gain shall not be allowed without my written permission. It is also understood that due recognition shall be given to me and to the University of Saskatchewan in any scholarly use which may be made of any materials in my thesis.

Requests for permission to copy or make other use of material in this thesis in whole or in part should be addressed to:

Head of the Department of Biochemistry

University of Saskatchewan

Saskatoon, Saskatchewan S7N 0W0

ABSTRACT

M-DNA is a complex between DNA and cobalt(II), nickel(II) or zinc(II) that forms under alkaline conditions. It has been postulated that the imino proton of guanine or thymine is replaced by the metal cation in each base-pair. The complex is thought to maintain a double-helical structure similar to B-DNA but has unusual properties. M-DNA acts as an electron conductor making it a potential candidate for future nanotechnology applications.

In this work the interactions of cobalt(II), nickel(II) and zinc(II) with DNA were studied. This was done in order to gain knowledge concerning the interactions of these metal cations with B-DNA and to assess aspects of the proposed M-DNA structural model. Firstly, experiments that demonstrated ionizing or ultraviolet radiation induced interstrand crosslinking in M-DNA are consistent with the hypothesis that M-DNA maintains a double-helical structure in which guanine binds with cytosine and adenine with thymine. These experiments also provide new insights into the effects of radiation on DNA in the presence of various metal ions at physiological and alkaline pHs.

Secondly, a titration experiment was performed in which it was shown that for each metal cation that binds to M-DNA, approximately one proton is released. This result is consistent with the hypothesis that imino protons are released during M-DNA formation.

Thirdly, crystals of the sequence d(GGCGCC) complexed with cobalt, nickel and zinc were grown. They did not grow in conditions above pH 8.1 and thus do not provide a solid state structural model for M-DNA. Interestingly, x-ray diffraction experiments revealed metal binding only to terminal N(7) positions of guanine residues with coordinated water molecules interacting with neighboring

guanine residues affecting the propeller twist. Though the crystals had a high solvent content, it is interesting that the few interactions involving the metal cations were sufficient to stabilize the crystal lattice.

Finally, conditions for growing crystals with DNA containing 5-fluorouracil at alkaline pH in the presence of cobalt were also discovered. This is a critical step because the presence of 5-fluorouracil allows DNA sequences to more readily form M-DNA at lower pH.

PUBLISHED WORKS

Articles in refereed journals resulting from work presented in this thesis:

Labiuk, S. L., Delbaere, L. T. J. and Lee, J. S. (2003) Cobalt(II), Nickel(II) and Zinc(II) Do Not Bind to Intra-Helical N(7) Guanine Positions in the B-Form Crystal Structure of d(GGCGCC). *J. Biol. Inorg. Chem.* (Accepted).

Labiuk, S. L., Delbaere, L. T. J. and Lee, J. S. (2001) Gamma and Ultraviolet Radiation Cause DNA Crosslinking in the Presence of Metal Ions at High pH. *Photochem. Photobiol.* 73: 579-584.

Aich, P., Labiuk, S. L., Tari, L. W., Delbaere, L. T. J., Roesler, W. J., Falk, K. J., Steer, R. P. and Lee, J. S. (1999) M-DNA: A Complex Between Divalent Metal Ions and DNA which Behaves as a Molecular Wire. *J. Mol. Biol.* 294: 477-485.

ACKNOWLEDGMENTS

I owe much gratitude to both of my supervisors, professors Jeremy Lee and Louis Delbaere who gave me the opportunity of working on such an exciting project. Both have been a tremendous inspiration and have always made themselves freely available for guidance, support and advice. I would also like to thank the members of my graduate advisory and examining committee for their guidance.

Gratitude is extended to all of the members of the labs where this work was carried out. Their support has been both necessary and appreciated. Recognition goes out to colleagues who provided technical assistance and advice. These include, but are not limited to, Dr. Lata Prasad, Dr. Palok Aich, Dr. Les Tari, Koto Hayakawa, and Yvonne Leduc. Carla Angelski was involved in setting up initial crystallization experiments for the sequence containing 5-fluorouracil. Helpful discussions were also enjoyed with others who worked on the M-DNA project: Dr. Shawn Wettig, Ryan Skinner, David Wood, Angela Brown and Michael Dinsmore.

Thanks are also due to my parents and family who put up with so much from me during this work. Their support and encouragement is most appreciated.

Finally, gratitude belongs to all of my fellow graduate students and friends who have played their part in making this time such a meaningful and enjoyable part of my life. They all provided help and encouragement at sundry times and in many ways known between them and myself. The acquaintanceships, companionships and friendships that were formed shall not be forgotten.

Financial support for these studies was provided by scholarships from the College of Medicine and the College of Graduate Studies and Research at the University of Saskatchewan as well as research grants from the Canadian Institutes of Health Research to professors Jeremy Lee and Louis Delbaere.

Use of the Advanced Photon Source was supported by the United States Department of Energy, Basic Energy Sciences, Office of Science, under Contract No. W-31-109-Eng-38. Use of the BioCARS Sector 14 was supported by the National Institutes of Health, National Center for Research Resources, under grant number RR07707.

DEDICATION

With love,

to my parents, Ernest and Diane, my brother Ryan and my sisters Kara and Kyla;

through whom much that is unattainable has been so graciously bestowed.

Ad majorem Dei gloriam.

TABLE OF CONTENTS

LIST OF TABLES

LIST OF FIGURES

LIST OF ABBREVIATIONS

A	adenine
A_{260}	absorbance at 260 nm
BICINE	N,N-bis(2-hydroxyethyl)glycine
5BrU	5-bromouracil
C	cytosine
d	deoxyribo prefix
DNA	deoxyribonucleic acid
EDTA	ethylenediaminetetraacetic acid
5FU	5-fluorouracil
G	guanine
HEPES	N-(2-hydroxyethyl)piperazine-N'-(2-ethanesulfonic acid)
I	inosine
M^{2+}	divalent metal cation
MPD	2-methyl-2,4-pentanediol
pH	negative logarithm of the hydrogen ion concentration
pK_a	negative logarithm of the dissociation constant of an acid
T	thymine
TAPS	N-tris-[hydroxymethyl]methyl-3-aminopropanesulfonic acid
T_m	melting temperature for DNA
TRIS	tris(hydroxymethyl)aminomethane
U	uracil
UV	ultraviolet
W_{dd}	water molecule in the distal-down position
W_{du}	water molecule in the distal-up position

W_{pd}	water molecule in the proximal-down position
W_{pu}	water molecule in the proximal-up position
W_t	water molecule in the trans position

1.0 INTRODUCTION

Deoxyribonucleic acid (DNA) was discovered in 1869 by Friedrich Miescer (Portugal and Cohen, 1977) and this represented the first step in both the biological and structural understanding of the macromolecule. Miescer's original term for DNA was "nuclein" and its importance was little understood and only partly correct. Miescher determined, correctly, that nuclein is a major component of the nucleus and distinguished from proteins, which had been discovered some thirty years earlier, by its phosphorous content. Its function, however, was thought to be simply a way of storing phosphorous in the cell. In 1889, Richard Altmann was the first to prepare protein-free nuclein and suggested the name nucleic acid due to the acid character of the substance.

By the early 1900s, all of the bases that are normally found in nucleic acids, adenine (A), guanine (G), cytosine (C), thymine (T) and uracil (U), had been discovered. Albert Kossel was a prominent investigator involved in much of this early work and was also the first to observe a carbohydrate component. By 1935, Phoebus Levene proposed a structure for the primary sequence of nucleic acid with the correct linkages between nucleotides (Levene and Tipson, 1935) which was confirmed in 1953 by Todd (Dekker *et al.*, 1953). It wasn't until 1944 that Avery proved that DNA

was the genetic material of living cells (Avery *et al.*, 1944; McCarty and Avery, 1946). Until then, it was commonly believed that only proteins had the requisite complexity to be the genetic material.

Thus, by the early 1950s, the primary structure of DNA was known but this in itself did not make clear how DNA could act as the genetic material responsible for coding protein sequences. An important observation was that the base composition of DNA consists of equal numbers of A and T residues and equal numbers of G and C residues (Chargaff *et al.*, 1951). The researchers were at a loss to explain these results, however, concluding that "the time has not yet come to attempt an answer."

An answer to the enigma did come in a very short time with some of the first fiber diffraction x-ray studies on DNA (Wilkins *et al.*, 1953; Franklin and Gosling, 1953). These observations were combined with those of Chargaff *et al.* (1951) by Watson and Crick, who proposed their model for the secondary structure of DNA (Watson and Crick, 1953a). Their structural model provided a rationale for the biological mechanisms observed in living systems (Watson and Crick, 1953b), propelling the biological sciences forward. Today, much detail about the structure of DNA is known. It has also been realized that other factors besides those inherent in the DNA are important in determining the structure and properties of the macromolecule.

Metal ions affect the stability of DNA structures and they are even implicated in the formation of alternative structures such as triplexes and quadruplexes. With the discovery of M-DNA (Lee *et al*, 1993), it has also been shown that not only the conformation, but also other properties of the DNA, such as electrical conductivity, can be profoundly affected by its interactions with metal ions.

The work presented in this thesis attempts to improve the understanding of important structural features of the M-DNA conformation as well as metal ion binding interactions with B-DNA. Knowledge of DNA structure will be necessary to accomplish this goal. With this in mind, a general introduction to DNA structure will be presented followed by an outline of metal cation interactions with DNA and how they affect DNA structure. This will include a literature review of the current state of knowledge concerning Co^{2+}, Ni^{2+} and Zn^{2+} interactions with DNA as elucidated by x-ray crystallography. Finally, a brief description of the properties of M-DNA will be given along with a detailed review describing the current state of knowledge regarding M-DNA structural features.

1.1 Structure of DNA

1.1.1 Primary DNA Structure

The primary structure of DNA consists of a polymer of deoxynucleotides. Each deoxynucleotide consists of a nitrogenous base attached to cyclic 2'-deoxy-D-

ribose, which in turn is attached to a phosphate group. Figure 1.1 depicts the four bases commonly found in DNA as well as the 2'-deoxy-D-ribose sugar. The bases are planar and of two general types: purine or pyrimidine. Purine bases consist of two aromatic rings of the types shown whereas pyrimidines consist of a single aromatic ring. Note the numbering schemes in each case. The bases A and G are of the purine type whereas C and T are of the pyrimidine type. In a deoxynucleotide, the 2'-deoxy-D-ribose is phosphorylated and a base is connected to the 1' position via a β-glycosyl C1'-N linkage. If the sugar is not phosphorylated, the entity is referred to as a deoxynucleoside.

The deoxynucleosides of A, G, C and T are named deoxyadenosine, deoxyguanosine, deoxycytidine and deoxythymidine, respectively. The deoxynucleotides are given the same prefix followed by the term monophosphate. Thus, for example, the deoxynucleotide of A having a phosphate group attached to the 5' position would be 5'-deoxyadenosine monophosphate, or simply 5'-dAMP, the prefix "d" standing for "deoxyribo." If no "d" is present, the entity is a nucleotide having a ribose sugar instead of 2'-deoxyribose.

A DNA strand, then, consists of a series of deoxynucleosides, each of which is joined to one neighbor *via* a phosphate group on the 5' oxygen and to another neighbor *via* a phosphate group on the 3' oxygen as represented in Figure 1.2. The end on which no residue is attached to the 5' oxygen is referred to as the 5'-end

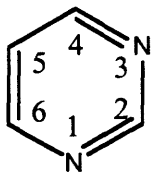

Pyrimidine

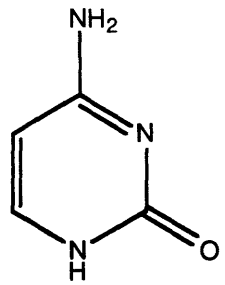

C

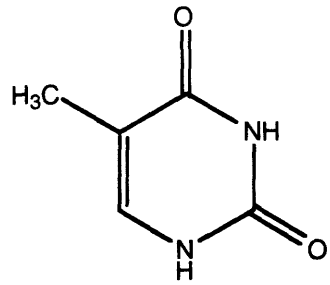

T

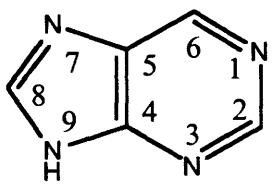

Purine

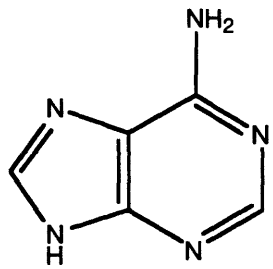

A

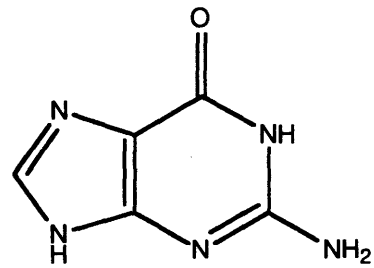

G

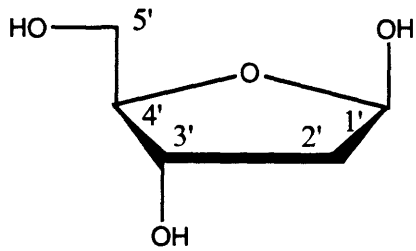

2'-deoxy-D-ribose

Figure 1.1. The constituents of DNA. The numbering schemes for pyrimidine bases, purine bases and 2'-deoxy-D-ribose are shown.

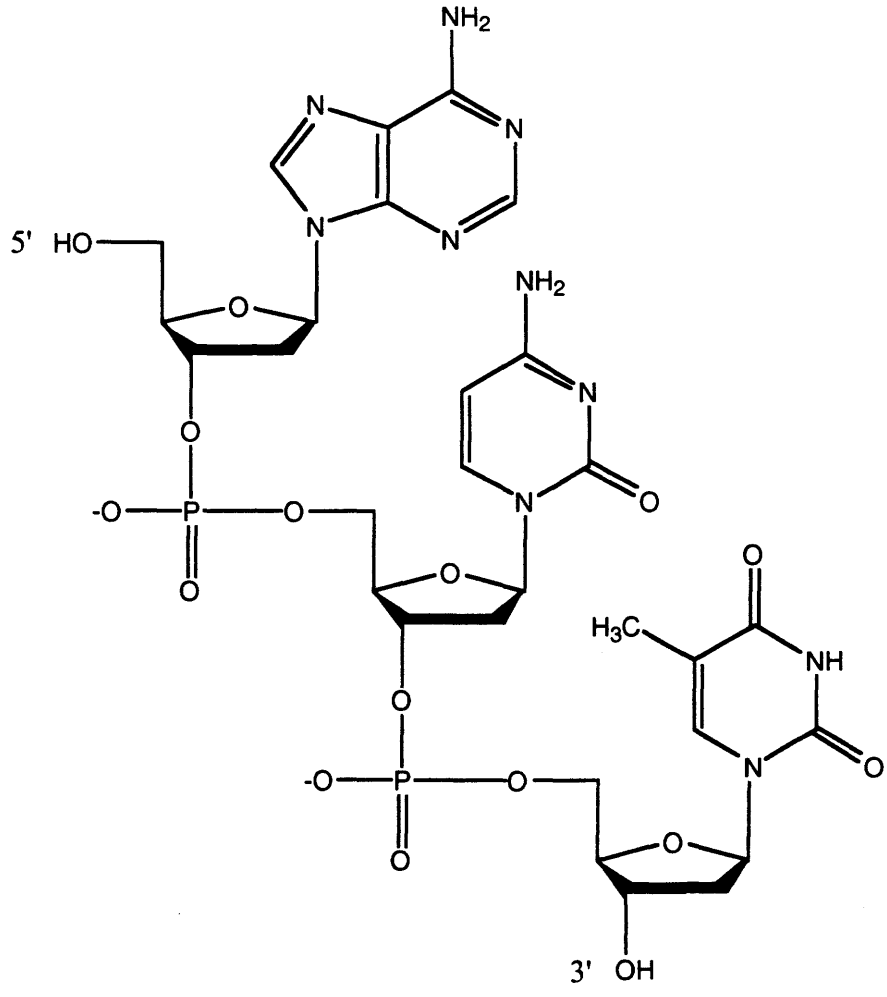

Figure 1.2. The deoxytrinucleotide d(ACT). Phosphodiester bonds link neighboring nucleosides in the 5' to 3' direction.

whereas the end on which no residue is attached to the 3' oxygen is referred to as the 3'-end. The ends of the strand may or may not be phosphorylated.

To describe the primary structure of DNA, an abbreviated form is used. The sequence is always written from the 5'-end to the 3'-end and given the prefix d. For example, d(GpGpCpGpCpCp), equivalent to d(GGCGCCp), describes a strand of DNA consisting of six deoxynucleotides, having a phosphate group on the 3'-end but none on the 5'-end. If the prefix "poly" is used, the sequence within brackets is repeated. For example, poly[d(TG)] indicates that the DNA sequence d(TG) is repeated. In this case, the complementary strand would be denoted as poly[d(CA)] and the duplex structure would be described as poly[d(TG)]•poly[d(CA)].

1.1.2 Secondary DNA Structure

The secondary structural description of DNA is usually given either as atomic coordinates or torsion angles along with bond lengths and bond angles (Seeman *et al.*, 1976; Saenger, 1984). Along the sugar-phosphate backbone, the conformation is described by six torsion angles: α, β, γ, δ, ε and ζ (Figure 1.3). The glycosyl bond is given by the torsion angle χ. These torsion angles allow flexibility in the chain that makes possible multiple categories of DNA secondary structure. The torsion angles are restricted to certain sterically-allowed values. The glycosyl bond, for example, is

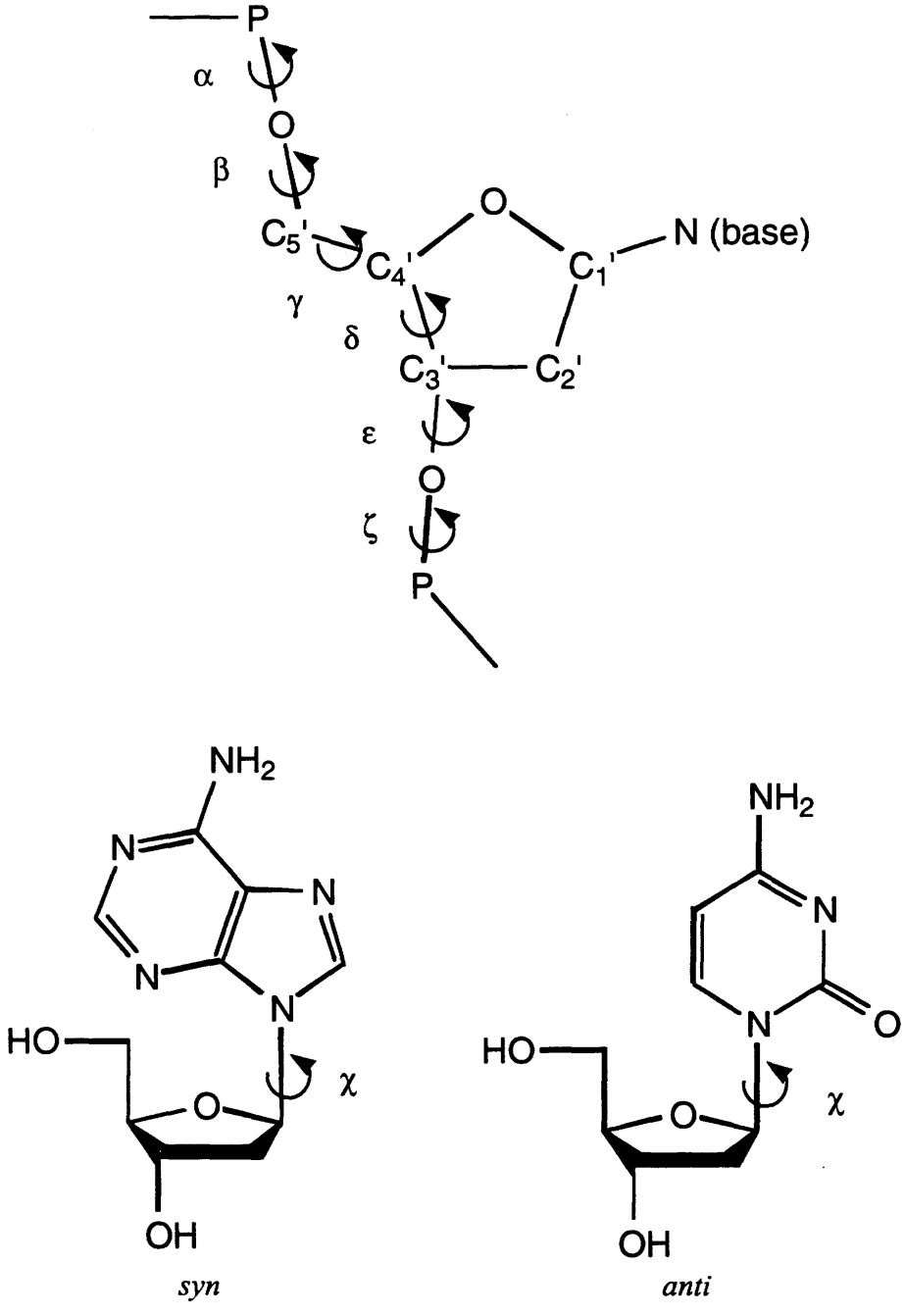

Figure 1.3. Torsion angles in a DNA strand. Shown are the torsion angles describing the conformation along the sugar-phosphate backbone of a strand of DNA (top) and the glycosyl bonds of deoxyadenosine and deoxycytidine deoxynucleosides (bottom). The glycosyl bond can be in either the *syn* or *anti* conformation.

generally found in one of only two stable positions: *anti* or *syn* (Figure 1.3). The *anti* conformation is most often observed in deoxynucleosides since there is least steric hindrance in this position. The *syn* conformation may occur when purine bases are present on the deoxynucleoside but is observed only rarely with pyrimidine bases. These trends are also followed in deoxypolynucleotides.

In the sugar residue, four of the five atoms constituting the ring are usually nearly coplanar, the fifth atom being outside of this plane by approximately 0.5 Å. This is known as the half-chair conformation (Figure 1.4). It is *endo* if the atom that is out-of-plane is on the same side of the ring as the C5' atom, otherwise, it is *exo*. Normally it is either the C2' or C3' atom that is out-of-plane. The sugar pucker determines the orientation of the phosphate group relative to the sugar residue.

1.1.2.1 A- and B-DNA

X-ray diffraction experiments on fibrous samples combined with detailed structural information from crystal studies of DNA constituents revealed some of the first details of DNA secondary structure. Fiber diffraction experiments yield overall or average features of a particular DNA conformation. Thus, when Franklin and Gosling (1953) published their results on fiber diffraction of DNA from calf thymus, they were able to distinguish between two different helical structures present under different conditions. Structure A was present under conditions of low humidity and

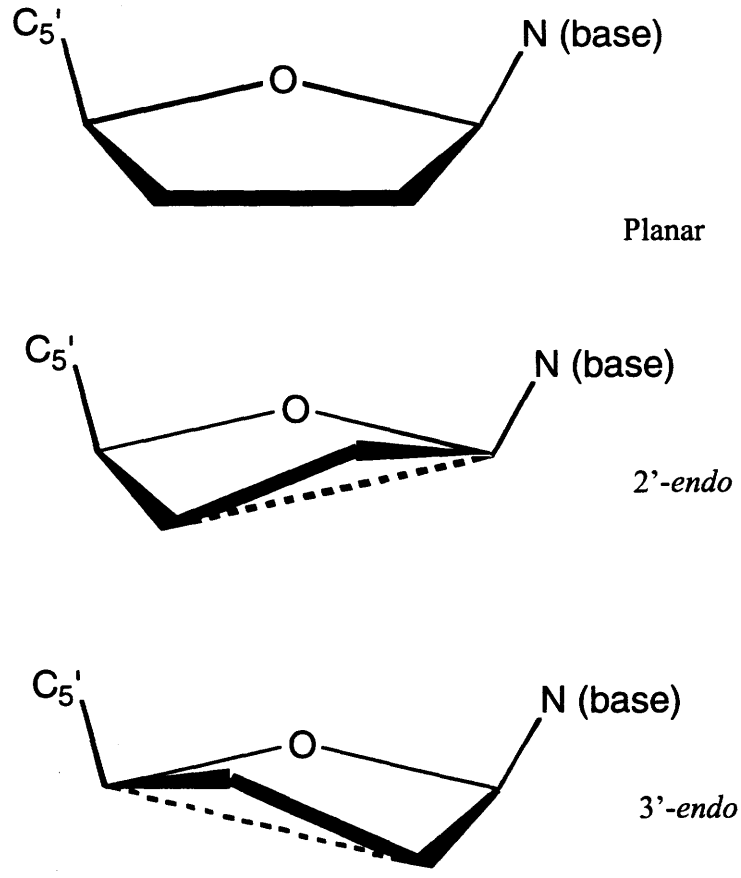

Figure 1.4. Diagram of the 2'-*endo* and 3'-*endo* conformations commonly adopted by the ribose ring. For simplicity, atoms bound to most of the carbon atoms have been omitted.

salt concentration. Structure B was present under conditions of high relative humidity with higher salt concentrations. The general outlines of Structure B were proposed based on these results. It is helical with the phosphate groups lying on the outside and the bases on the inside, the helix diameter being approximately 20 Å. The fiber axis displays a period of 34 Å with bases having a separation of 3.4 Å meaning that there are 10 residues per helical turn (Franklin and Gosling, 1953; Wilkins *et al.*, 1953).

These results provided evidence for the structural scheme put forward by Watson and Crick (1953b) for the B form of DNA. They proposed that the structure has two helical chains wrapped around a common axis in a right-handed fashion. The chains are antiparallel with bases on the inside and the sugars being approximately perpendicular to them. They also explained the observations of Chargaff (1951) and others (Wyatt, 1952), proposing that bases pair with each other along the helix in such a way that A always hydrogen bonds with T and G with C (Figure 1.5) giving a purine : pyrimidine ratio of one. The A•T and G•C base-pairs interact through two and three hydrogen bonds, respectively. In this scheme, the purine•pyrimidine pairs are isomorphous, that is, they have the same C1'-C1' bond lengths and the same N9-C1'-C1' and N1-C1'-C1' bond angles. Thus, any sequence can make up one strand but the other must be its complement in order to form a stable helix. This proposal has been corroborated by many sets of fiber diffraction experiments on DNA from other species and under varying humidity and salt conditions (Arnott, 1970).

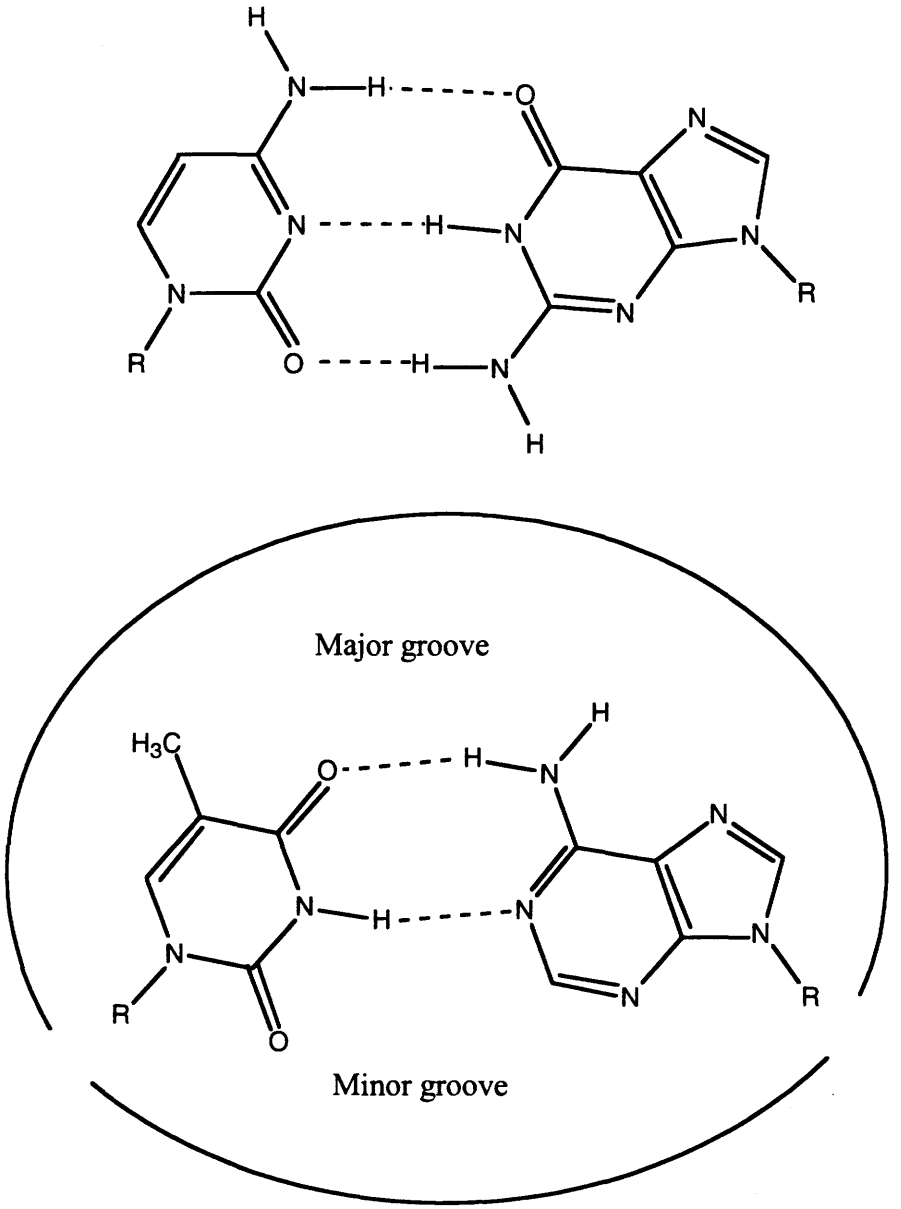

Figure 1.5. Watson-Crick base-pairing in duplex DNA. C•G base-pairs (top) interact *via* three hydrogen bonds whereas T•A base-pairs (bottom) interact *via* two. The major and minor grooves are indicated with the T•A base-pair. In both diagrams, R represents atom C1' of the 2'-deoxyribose sugar.

Development of techniques that allowed for the synthesis of large quantities of DNA having a specific sequence (Itakura *et al.*, 1975) allowed for x-ray studies on single crystals of deoxyoligonucleotides, further refining knowledge about DNA secondary structure. These structures have been extensively reviewed (Dickerson *et al.*, 1982; Drew and McCall, 1988) and conclusions have been drawn concerning general structural features of both the A- and B-DNA conformations (Saenger, 1984; Dickerson, 1992).

B-DNA has a right-handed helix with a diameter of approximately 20 Å, 10 base-pairs per helical turn and a twist of 36° per base-pair. On average, the base tilt is 6° normal to the helix axis. The double helix has a major groove that is wide and deep and a minor groove that is narrow and deep. The sugar pucker is C2'-*endo* while the glycosyl bond is in the *anti* conformation. This conformation is predominant in biological systems.

A-DNA also displays a right-handed helical sense with the two strands being antiparallel and the glycosyl bond maintaining an *anti* conformation. Several differences exist, however, and A-DNA has a somewhat larger diameter of approximately 26 Å, 11 base-pairs per helical turn and a helical twist per base-pair averaging 33°. The rise per base-pair is only about 2.6 Å, giving A-DNA a more compact structure. The tilt of base-pairs normal to the helix axis is as large as 20° and the major groove is narrow and deep compared to B-DNA, while the minor groove is

wider and shallower. A major distinguishing feature is that the sugar residues in A-DNA have a sugar pucker that is C3'-*endo*. When observing a strand of A-DNA along the helical axis, an obvious feature is the pronounced axial hole. Hydrogen bond lengths between base-pairs normally vary between approximately 2.7 Å and 3.2 Å for either A- or B-DNA.

1.1.2.2 Base Stacking Interactions

Though hydrogen bonding between base-pairs provides specificity in the interaction between the strands that compose the double helix, base stacking interactions are principally responsible for stabilizing it. These interactions are also known as π-π interactions. A major driving force is the tendency for minimization of the surface area of bases exposed to water, known as the hydrophobic effect (Calladine and Drew, 1992). Thus, when the solvent contains less water, the tendency is for this factor to be lessened and structures such as A-DNA emerge, which have bases with more surface area exposed. The effect is also observed in the presence of organic solvents such as ethanol (Urpí *et al.*, 2000).

Additionally, four other factors have been defined (Hunter and Sanders, 1990; Hunter, 1993). Briefly, π-π interactions are affected by van der Waals' interactions, electrostatic interactions between partial atom charges, electrostatic interactions between the charge distributions associated with the π-electron density and

interactions between partial atom charges and π-electron density. These latter four effects are more important in describing the relationship between sequence and the three-dimensional structure of DNA.

Van der Waals' interactions are largely attractive and act to maintain the base-pairs in contact, but become repulsive if the base-pairs are too close together. The surface that a base-pair encounters on its neighboring base-pair is not uniform. The charges due to electronegative atoms such as oxygen and nitrogen make for an uneven charge distribution. Of especial importance is the G residue which has a large region of negative charge associated with atom O(6) and extending to atom N(7). The C residue is associated with a large region of positive charge centered around atom C(6). Bases will tend to maximize the attractive forces between these positive and negative regions when they stack.

Base pairs also have an electron density distribution that has been characterized as a "sandwich." That is, they display a positively-charged central plane sandwiched between two negatively-charged regions of π-electron density above and below. Repulsion between the negatively-charged electron density results in a tendency for bases to repel each other and not stack directly on top of one other. The interactions become more favorable when the bases are offset such that the negatively-charged electron density can interact with the positively-charged central area of its neighbor. Finally, interactions between the π-electron density cloud and

partial atomic charges must be considered. An example is the tendency for G residues to stack such that the large region of negative charge is not directly above the π-electron density cloud of its neighbor.

1.1.3 Describing Base-Pair Geometry

The overall structure of double helical DNA may not reflect more subtle variations in local structure such as the orientation of bases relative to each other within the base-pairs and the orientations of neighboring base-pairs to one another. It is useful to define these geometric aspects as base-pair and base-pair step parameters, respectively. Average base-pair and base-pair step parameters can be considered in order to gain some idea about the overall conformation of a double helix because some of the parameters will differ between different conformations of DNA and from one sequence to another. However, it is often the case that local variations occur in which case local base-pair and base-pair step parameters will differ from the overall average for any particular conformation.

To describe these parameters, a standard reference frame is used (Dickerson *et al.*, 1989; Olson *et al.*, 2001). For base-pair parameters, a set of axes is constructed with reference to an ideal base-pair such that the *x*-axis points toward the major groove along the short axis of the base-pair. If a straight line were drawn between both C1' atoms of the base pair, the *x*-axis would be perpendicular to it and would

cross the midpoint of the line. It would have its origin at the intersection with the *y*-axis at the pseudo-dyad axis of the base-pair. The *y*-axis runs along a line connecting the C6 atom of the pyrimidine and the C8 atom of the purine. The *z*-axis has its origin at the intersection of the *x*- and *y*-axes and runs along the 5' to 3' direction of the sequence strand so that a right-handed rule is obeyed.

For base-pair step parameters, angles and distances are often calculated with reference to an average helical axis constructed between the neighboring base-pairs. When analyzing base-pair step parameters in bent DNA structures, it is critical that the axis chosen be independent of the global helix axis.

The diagram in Figure 1.6 visually shows the coordinate frame of reference for base-pair parameters. Also shown are schematic diagrams of the base-pair and base-pair step parameters. Shear, stretch and stagger describe the separation of two bases of a base-pair along the short axis, long axis and vertical axis, respectively. Buckle, propeller twist and opening describe the relative rotation of bases in a base-pair about the short axis, the long axis and the vertical axis, respectively. Shift, slide and rise measure the sliding of one base-pair relative to the next base pair along the short, long and vertical axes, respectively. Tilt, roll and twist measure the rotation of one base-pair with respect to the other about the short, long and vertical axes, respectively. The "local" helical parameters describe the geometry of the base-pair's vertical axis in relation to the global helix axis. Thus, x-displacement and y-

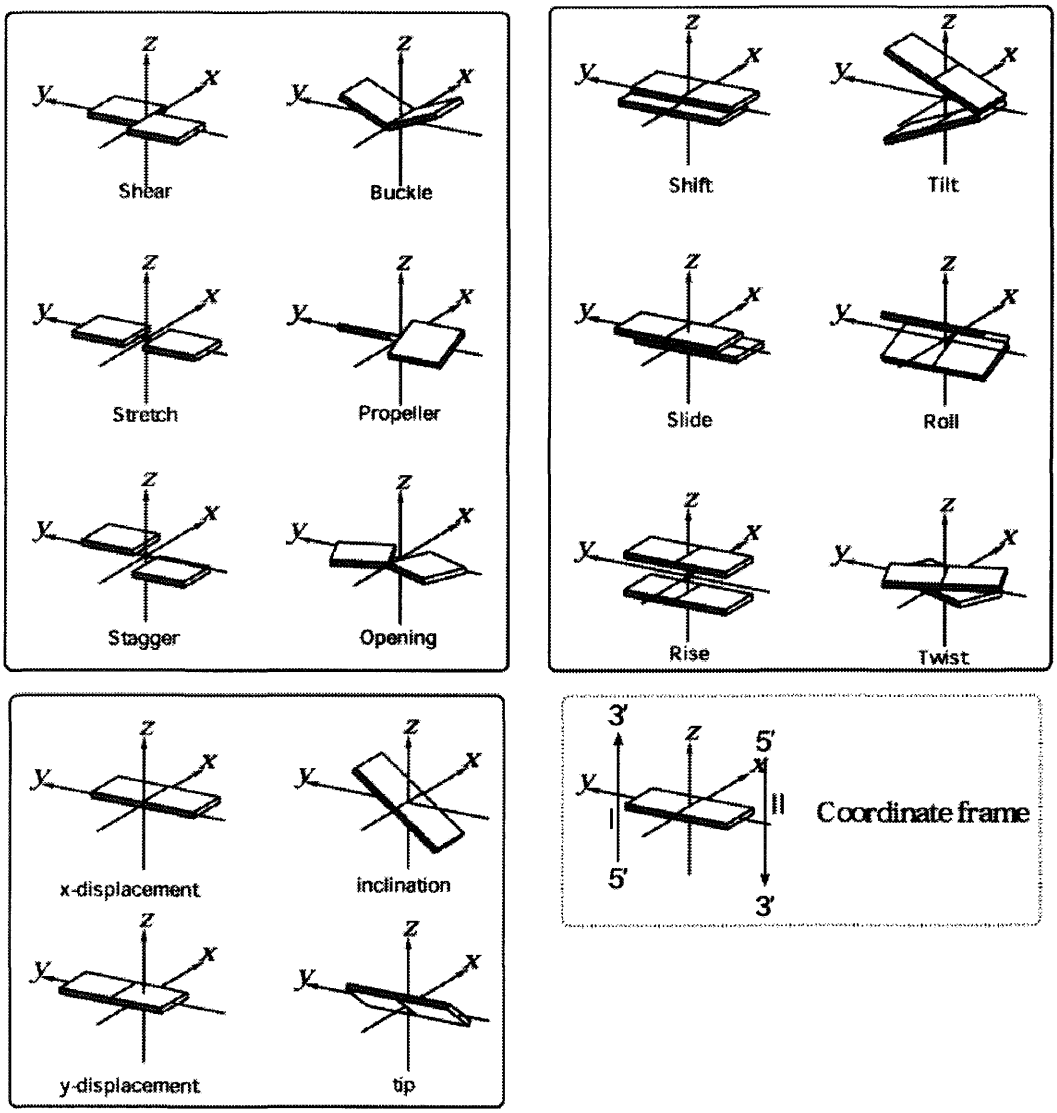

Figure 1.6. Base-pair and base-pair step parameters for duplex DNA. The illustrations demonstrate positive values for the base-pair parameters (upper left), base-pair step parameters (upper right) and local helical parameters (lower left). The coordinate frame is also shown (lower right), demonstrating the positions of the x, y and z-axes relative to the base-pairs. From Lu, 2002.

displacement measure the displacement of the base-pair along the x- and y-axis, respectively. Inclination and tip measure the rotation of the base-pair's vertical axis about the x- and y-axis, respectively.

Average values obtained from high-resolution x-ray crystallographic structures for many of these parameters vary between B- and A-DNA (Table 1.1). A-DNA tends to have lower twist and slide, but increased roll compared to B-DNA. The other base-pair step parameters and all of the base-pair parameters are generally not useful in distinguishing A-DNA from B-DNA, but x-displacement has a more negative value for the former.

The pitch of the double helix is defined as the translation along the vertical z-axis for a complete helical turn. Thus, the number of base-pairs per helical turn is calculated by dividing the pitch by the rise.

1.1.4 Denaturation and Renaturation of DNA

Denaturation of DNA occurs when the hydrogen bonds between base-pairs are broken and the double helix becomes two separate single strands of DNA. This commonly occurs at high temperatures, where it is referred to as melting and can be measured with a thermal denaturation experiment. Single strands of DNA have a higher absorbance at 260 nm (A_{260}) than does a double helix and this change is used

Table 1.1. Average values for base-pair, base-pair step and helical parameters in B- and A-DNA structures. Adapted from Olson *et al.*, 2001

Parameter	B-DNA	A-DNA
Base-pair parameters		
Shear (Å)	0.00 ± 0.21	0.01 ± 0.23
Stretch (Å)	-0.15 ± 0.12	-0.18 ± 0.10
Stagger (Å)	0.09 ± 0.19	0.02 ± 0.25
Buckle (°)	0.5 ± 6.7	-0.1 ± 7.8
Propeller twist (°)	-11.4 ± 5.3	-11.8 ± 4.1
Opening (°)	0.6 ± 3.1	0.6 ± 2.8
Base-pair step parameters		
Shift (Å)	-0.02 ± 0.45	0.00 ± 0.54
Slide (Å)	0.23 ± 0.81	-1.53 ± 0.34
Rise (Å)	3.32 ± 0.19	3.32 ± 0.20
Tilt (°)	-0.1 ± 2.5	0.1 ± 2.8
Roll (°)	0.6 ± 5.2	8.0 ± 3.9
Twist (°)	36.0 ± 6.8	31.1 ± 3.7
Local helical parameters		
X-displacement (Å)	0.05 ± 1.28	-4.17 ± 1.22
Y-displacement (Å)	0.02 ± 0.87	0.01 ± 0.89
Inclination (°)	2.1 ± 9.2	14.7 ± 7.3
Tip (°)	0.0 ± 4.3	-0.1 ± 5.2

to measure the temperature at which half of the DNA has denatured (T_m). The T_m gives an indication of the stability of the DNA helix under study.

A major intrinsic property of the DNA that affects its stability is the G•C content. DNA that has a higher G•C content denatures at a higher temperature than does DNA with a higher A•T content when measured under similar solvent conditions. Thus, at pH 7 with an NaCl concentration of 0.15 M, the bacterial DNA from *Clostridium perfringens* has a G•C content of 27% and a T_m of 80.5 °C while DNA from *Micrococcus lysodecticus* has a G•C content of 72% and a T_m of 99.5 °C. *Echerichia coli* has a G•C content of 50% and a T_m of 90.5 °C, intermediate between the other two (Marmur and Doty, 1962). Calf thymus DNA has a G•C content of 42% and a T_m of 87 °C.

Although T_m is proportional to G•C content, it is evidently not the case that the number of hydrogen bonds between base pairs determines the stability of a helix. This is especially obvious in synthetic sequences having the same G•C content but differing in the sequence. In many cases, these have been shown to have different T_m values. For example, poly[d(TTG)]•poly[d(CAA)] has a T_m of 65 °C whereas poly[d(TTC)]•poly[d(GAA)] has a T_m of 58.5 °C (Lee *et al.*, 1984). It is thus stacking interactions that are principally responsible for variations in duplex stability, certain base-pairs stacking more favorably than others.

DNA melting is a reversible process. If a solution of completely denatured DNA is incubated at a temperature approximately 25 °C below its T_m, it eventually completely renatures. However, if the temperature is lowered too quickly, the DNA will only base-pair partially and this may be either intermolecularly or intramolecularly. Because renaturation is a cooperative process, DNA that is not completely denatured will properly renature much more readily even at lower temperatures (Saenger, 1984).

Besides thermal denaturation profiles, an effective way of measuring denaturation takes advantage of the increased fluorescence of ethidium (Figure 1.7) when bound to duplex DNA. The x-ray crystallographic structure of ethidium bound to a dinucleotide demonstrates that the drug molecule intercalates between base-pairs in DNA (Tsai *et al.*, 1975) such that the phenyl ring and the ethyl group are in the minor groove with the amino groups forming weak hydrogen bonds with the oxygen atoms of the phosphate backbone. The net positive charge makes the interaction more favorable because it reduces repulsive forces between π-electron clouds. When bound, there is an accompanying lengthening of the double helix and the adjacent base-pairs are separated by approximately 6.8 Å. When DNA is denatured, there is a sharp drop in ethidium fluorescence (LePecq and Paoletti, 1967). The large fluorescence enhancement of ethidium when bound to duplex DNA makes it a useful drug in many assays (Morgan *et al.*, 1979a; Morgan *et al.*, 1979b).

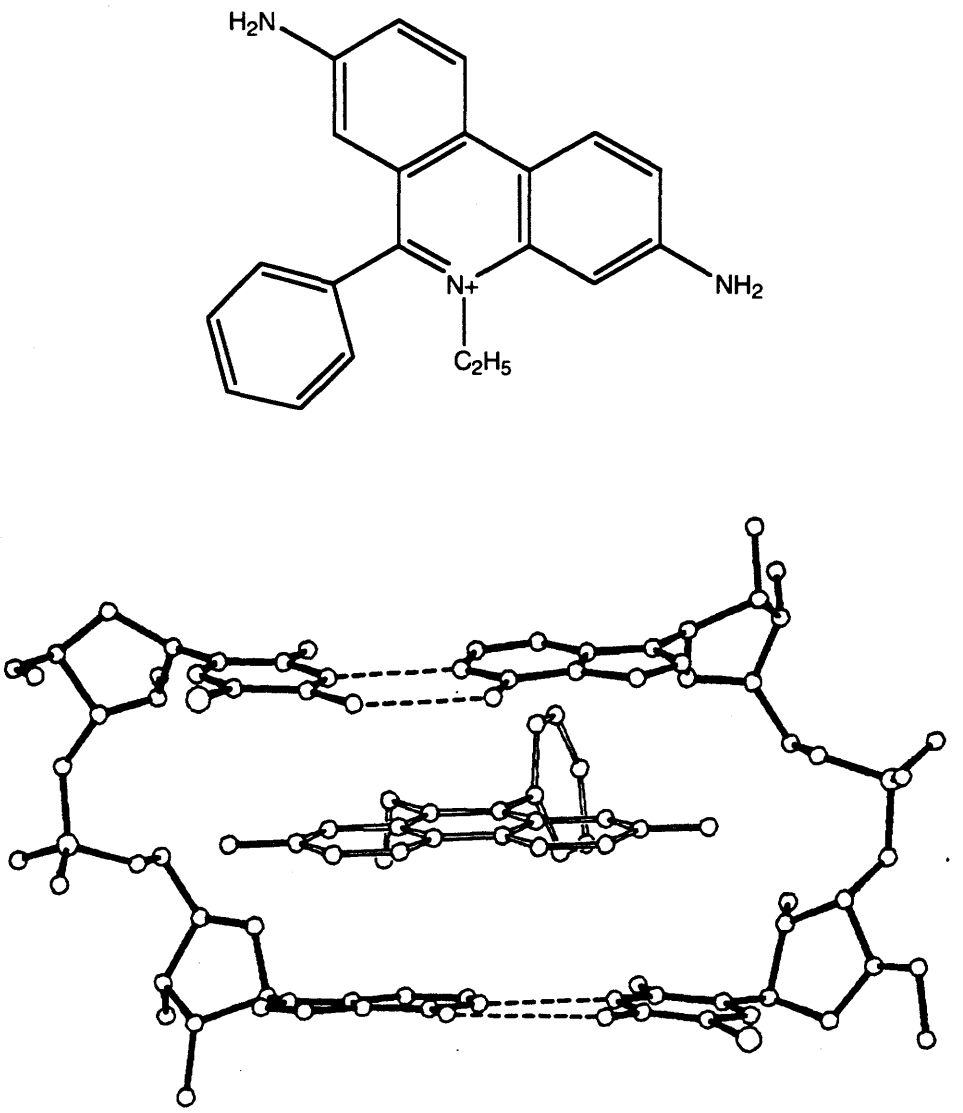

Figure 1.7. Intercalation of ethidium. Shown are the structure of the ethidium molecule (top) and the manner of intercalation in the crystal structure with 5-iodo-UpA (bottom). Adapted from Tsai *et al.*, 1975.

Other factors that can induce the denaturation of DNA include extremes of pH and metal cations. At very high or low pH values, atoms on the bases may become deprotonated or protonated, causing disruption in the hydrogen bonding between base-pairs. The stability of the helix, determined partially by G•C content, will determine the pH at which denaturation will occur. Metal cations may cause stabilization or destabilization of the double helix depending on type and concentration and this will be the focus of the next section.

1.2 DNA-Metal Cation Interactions

Metal cations interact extensively with DNA in solution (Kazakov, 1996) and must be considered along with the DNA structure. In fact, with very low concentrations of metal cations, DNA denatures even at relatively low temperatures. Often, changes in the stability or conformation of the DNA result from interactions with various metal cations at different sites on the DNA.

1.2.1 Metal Cation-Ligand Interactions

Group 1 and group 2 metal cations generally dissolve in water giving complete charge separation and their interactions are largely ionic. For example, NaCl dissolved in water gives the Na^+ and Cl^- cation and anion, each interacting

ionically with water molecules. Transition metal compounds do not usually follow this trend.

In general, the reaction of a transition metal cation (M^{m+}) with a donor ligand (L^{n-}) may be expressed as:

$$M^{m+} + L^{n-} \rightarrow ML^{(m-n)+} \qquad \text{(Equation 1.1)}$$

where $ML^{(m-n)+}$ is the complex formed, m is the charge of the metal cation and n is the charge of the ligand. The charge on the cation is generally +1, +2 or +3. The bond formed between the donor ligand and the metal cation is referred to as a coordinate bond (Gerloch and Constable, 1994). The ligand acts as an electron pair donor, contributing both electrons toward the formation of the coordinate bond.

In dilute aqueous solution, transition metal cations form complexes with water so that Equation 1.1 is more properly expressed as:

$$M(OH_2)_x^{m+} + L^{n-} \rightarrow M(OH_2)_{x-1}(L)^{(m-n)+} + H_2O \qquad \text{(Equation 1.2).}$$

It should not be imagined that the coordinate bonds between ligand atoms and the metal cation center are purely ionic or covalent. They are best described as intermediate between these two extremes. The electroneutrality principle has been used as a model to describe this type of bonding and states that the charge distribution in such a complex will ideally leave the metal with a neutral charge (Gerloch and Constable, 1994).

Thus, for example, if M^{m+} in Equation 1.2 were Co^{2+} and x were equal to six, a purely ionic description would have a charge of +2 on the metal center and a purely covalent description would have a charge of –4 on the metal center and a charge of +1 on each oxygen atom. Applying the electroneutrality principle, we obtain a more reasonable distribution with the metal center having a charge of 0 and each oxygen atom a charge of +1/3. This principle can be extended to metal cation-ligand interactions in general.

Of the metal cations in the first transition series this work is primarily concerned with Co^{2+}, Ni^{2+} and Zn^{2+} though other divalent metal cations (M^{2+}) in this series generally behave in a similar manner. In aqueous solutions, they are octahedrally coordinated to six water molecules (Cotton *et al.*, 1999). Thus, under these conditions, Zn^{2+} is found as the $[Zn(OH_2)_6]^{2+}$ species. If the solution were to be made basic, the loss of a proton would cause the formation of $[Zn(OH)(OH_2)_5]^{+}$. The loss of another proton would result in $[Zn(OH)_2(OH_2)_4]^{0}$ and precipitate would be observed. At very high pH, the complex would obtain an overall negative charge.

Coordinated to a ligand, Zn^{2+} is most commonly found with a tetrahedral, trigonal-bipyrimidal, square-pyrimidal or octahedral geometry although linear, trigonal-planar as well as 7 and 8 coordinated species are also known (Cotton *et al.*, 1999). Zn^{2+} has also been observed with a distorted square-planar geometry (Mamula *et al.*, 2000). For Co^{2+} and Ni^{2+}, trigonal, tetrahedral, square-planar, trigonal-

bipyrimidal, square-pyrimidal and octahedral geometries have all been observed, tetrahedral and octahedral being most common but Ni^{2+} often favoring a square-planar geometry.

1.2.2 Interaction Classification Schemes

In order to categorize metal interactions with DNA, we first consider the atoms on deoxynucleoside monophosphates and their ability to act as electron pair donating ligands. The principal sites to which metal cations coordinate can be grouped in decreasing order of proton affinity (with their approximate pK_as). Thus, T N(3) (10.0) > U N(3) (9.4) ≈ G N(1) (9.4) > C N(3) (4.3) > A N(1) (3.8) > G N(7) (2.4) > A N(7) (Martin and Mariam, 1979). The proton affinity of a site gives an indication of its basicity and can thus indicate its metal binding capacity. Because the first three of the series will be protonated under neutral conditions, the order with which the atoms are able to bind metal cations can be given as C N(3) > A N(1) > G N(7) > A N(7) > G N(1) ≈ U N(3) > T N(3). The latter three become more accessible under alkaline conditions.

Purine N(3) positions are not generally available for metal coordination because of steric hindrance with the sugar. Primary amino groups do not participate in metal ion coordination because there is delocalization of the lone pair of electrons into the aromatic ring system resulting in significant double-bond character making

these types of amino groups non-basic. Furthermore, primary amino groups are difficult to deprotonate (pK_a > 12). The oxygen atoms of the bases can also be involved in metal cation binding with O(2) of C being most common. The oxygen atoms of phosphate groups bind metal ions readily. In duplex DNA, many sites are not as easily accessible because of hydrogen bonding between base-pairs, base stacking interactions and other steric constraints.

The preference of different metal cations for particular donor atoms in DNA has been classified by Angelici (1973). Class A, or hard metal cations include alkali metals and alkaline earth metals such as Na^+, K^+, Mg^{2+} and Ca^{2+}. These typically have relatively small radii, high positive charges and no unshared electrons in their valence shells. The high ratio of positive charge to size results in a low polarizability and these tend to form ionic bonds with highly electronegative donor atoms that also have low polarizability (termed hard donor atoms or hard Lewis bases).

Class B, or soft metal cations include Cu^+, Ag^+, Au^+, Hg^{2+} and Pt^{2+}. These typically have a low ratio of positive charge to size compared to the class A metal cations and have unshared valence electrons. Class B metal cations are thus much more polarizable and correspondingly form the most stable complexes with highly polarizable donor atoms that have low electronegativities (termed soft donor atoms or soft Lewis bases). The resulting interactions have more covalent character than the interactions that involve class A metal cations.

In this classification scheme, some metal cations fall between the two extremes and are termed borderline. These include many of the metal cations of the first transition series, namely Fe^{2+}, Co^{2+}, Ni^{2+}, Cu^{2+}, and Zn^{2+}. Borderline metal ions will coordinate with both soft and hard donor atoms.

These trends are generally observed with DNA-metal ion interactions. Hard ligand donor atoms, such as the negatively charged oxygen atoms of the phosphate backbone are most often bound to class A metal cations such as Na^{+} and Mg^{2+}. Additionally, these interactions tend to have a largely ionic character, forming and breaking quite rapidly. Contrariwise, ligand donors that are softer and have a higher polarizability, such as the nitrogen atoms of the nitrogenous bases, prefer to bind class B metal ions like Ag^{+} and Hg^{2+}, the coordination having a more covalent character. First row transition metal cations that are classified as borderline interact with both phosphate oxygen atoms and atoms of the nitrogenous bases.

1.2.3 Duplex Stability

There is often a change in the stability of DNA when metal ions interact with it (Kazakov, 1996; Saenger, 1984). In general, the interaction of metal cations with negatively charged phosphate oxygen atoms is nonspecific and serves to stabilize the DNA duplex due to shielding of the negative charges of the phosphate backbone. Coordination to specific electron-donor atoms may follow this initial non-specific

interaction. The tendency is for destabilization of the duplex when metal cations coordinate to atoms on the nitrogenous bases because this interaction can destabilize the stacking interactions and hydrogen bonding.

The stabilization or destabilization of the double helix is often determined by thermal denaturation profiles. Thus, metal ions that stabilize the DNA helix will increase the T_m while those that destabilize the DNA helix will decrease the T_m. For example, K^+ stabilizes the DNA helix by interacting principally with the phosphate oxygen atoms. This is reflected in an approximate 27 °C increase in T_m for duplex *E. coli* DNA when the concentration of K^+ is increased to 1.0 M from 0.01 M (Marmur and Doty, 1962). Similar trends are observed with Na^+ and Mg^{2+} (Thomas, 1954). On the other hand, metal cations such as Ag^+ causes a decrease in T_m because of binding to the nitrogenous bases (Guay and Beauchamp, 1979).

The trend observed by Eichorn and Shin (1968) also correlates well with the class A *versus* class B classification scheme described above. Using thermal denaturation profiles, it was observed that a series of metal cations could be described, Mg^{2+}, Co^{2+}, Ni^{2+}, Mn^{2+}, Zn^{2+}, Cd^{2+}, Cu^+, in order of decreasing ability to stabilize the DNA helix. Hence, those metal ions that have more class B character have an increased propensity to bind the nitrogenous bases and cause denaturation of the double helix. Those that have more class A character tend rather to stabilize the double helix.

1.2.4 Crystallographic Studies

The first DNA-metal interactions that were studied using x-ray crystallography involved single bases, nucleosides and nucleotides (Swaminathan and Sundaralingam, 1979; Gellert and Bau, 1979). More recently, several deoxyoligonucleotide structures have become available (Aoki, 1996). In this section unmodified nucleotide, deoxynucleotide and deoxyoligonucleotide complexes with Co^{2+}, Ni^{2+} and Zn^{2+} will be reviewed.

1.2.4.1 Co^{2+}

For purine nucleotides, this group includes Co^{2+}-5'-GMP and Co^{2+}-5'-IMP (De Meester *et al.*, 1974a), Co^{2+}-5'-dGMP (Gellert *et al.*, 1979) and Co^{2+}-5'-dIMP (Poojary and Manohar, 1986) to date. These structures all show the metal bound to the N(7) position of the purine with five water molecules arranged in a square pyrimidal fashion to complete an octahedral coordination. They thus have the general formula $M^{2+}(5'\text{-NMP})(H_2O)_5nH_2O$. Interactions are observed between water molecules of the hydration sphere of the metal and oxygen atoms of the nucleotide phosphate groups and the O(6) position of purines. Interestingly, no Co^{2+} binds to the phosphate groups themselves. The Co^{2+}-N(7) bond lengths range between approximately 2.13 Å and 2.16 Å while the Co^{2+}-oxygen bond lengths range between

2.06 Å and 2.17 Å. The nucleotides display the *anti* conformation in the glycosyl bond and the sugars have a C3'-*endo* conformation.

Solid state studies of pyrimidine nucleotide-Co^{2+} complexes include Co^{2+}-5'-CMP (Clark and Orbell, 1975) and Co^{2+}-5'-UMP (Cartwright *et al.*, 1977). Both of these structures are polymeric. The C nucleotide displays metal binding *via* N(3), two oxygen atoms of different phosphate groups on neighboring moieties, one water molecule and a weak interaction with O(2) to give the metal an approximate tetrahedral coordination. The U nucleotide complex only shows binding to four phosphate groups and two water molecules giving Co^{2+} an octahedral coordination.

The first Co^{2+} deoxyoligonucleotide complex to be studied by x-ray crystallography involved Co^{2+} soaked into crystals of Z-DNA (Gao *et al.*, 1993). In these d(CGCGCG) and d(CGCGTG) structures, Co^{2+} binds to the N(7) position of G moieties both at the ends of the helix and within it. Areas containing alternating GC residues within the helix next to a derivative of the daunorubicin drug molecule displayed a distorted B-DNA conformation. Interestingly, no Co^{2+} binding was observed to G residues at this site, although Co^{2+} atoms were bound to sites still having the Z-DNA conformation. In this case a normal octahedral coordination was observed.

Based on modeling studies, the authors proposed that Co^{2+} cannot form a stable interaction with the G N(7) position within a B-DNA helix because the

octahedral coordination sphere clashes with the base at its 5' side. Normally, the proximal-up (W_{pu}) or proximal-down (W_{pd}) water molecule is hydrogen bonded to O(6) of the same G. The hydrogen bond restraints cause the water molecules to be out-of-plane relative to the G base, and the water molecules are named accordingly (Figure 1.8). In the example shown, W_{pd} would clash with the neighboring base in B-DNA.

More recently, several structures with Co^{2+} have appeared in the literature with the sequences d(CGTACG) (Adams *et al.*, 2000; Yang *et al.*, 2000) and another containing 5-bromouracil (5BrU) that has a Br atom attached to the 5 position of U: d[CG(5BrU)ACG] (Thorpe *et al.*, 2000). Again, the Co^{2+} atoms only bind to G residues. In all of these structures, there is a drug molecule bound and fraying of the terminal base-pairs is observed resulting in no G residues being present within a section of B-DNA. It is thus impossible to make any conclusions about whether Co^{2+} binds to G positions within a sequence of DNA that has the B conformation based on these studies.

The Yang *et al.* (2000) structure was calculated from high resolution data (1.1 Å) making it possible to locate water molecules within the coordination sphere of Co^{2+}. In this case, the Co^{2+} bound to the N(7) position of G residues also bound five water molecules giving M^{2+} octahedral coordination reminiscent of the studies in single G nucleotides.

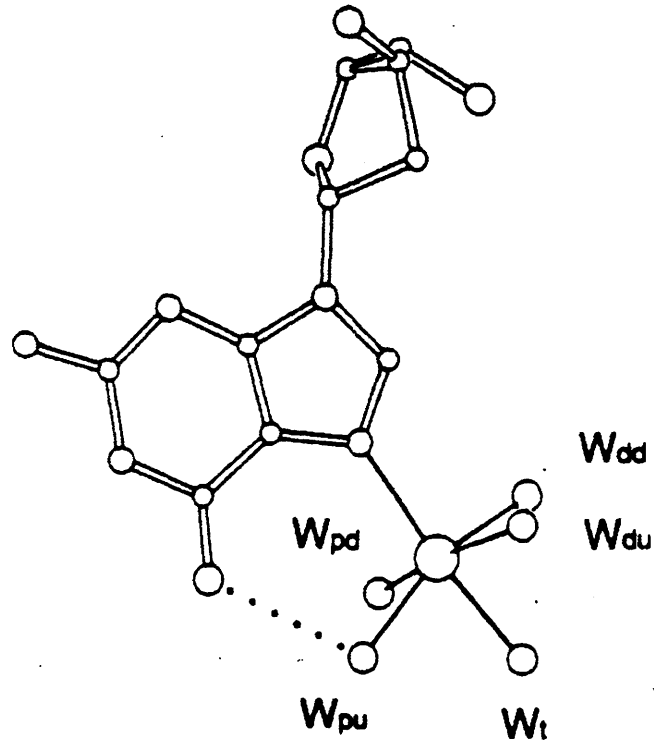

Figure 1.8. Hydration sphere of M^{2+} bound to the N(7) position of G. Shown are five water molecules coordinated to Co^{2+}. Water molecules are named W_{pd} (proximal-down), W_{pu} (proximal-up), W_{dd} (distal-down), W_{du} (distal-up) and W_t (trans). From Gao *et al.*, 1993.

1.2.4.2 Ni^{2+}

The first Ni^{2+}-nucleotide x-ray crystallographic structure to appear in the literature was that of Ni^{2+}-5'-GMP (De Meester *et al.*, 1974c). Subsequently there have been three more: Ni^{2+}-5'-AMP (Collins *et al.*, 1975), Ni^{2+}-5'-IMP (Clark and Orbell, 1974) and Ni^{2+}-5'-dGMP (Gellert *et al.*, 1979). All of these structures are similar to the purine nucleotide-Co^{2+} complexes and have the formula M^{2+}(5'-NMP)$(H_2O)_5 nH_2O$. The Ni^{2+}-N(7) bond lengths range from 2.08 Å to 2.12 Å while Ni^{2+}-oxygen atom bond lengths range from 2.02 Å to 2.13 Å.

The first oligonucleotide to be crystallized in the presence of Ni^{2+} was reported in 1999 (Abrescia *et al.*, 1999a). In this 3.0 Å structure, the self-complimentary sequence d(CGTATATACG) adopted a B-like conformation except at the terminal residues. The terminal G residue is found to interact with the minor groove of a neighboring decamer to form a G•C• G base triplet, stabilizing the crystal lattice. Among the four strands of DNA in this structure, three of the terminal C residues could not be located due to the limited resolution of the data. The one that was found, however, was not base-paired to its complimentary G base. Rather, it was found to interact with a neighboring strand. Interestingly, Ni^{2+} bound only to the N(7) position of every G residue and not to any of the A residues.

In a related structure (Abrescia *et al.*, 1999b), the same DNA sequence was crystallized in a different space group and gave a higher resolution structure. In this

1.58 Å structure, it was confirmed that Ni^{2+} was coordinated to five water molecules as well as to the N(7) position of the terminal G residues. The water molecules were arranged octahedrally in a similar manner to those seen in the nucleoside monophosphate structures. Based on the work of Gao *et al.* (1993), it was proposed that in deoxyoligonucleotides, metal ions similar to Ni^{2+} might interact specifically with G residues in unusual conformations or residues located at terminal positions.

This was confirmed when it was shown that in the crystal structure of Ni^{2+} and d(CGTGTACACG), Ni^{2+} binds only to G residues in terminal positions or in extrahelical positions (Abrescia *et al.*, 2002). Ni^{2+} did not bind to the G residue located in the center of the helix. The question remains whether this is a general phenomenon or whether it is limited to specific sequences.

1.2.4.3 Zn^{2+}

The purine nucleotide structure with Zn^{2+}, Zn^{2+}-5'-IMP (De Meester *et al.*, 1974b) differs from the corresponding structure with either Co^{2+} or Ni^{2+} in various ways. Zn^{2+} is bound to both the N(7) position and to three phosphate groups of neighboring nucleotides such that a polymeric structure is formed with each Zn^{2+} having a distorted tetrahedral coordination. The Zn^{2+}-N(7) bond length is 1.99 Å. The glycosyl bond is *anti* with the sugar conformation being C3'-*endo*.

In the pyrimidine nucleotide-Zn^{2+} complex, Zn^{2+}-5'-CMP (Aoki, 1976) also has a polymeric structure with C binding the metal *via* N(3). Zn^{2+} is also bound to two oxygen atoms of different phosphate groups on other moieties, one water molecule and has a weak interaction with O(2) to give it an approximate tetrahedral coordination.

In the deoxypolynucleotide structure of d(CGCAATTGCG), Zn^{2+} was shown only to interact with extra-helical G residues or those at the terminal ends of the helix (Soler-López *et al.*, 2002). In this structure, fraying of the ends is also observed so that the second G in the sequence is actually a terminal G. No Zn^{2+} binds to the eighth G in the sequence. Thus there is good evidence that transition metals do not form an inner sphere complex with the N(7) atom of G residues within a B-DNA helix except at the ends.

1.2.5 Induction of Alternative Conformations

Other structures composed of DNA strands have been discovered since the elucidation of the A- and B-DNA conformations, many of which are stabilized by metal cations. These include Z-DNA, as well as conformations containing more than two strands of DNA, namely triplex DNA and quadruplex DNA.

1.2.5.1 Z-DNA

The most striking difference between the Z-DNA conformation and that of A- or B-DNA is that the Z-DNA double helix is left-handed. Evidence for this structure was first observed in circular dichroism experiments that showed an inversion of the spectrum (Pohl and Jovin, 1972) for poly[d(GC)]•poly[d(GC)] at Na^+ or Mg^{2+} concentrations in the 0.7 to 3 M range. The structure was later confirmed by x-ray crystallography experiments with the d(CGCGCG) sequence (Wang *et al.*, 1979). The diameter of Z-DNA is smaller than either A- or B-DNA, being only about 18 Å. There are approximately 12 base-pairs per helical turn with an average rise per turn of 45 Å and a rise per base-pair of 3.7 Å. Compared to the other conformations, the major groove is rather flat and exposed but the minor groove is narrow and deep.

The glycosyl bond shows an *anti* conformation for pyrimidine bases, but surprisingly has a *syn* conformation for purine bases. The sugar pucker is C2'-*endo* for pyrimidines but C3'-*endo* for purine bases. While the Z-DNA structure is usually associated with DNA strands having alternating purines and pyrimidines, there are known examples of Z-DNA structures in sequences without alternating purines and pyrimidines (Wang *et al*, 1985). In this crystal structure, d(CGATCG) with C residues brominated or methylated on the C(5) atoms displays the Z-DNA conformation.

Besides methylation or bromination of C residues, it has been found that the Z-DNA conformation is stabilized by high metal ion concentrations. Whereas alkaline and alkaline earth metal cations such as Na^+ and Mg^{2+} are required in high concentrations, transition metal cations, especially Mn^{2+}, Ni^{2+}, Cd^{2+}, Zn^{2+} and Cu^{2+}, effectively stabilize the conformation even at sub-millimolar concentrations (Van de Sande *et al.*, 1982; Taboury *et al.*, 1984).

Class A metal cations stabilize the Z-DNA conformation principally by shielding the negatively charged phosphate groups from each other. In Z-DNA, these groups are very close to each other (8 Å compared to 12 Å in B-DNA). It is thought that the transition metal cations stabilize Z-DNA more effectively by also binding to G residues at the N(7) position (Kagawa *et al.*, 1991; Gao *et al.*, 1993). In Z-DNA, this position is much more exposed than in A- or B-DNA so that the metal cation can only bind when the DNA is in the Z conformation.

The Z-DNA conformation has also been observed to form more easily under conditions of negative superhelical stress as well as when C is methylated at the C(5) position, even under physiological metal cation concentrations (Herbert and Rich, 1996). This has raised much excitement because methylation of C at C(5) and negative superhelical stress are both common biologically. Evidence for *in vivo* formation of Z-DNA in prokaryotic systems has been put forward (Jaworski *et al.*, 1987). Here, *Eco*RI restriction sites were inserted into regions of plasmids containing

sequences that had various capacities of forming Z-DNA. In *E. coli* cells it was found that those that were more likely to be in the Z-DNA conformation did not become methylated in the presence of *Eco*RI methylase. In eukaryotic systems, the evidence for the existence of Z-DNA that has been presented is more indirect. Antibodies against Z-DNA have been shown to bind to eukaryotic chromosomes and proteins have been isolated from eukaryotic systems that bind Z-DNA (Herbert and Rich, 1996).

Various biological roles for Z-DNA have been postulated (reviewed in Rich *et al.*, 1984; Herbert and Rich, 1996). It may function to regulate gene expression because it would present an alternate structure that could be recognized by DNA-binding proteins such as transcription factors. Further, the conformation may be important in recombination because alternating purine•pyrimidine tracts have been associated with recombination hotspots. Additionally, transcription by RNA polymerase is inhibited by the Z-DNA conformation. Because negative topological strain is generated behind RNA polymerase as it transcribes, this may be important in regulating subsequent RNA polymerase activities.

1.2.5.2 Triplex DNA

Another form of DNA that can be stabilized by metal cations is triplex DNA (Soyfer and Potaman, 1996). This conformation forms with homopurine –

homopyrimidine tracts. It was first shown experimentally by Felsenfeld *et al.* (1957) using poly(A) and poly(U) which formed a structure having one strand of the former and two of the latter in the presence of Mg^{2+}. Shortly after these initial experiments, x-ray crystal data revealed an A•T base-pair having T hydrogen bonding *via* its N(3) and O(4) positions to A at positions N(7) and N(6), respectively (Hoogsteen, 1959; Hoogsteen, 1963). This type of hydrogen bonding scheme was dubbed Hoogsteen base-pairing and explains how triplex DNA forms.

Triplex DNA consists of base-triads having Watson-Crick type pyrimidine•purine base-pairing with an additional pyrimidine or purine residue hydrogen bonded to the purine residue in a fashion that can either be described as Hoogsteen or reverse-Hoogsteen (Figure 1.9). It is reverse-Hoogsteen if the third residue is in the opposite direction as that observed by Hoogsteen (1959), that is, if the third strand is antiparallel to the purine strand.

When describing base-triads, it is common to abbreviate them in the following manner. The first and second positions are reserved for the pyrimidine and purine of the Watson-Crick base-pair, respectively. The third position is given to the residue that is bound by Hoogsteen base-pairing. Thus, T•A•A describes a base-triad with A hydrogen bonded to T in a Watson-Crick fashion and to another A in a Hoogsteen fashion.

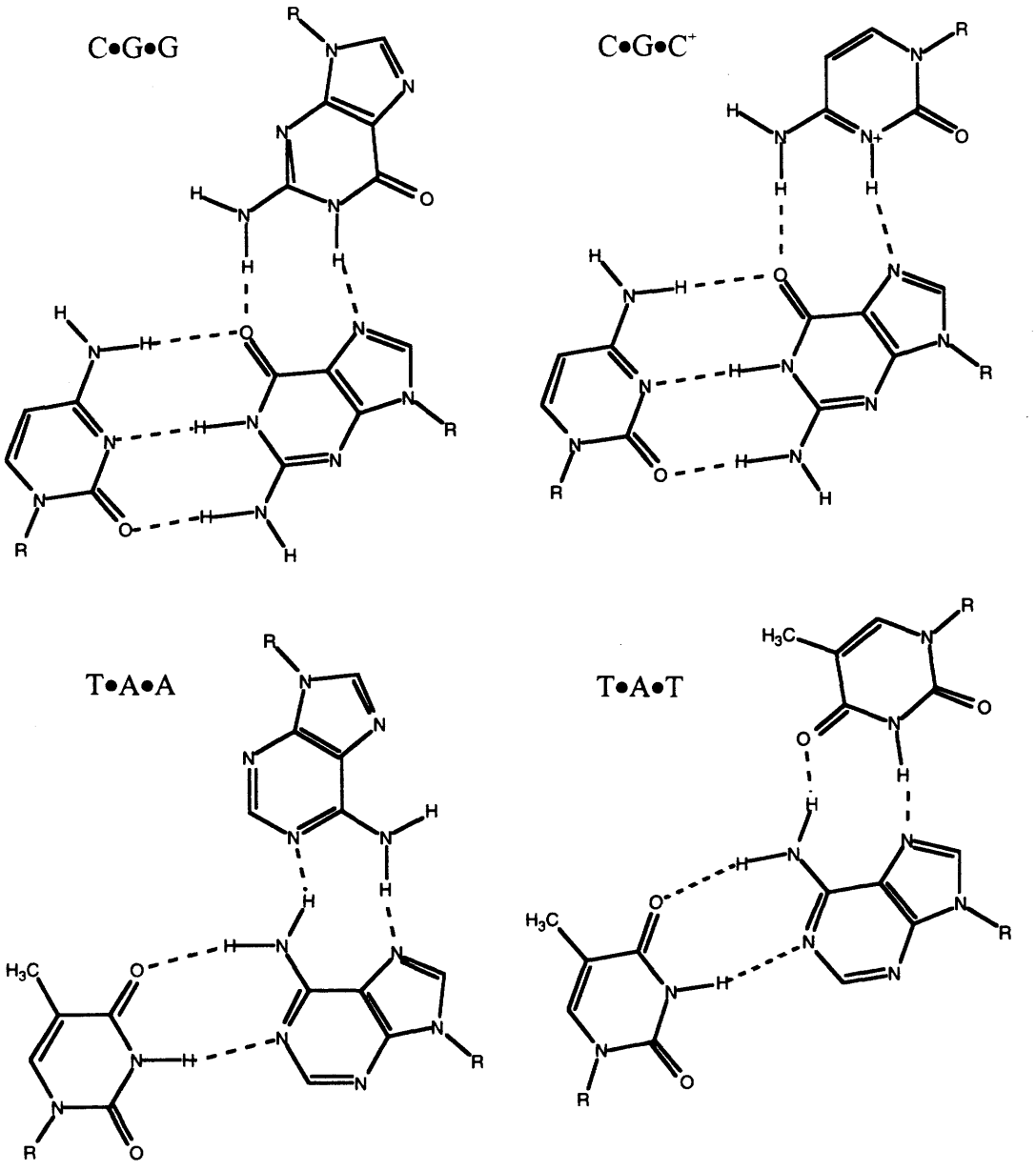

Figure 1.9. Common base-triads in triplex DNA structures. The structures on the left depict the third residue hydrogen bonded in a reverse-Hoogsteen fashion whereas those on the right have the third residue hydrogen bonded in a Hoogsteen fashion. In each case, R represents atom C1' of the 2'-deoxyribose sugar.

Triplex DNA can form with homopurine and homopyrimidine tracts having mixed sequences (Morgan and Wells, 1968). The overall geometry of the triple helix shares similarities with A- or B-DNA but can be highly variable depending on the particular sequences in question. The conformation is often dependent on an acidic environment, since C•G•C^+ and C•G•A^+ base-triads must be protonated at either the C or A residue in order to participate in Hoogsteen base-pairing (Lee *et al.*, 1979). Blocking Hoogsteen base-pairing sites can inhibit triplex formation. Thus, alkylation of A at position N(6), methylation of purine residues at position N(7), or the incorporation of 7-deazaadenine, which has no nitrogen atom at position seven, all inhibit triplex formation (Soyfer and Potaman, 1996).

Triplex structures are dramatically stabilized when metal cations are present because the negative charges on the phosphate groups are thereby shielded from each other. It has been shown that in order to obtain formation of triplexes at a level similar to that with 0.6 M Na^+, concentrations under 10 mM are sufficient for Mg^{2+}, Ca^{2+}, Mn^{2+} and Zn^{2+} (Felsenfeld and Rich, 1957).

As in the case with Z-DNA, evidence suggests that triple-helical DNA exists *in vivo* (reviewed in Soyfer and Potaman, 1996). Purine•pyrimidine tracts long enough to form triplex structures are found in up to 1% of the genome in eukaryotes. Several single stranded DNA-binding proteins have been discovered that bind to homopurine or homopyrimidine tracts that would be expected upon triplex formation.

Additionally, antibodies against triplex DNA have been shown to bind eukaryotic chromosomes (Lee *et al.*, 1987).

Various biological roles for triplex DNA have been proposed (reviewed in Soyfer and Potaman, 1996). It is conceivable, for example, that the formation of triplex DNA disrupts sites for DNA-binding proteins thereby playing a part in transcriptional regulation. Triplex DNA is also thought to interfere with DNA replication and is also likely involved in DNA condensation.

1.2.5.3 Quadruplex DNA

A model for quadruplex DNA was first proposed by Rich (1958) based on fiber x-ray diffraction experiments on poly(dI) sequences. These experiments pointed to a structure containing four strands. The first single crystal x-ray structure showed that the sequence d(GGGGTTTTGGGG) formed a complex whereby two of these sequences interacted with each other such that four G residues hydrogen bonded to form a quadruplex structure (Figure 1.10) (Kang *et al.*, 1992). The T sequences formed loops, one at either end of the complex so that two of the G segments ran antiparallel to the other two with all strands taking on an overall right-handed conformation. The stretches of G alternated in *syn* and *anti* conformation for the glycosyl bond. Interestingly, K^+ cations were located near the center of the quartets

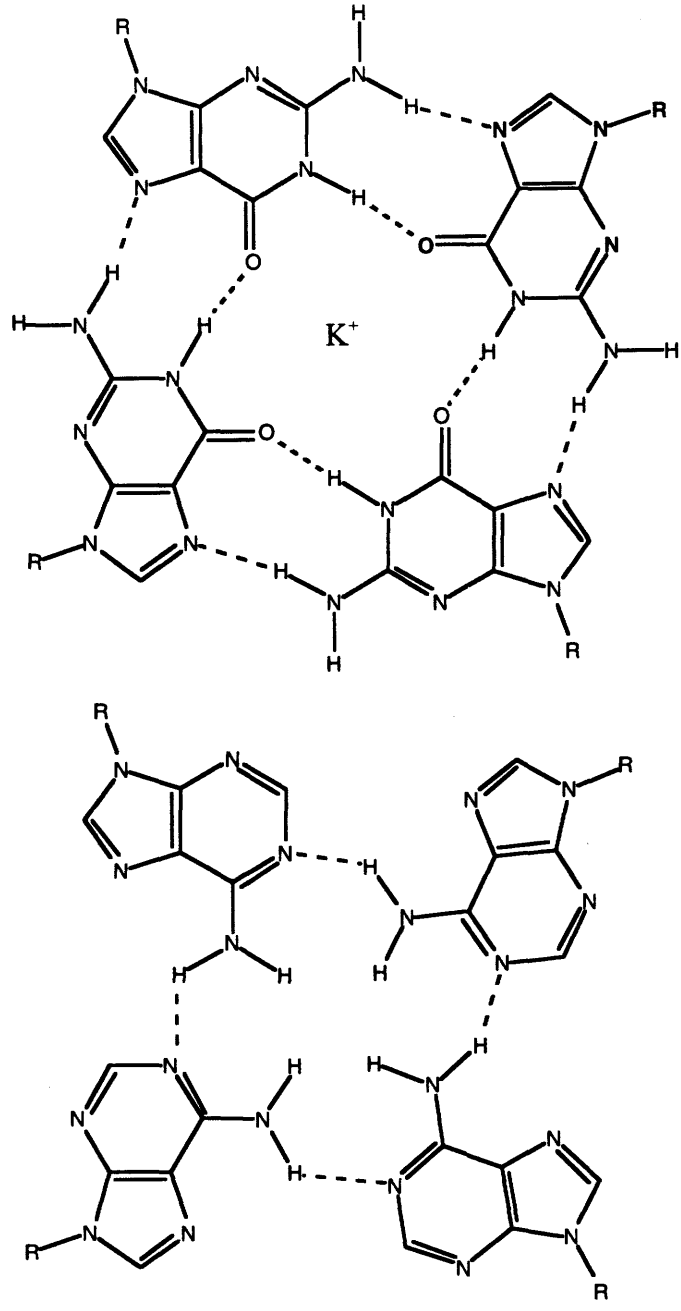

Figure 1.10. Quadruplex structures. Shown are a G-quartet (top) and an A-quartet (bottom). These structures are stabilized by monovalent cations such as K^+, as depicted for the G-quartet. R represents atom C1' of the 2'-deoxyribose sugar.

but because of the relatively low resolution of the data (2.5 Å), their locations were not definitively determined.

Two years later, a second structure was published showing that the sequence d(TGGGGT) crystallized with all four strands parallel (Laughlan *et al.*, 1994). This was a much higher resolution structure (1.2 Å) and metal cations could therefore be observed with much greater clarity. In this structure, Na^+ cations were found both between and within the planes of the bases providing a rationale for the need of metal cations to stabilize this structure.

It was also discovered that A residues can participate in this type of structure when studies were performed using poly[d(GGA)], poly[d(GA)] and poly[d(GAA)] (Lee, 1990). In the case of poly[d(GGA)], it was found that Ca^{2+} and Ba^{2+} were better able to stabilize the quadruplex than K^+.

In humans, the sequence d(TTAGGG) is repeated for long stretches at the ends of chromosomes and in other eukaryotes, similar phenomena are observed (Mergny and Hélène, 1998; Phan and Mergny, 2002). Because these telomeric regions are G-rich, it is thought that they are involved in quadruplex DNA formation. The formation of this structure may in part regulate telomerase because the function of this enzyme is inhibited by it (Zahler *et al.*, 1991). Evidence for the existence of this structure *in vivo* includes the binding of antibodies against guanine-quadruplex DNA in eukaryotic nuclei (Schaffitzel *et al.*, 2001).

1.3 M-DNA

Another conformation of DNA stabilized by M^{2+} has been described more recently (Lee *et al.*, 1993). It has been dubbed M-DNA due to its intimate association with certain metal cations.

1.3.1 Properties

The M-DNA conformation forms only with Co^{2+}, Ni^{2+} and Zn^{2+} at pH values above 8, although intermediate formation is observed at pH 8 (Lee *et al.*, 1993). It does not form with Ag^{+}, Ca^{2+}, Cu^{2+}, Mg^{2+} or Mn^{2+}. Once formed M-DNA does not bind ethidium and this provides for a convenient detection method and way to assess formation kinetics. A fluorescence assay solution was developed wherein M-DNA does not readily form but remains stable if already formed. The assay solution consists of 5 mM tris(hydroxymethyl)aminomethane (TRIS)-HCl (pH 8.0), 200 μM Zn^{2+} and 0.5 μg/mL ethidium. If the pH of the solution is lowered or ethylenediaminetetraacetic acid (EDTA) is added, M-DNA readily reverts back to the B-DNA conformation.

With fluorescence studies, the formation of M-DNA was shown to be dependent on the M^{2+} concentration, forming more rapidly and to a greater extent with higher concentrations. Formation is also dependent on temperature, M-DNA

forming only slowly near 0°C but more quickly with increasing temperatures up to 37 °C (Lee *et al.*, 1993).

It was also reported that at pH 6.5, the maximum stabilization provided by Zn^{2+} is approximately 3 °C as assessed by T_m measurements on calf thymus DNA. At concentrations above approximately 75 μM, Zn^{2+} increasingly destabilizes the DNA helix. This coincides well with the results of Eichorn and Shin (1968) who showed that Zn^{2+} is mostly destabilizing to DNA duplexes. On the other hand, at pH 9.0 where the M-DNA conformation would be expected to form, Zn^{2+} is mostly stabilizing with the T_m increasing as much as 12 °C.

The formation of M-DNA does not seem to be dependent on base composition. Thus, M-DNA forms at the same rate with *M. luteus*, *E. coli* and *C. perfringens* DNA which have 72%, 50% and 27% G•C content, respectively. The extent of formation does, however, vary with different synthetic sequences. Poly[d(TG)]•poly[d(CA)] forms most readily, followed by poly(dA)•poly(dT), poly[d(TCC)]•poly[d(GGA)], poly[d(TTC)]•poly[d(GAA) and poly[d(GC)]. Poly[d(AT)] forms M-DNA least favorably.

Of great interest, it has been found that the M-DNA conformation is capable of acting as a molecular wire (Aich *et al*, 1999). Duplexes were synthesized having an electron donor (fluorescein) at one end and an electron acceptor (rhodamine) at the

other. When M-DNA was formed with Zn^{2+}, the fluorescence of the fluorescein on a 20 base-pair sequence was 95% quenched. When the sequence was extended to 54 base pairs, quenching was still observed on the order of about 60% and this was attributed to electron transfer. When a DNA-binding protein specific for a portion of the 54 base-pair sequence was added, the transfer of electrons was inhibited and negligible loss of fluorescein fluorescence was observed.

Conduction has also been observed through 15 μm long Zn^{2+} M-DNA bundles dropped across two gold electrodes (Rakitin *et al.*, 2001). In this case, the conduction is more efficient than through normal B-DNA, which demonstrates only semiconductor-like behavior. It should be noted, however, that this technique measures conduction through DNA or M-DNA bundles consisting of approximately 100 molecules each.

It has been proposed in many of these studies that M-DNA could be useful for building nanoelectronic devices. Because DNA self-assembles, the components could be chemically synthesized, eliminating the need to build smaller machines capable of constructing even smaller mechanical devices. DNA can also be synthesized with whatever sequence is desired. This, in conjunction with its ability to bind other molecules such as drug molecules and proteins in a sequence-specific manner, makes DNA an exciting possibility for these nanoengineering enterprises (Ward, 2001; Wang, 2002; Richter, 2003).

On this front, some positive results have already been achieved (Aich *et al.*, 1999), a protein binding to a specific sequence having been shown to block electron transfer through M-DNA in a switch-like fashion. M-DNA formation also shows some sequence dependence meaning that DNA circuits could be constructed having certain regions more readily taking on the conductive M-DNA conformation than other regions. Thus, elements such as capacitors could potentially be built into such nanocircuitry quite readily.

1.3.2 Structure

Experimental results pointing to a structural elucidation for M-DNA will now be reviewed. It is thought that the structure has an overall topology that is similar to B-DNA. This is based on several lines of evidence. First, the formation of M-DNA is not dependent on DNA base composition and it will form with any sequence, including sequences containing inosine, 6-methyladenine and 7-deazaadenine (Figure 1.11). This, combined with the fact that M-DNA rapidly reverts to B-DNA by the addition of EDTA or a lowering of the pH suggests that it does not simply represent denatured DNA. It also indicates that G still base pairs with C and A with T since a rapid reversion would not be expected if this were not the case. Formation in the presence of 6-methyladenine and 7-deazaadenine eliminates the possibility of M-DNA requiring Hoogsteen base-pairs.

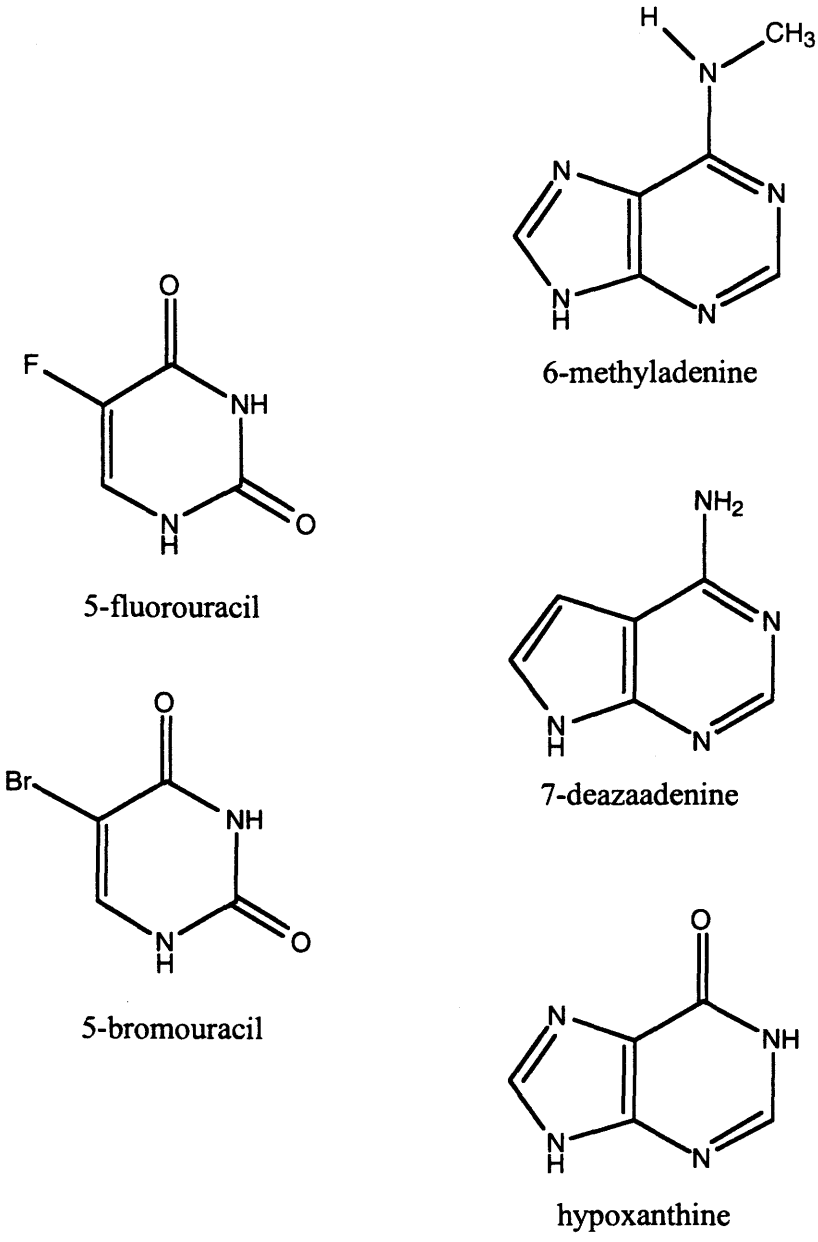

Figure 1.11. Modified bases that have been used to study M-DNA formation.

Second, the circular dichroism spectrum of calf thymus DNA at pH 9.0 in the presence of 1 mM Zn^{2+} is not significantly different from that of calf thymus DNA in the absence of Zn^{2+} (Lee *et al.*, 1993). Third, agarose gel electrophoresis experiments in the same study showed that with the addition of Zn^{2+} at pH 9.0, covalently closed circular and linear DNA behave similarly to B-DNA. This not only indicates that M-DNA does not simply represent precipitation or aggregation, but that it has a number of base-pairs per helical turn similar to that of B-DNA. Fourth, it was shown that a D-site binding protein recognized its binding site at the center of a 54-mer duplex and successfully blocked electron transport (Aich *et al.*, 1999) in the presence of Zn^{2+} at pH 9.0. The D-site binding protein is specific for duplex DNA and would not be expected to bind specifically to DNA having a conformation wildly different from the usual B-DNA conformation. These observations all suggest that the overall topology of M-DNA is similar to B-DNA, being right-handed with approximately 10.5 base-pairs per helical turn, A base-pairing with T and G base-pairing with C. We now examine some of the evidence that indicates where M^{2+} may be binding in this structure.

That an alkaline pH is necessary and that M-DNA will not bind ethidium suggest that one of the protons must be removed before formation and that the M^{2+} position must be such that ethidium intercalation is inhibited. Because the imino protons at G N(1) and T N(3) have high pK_a values, they are the most likely

candidates for M^{2+} binding (see Section 1.2.2). This proposal is especially favored when nuclear magnetic resonance experiments on the DNA sequence $d(TG)_{15}$•$d(CA)_{15}$ are considered (Lee *et al.*, 1993). In these experiments, it was shown that at pH 9.0, the peaks corresponding to the imino protons disappear in the presence of 2.0 mM Zn^{2+}. M^{2+} in this position would also be expected to inhibit ethidium binding since the positive charge would repel the positively charged ethidium ion.

Transition metal binding to this site within base-pairs is not unheard of and there are currently at least two x-ray crystal structures reporting this. The first is a complex of two T bases with Hg^{2+} binding to the N(3) position of each (Kosturko *et al.*, 1974). Although this does not form a standard base-pair, it does demonstrate the possibility of a transition metal cation being able to bind to the imino position to form a bridge between two bases. The second occurred in an RNA sequence with Au^{3+} (Ennifar *et al.*, 2003). In this structure, Au^{3+} replaces the imino proton of G, binding within the plane of the G•C base-pair with a distorted square-planar geometry. Although the metal cation caused the base-pairing to be distorted, with hydrogen bond distances being stretched to over 3.5 Å, it did not destroy the interaction. The stretching is likely due to the somewhat large ionic radius of Au^{3+} (0.82 Å) (Cotton *et al.*, 1999).

The observations discussed to this point suggested base-pair structures for M-DNA similar to those depicted in Figure 1.12 (Aich *et al.*, 1999). Molecular modeling

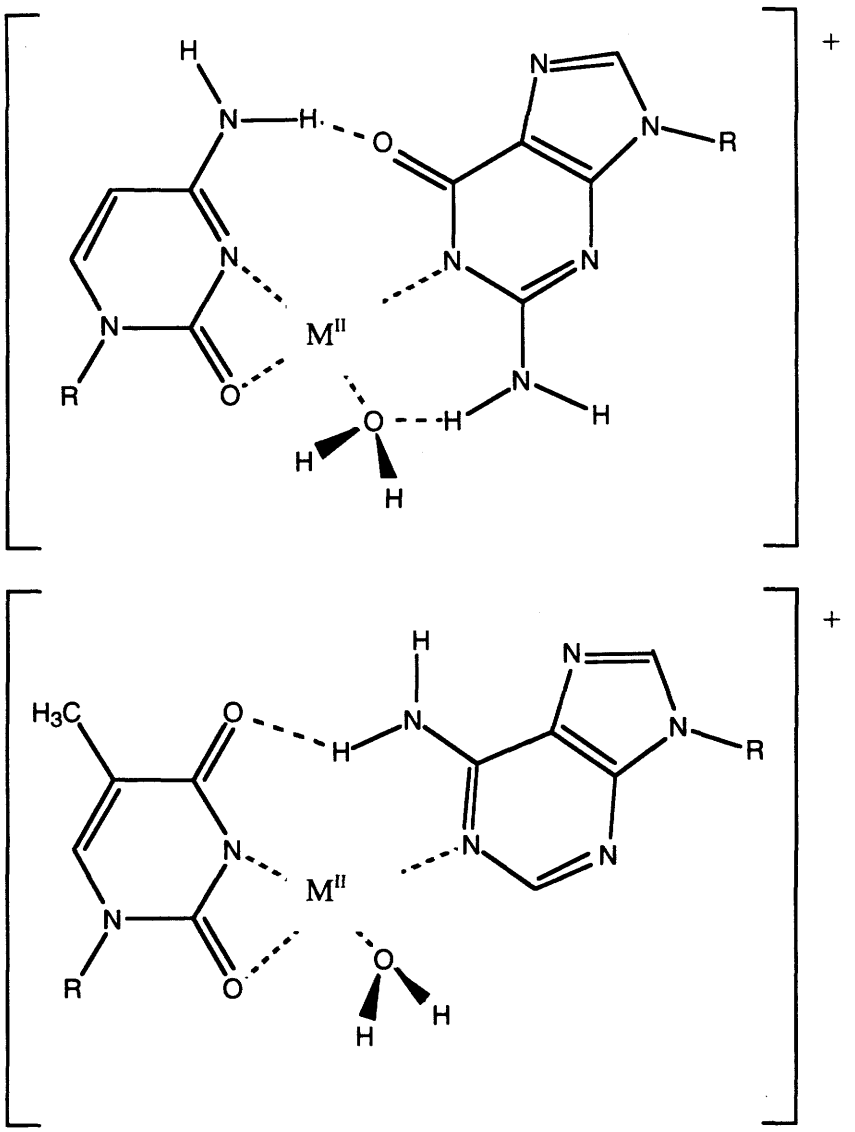

Figure 1.12. Proposed structure for the base-pairs of M-DNA. Shown are C•G (top) and T•A (bottom) base-pairs with M representing Co, Ni or Zn. R represents atom C1' of the 2'-deoxyribose sugar.

was performed with a 12 base-pair helix, replacing the imino protons with Zn^{2+} (Figure 1.13). In this proposed structure, both A•T and G•C base-pairs can accommodate the M^{2+} and are isomorphous. To accommodate the M^{2+}, the minor groove is widened by approximately 20° to 30°. In this scheme, the M^{2+} has a distorted square-planar arrangement with a water molecule completing the coordination. There also remains one hydrogen bond in each type of base-pair, providing a rationale for the observation that M-DNA rapidly reverts back to B-DNA upon removal of the M^{2+}. The helix shows approximately 11 base-pairs per helical turn which is similar to B-DNA. The distance between adjacent M^{2+} is approximately 4 Å, providing a route for electron transport through the helix.

As far as is known, the M-DNA conformation is only adopted with Co^{2+}, Ni^{2+} and Zn^{2+}. It is hypothesized that this is because the M^{2+} involved must have an appropriately small ionic radius (under approximately 0.74 Å), be able to form a M^{2+}-nitrogen atom bond with the appropriate bond length and be able to take on a distorted square-planar geometry. M^{2+}-N(7) bond lengths vary between approximately 2.0 Å and 2.2 Å in the nucleotide monophosphate structures described in section 1.2.4 for Co^{2+}, Ni^{2+} and Zn^{2+}. Although Cu^{2+} has a similar ionic radius to Co^{2+}, Ni^{2+} and Zn^{2+} and can conform to a square-planar coordination geometry (Cotton *et al.*, 1999), it prefers to form coordinate bonds with nitrogen atoms which are somewhat longer. Thus, in many similar structures, the Cu^{2+}-N(7) bond length varies between

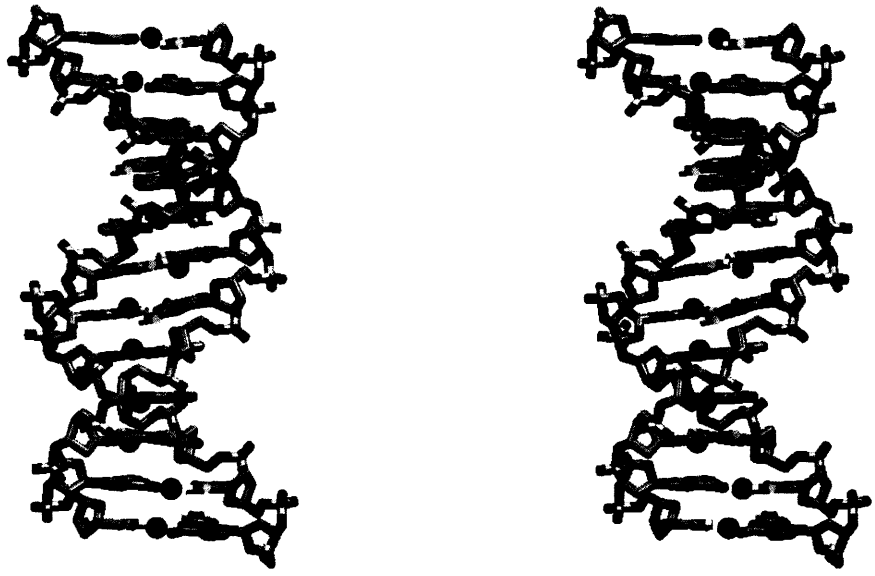

Figure 1.13. Stereo view of the M-DNA model. Twelve base pairs are shown with Zn^{2+} cations colored green, oxygen atoms red, phosphorus atoms yellow and carbon atoms gray. From Aich *et al.*, 1999.

approximately 2.2 Å and 2.6 Å (Sletten and Lie, 1976; Clark *et al.*, 1978; Kagawa *et al.*, 1991).

Recent experiments have corroborated many of the predictions based on the proposed structure for M-DNA. It has been demonstrated that if the modified bases 5-fluorouracil (5FU) or 5BrU (see Figure 1.11) are incorporated into DNA, the formation of M-DNA occurs under less alkaline conditions in the presence of Zn^{2+} (Wood *et al.*, 2002). DNA having a 54% G•C content has a value for pH_m of 8.4, pH_m representing the pH at which M-DNA formation is 50% complete. Incorporation of 5FU or 5BrU result in pH_m values of 7.9 and 8.0 respectively. These modified bases have pK_a values for the imino protons of 7.8 and 8.2, respectively. Compared to the pK_a value for the imino proton of T (9.9), this is a significant difference and the ease of formation supports the proposal that the M^{2+} are replacing the imino protons of T in M-DNA. Similarly, hypoxanthine (imino proton pK_a = 8.8) incorporation results in a pH_m of 8.1, showing a similar effect with purine bases. If both 5BrU and hypoxanthine are incorporated into the same DNA sequence, the resulting pH_m is 7.8. Not only do these results favor the hypothesis that M^{2+} is replacing the imino protons of G and T in M-DNA, they also provide a way in which to form M-DNA under less alkaline conditions. The exciting possibility of M-DNA formation *in vivo* will be discussed at greater length after the results of the current work are described.

1.4 Radiation Damage to DNA

Parts of this thesis deal with DNA damage caused by ionizing and ultraviolet (UV) radiation. Therefore, a brief overview of the effects caused by each of these radiation types will be given.

1.4.1 Ionizing Radiation

Gamma radiation is a type of ionizing radiation and causes nicking and damage to bases in DNA. These types of damage are attributable to one of two general processes (reviewed by Breen and Murphy, 1995). Absorption of ionizing radiation directly by the bases of DNA can occur. Alternatively, there can be formation of free radical species generated from water molecules that surround the DNA.

Generation of free radicals can occur in one of two ways. In the first process, radiation ionizes the water molecule to give a hydrated electron (e^-_{aq}) and $H_2O^{\bullet+}$:

$$H_2O \rightarrow H_2O^{\bullet+} + e^-_{aq} \qquad \text{(Equation 4.1).}$$

Additional reaction of the $H_2O^{\bullet+}$ species with water yields a hydroxyl radical ($^{\bullet}OH$):

$$H_2O^{\bullet+} + H_2O \rightarrow H_3O^+ + {}^{\bullet}OH \qquad \text{(Equation 4.2).}$$

And additional reaction of the solvated electron results in a hydrogen atom ($H^{\bullet}$) and a hydroxide ion (OH^-):

$$e^-_{aq} \rightarrow H^\bullet + {}^-OH \qquad \text{(Equation 4.3).}$$

In the second process, the water molecule is excited by ionizing radiation to give the excited species (H_2O^*) which undergoes homolysis to give $^\bullet OH$ and $H^\bullet$:

$$H_2O \rightarrow H_2O^* \rightarrow {}^\bullet OH + H^\bullet \qquad \text{(Equation 4.4).}$$

The free radicals that are generated by these processes react with DNA to cause damage.

Of the free radical species formed, $^\bullet OH$ is the most important and usually acts either by abstracting hydrogen atoms from the sugars of DNA or by addition to the double bonds of bases (Breen and Murphy, 1995). Although $^\bullet OH$ radicals can attack hydrogen atoms of all the sugar carbon atoms, attack at C4' is the most common, usually resulting in a single-strand break (Figure 1.14). The attack on the sugar moiety leads to release of the phosphate group either at the 3'-end or the 5'-end of the sugar. Because secondary radicals are more stable than primary radicals, release of the 3'-phosphate is most common. The positive charge thus generated is stabilized by the lone pair of electrons from the oxygen atom of the sugar ring.

Strand cleavage *via* hydrogen extraction at C1' can be enhanced under basic conditions (Figure 1.15). Oxidation of the radical results in an alkali labile hydrogen atom at C2' that results in cleavage at the 3' phosphate (Dizdaroglu *et al.*, 1977). This mechanism also results in the release of free base groups.

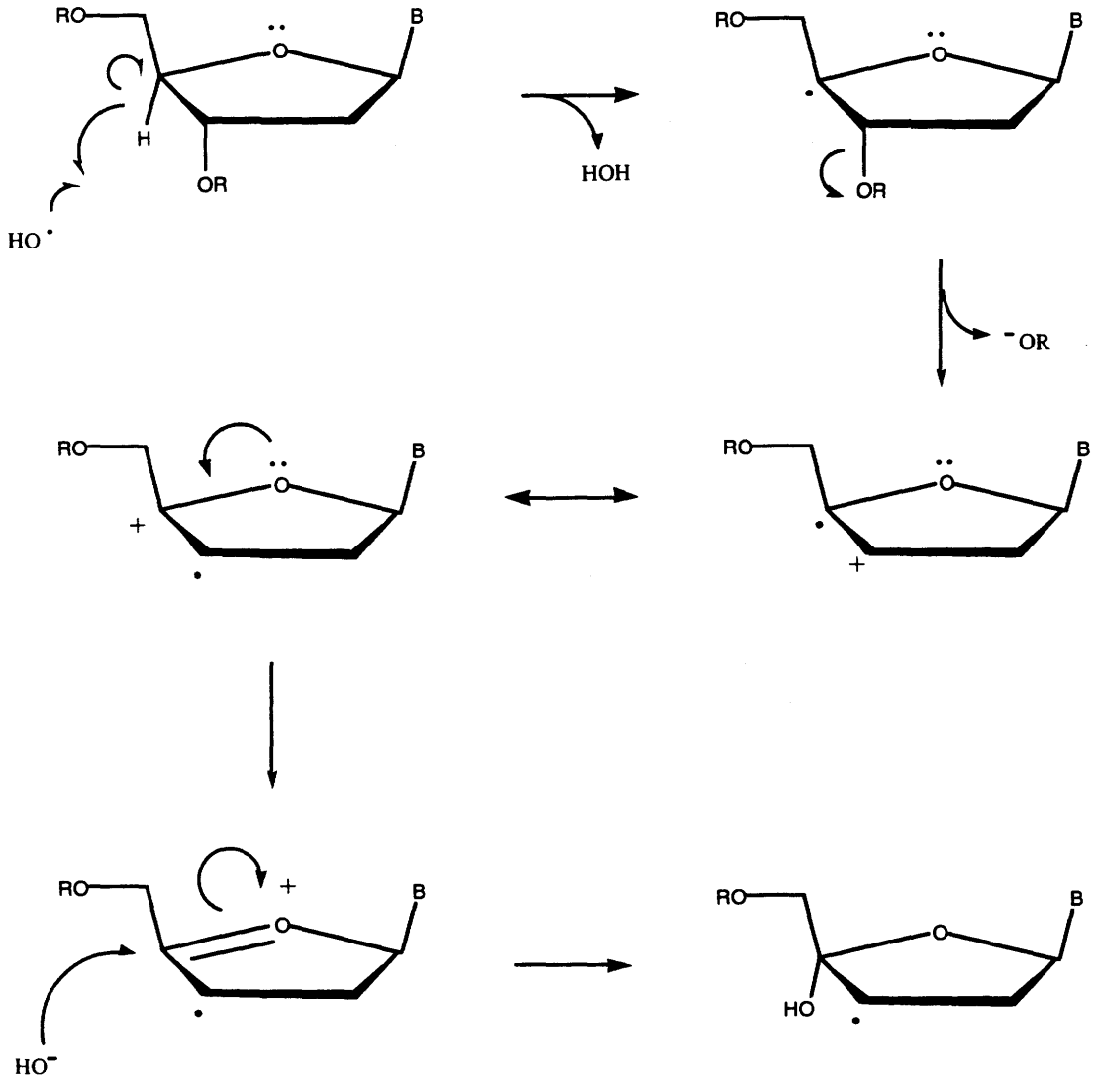

Figure 1.14. DNA strand cleavage after hydrogen abstraction at C4'. The B represents any base attached to the C1' atom of the sugar. Adapted from Breen and Murphy, 1995.

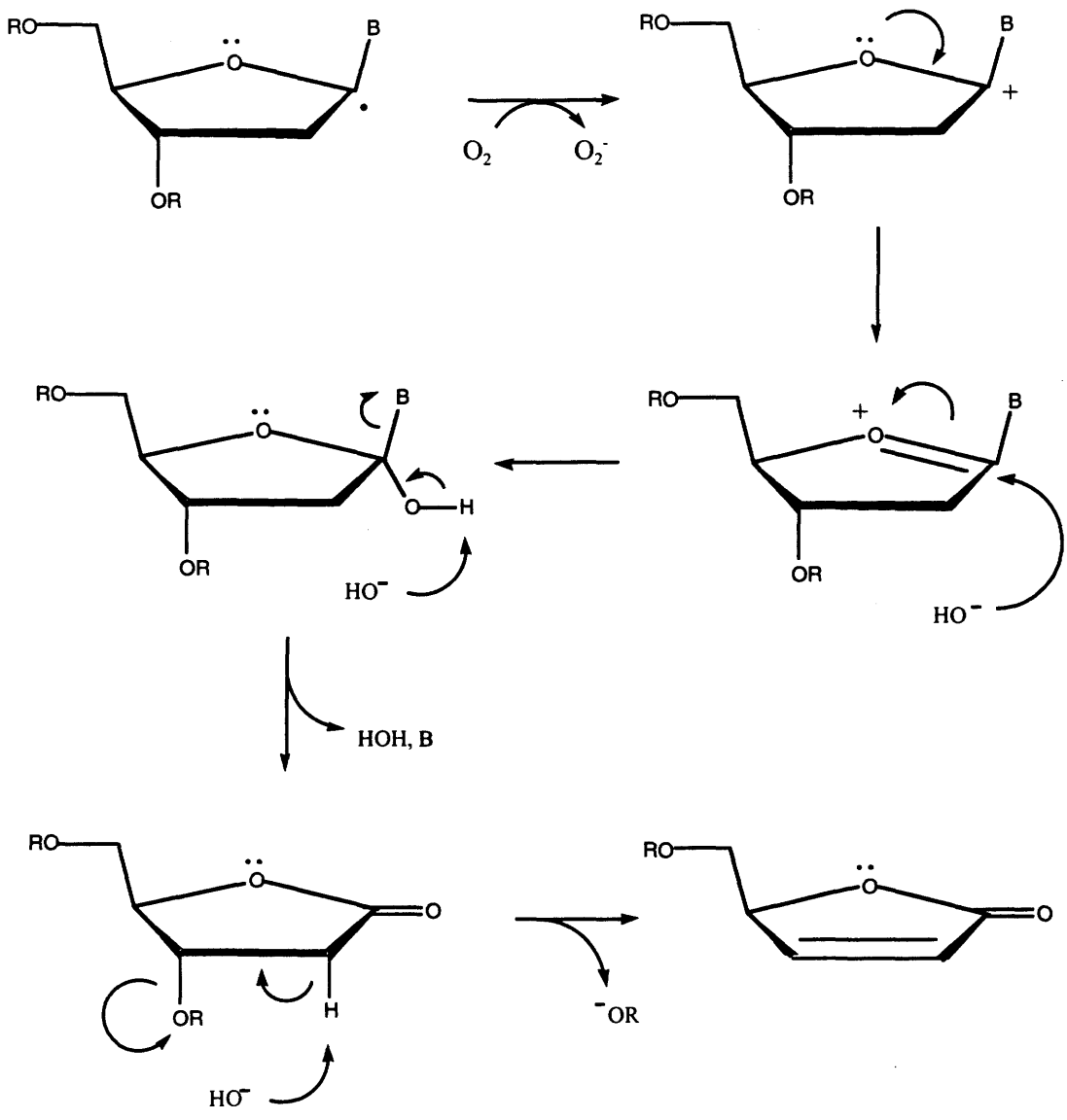

Figure 1.15. DNA strand cleavage after hydrogen abstraction at C1'. The B represents any base attached to the C1' atom of the sugar. Adapted from Breen and Murphy, 1995.

1.4.2 UV Radiation

The use of UV radiation in this work is limited to the UVC region, which occupies the electromagnetic spectrum with wavelength between 220 nm and 290 nm. UV radiation commonly results in mutagenic effects because DNA is a major cellular target (Ananthaswamy and Pierceall, 1990).

It is known that the main photoproducts of DNA irradiation by UV are cyclobutyl pyrimidine dimers and pyrimidine (6-4) pyrimidone photoproducts (Figure 1.16) (Douki and Cadet, 1995; Douki *et al.*, 1997). These generally occur between two T residues or a T and C residue that are next to each other on the same strand. Direct absorption of UV radiation by DNA can also result in strand breaks but in general the other types of damage predominate.

1.5 Justification and Objectives

This work is primarily concerned with structural aspects of Co^{2+}, Ni^{2+} and Zn^{2+} interactions with DNA. Two conformations, B-DNA and M-DNA have been explored in their interactions with these M^{2+} using various techniques. Since M-DNA has electronic and structural properties that differ from B-DNA, a different response to ionizing and UV radiation was anticipated in both cases. Further, it was predicted that a titration experiment should demonstrate that protons are released during M-DNA formation if the imino protons are being replaced by the M^{2+}. Both of these

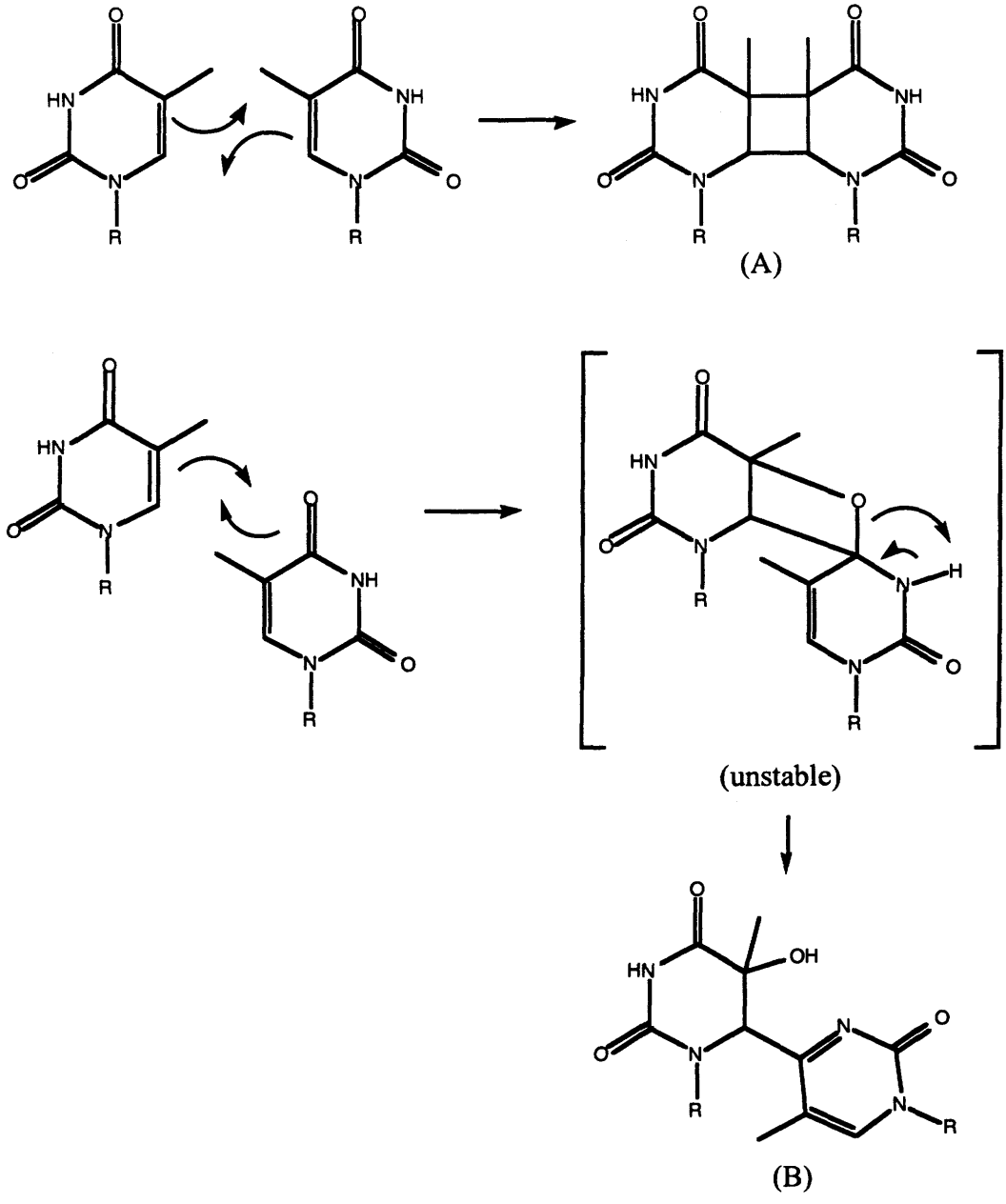

Figure 1.16. Cyclobutane dimer and pyrimidine (6-4) pyrimidone photoproducts. UV radiation induces a [2 + 2] photoreaction between the C5-C6 double bonds of neighboring T residues to form a cyclobutane dimer (A). Alternatively, a [2 + 2] photoreaction can occur between the C5-C6 double bond of one T and the carbonyl group of C4 on a neighboring T to yield a pyrimidine (6-4) pyrimidone photoproduct (B). Pyrimidine (6-4) pyrimidone photoproducts can also result between T and C residues. Adapted from Douki and Cadet, 1995.

experiments were designed to test various aspects of the proposed structural model for M-DNA.

Because there have been few x-ray crystallography studies with deoxyoligonucleotides in the presence of Co^{2+}, Ni^{2+} and Zn^{2+}, crystal structures of DNA with these M^{2+} are useful for studying their effects on DNA structure and crystal packing. Although it has been shown that these cations will not bind to N(7) positions on G residues within a B-DNA helix for the three sequences discussed in Section 1.2.4, it is of interest to see if they coordinate to the N(7) positions of G residues in other sequences. Additionally, the information gained from these structures will help develop a model for the structure of M-DNA since the manner of M^{2+} interaction with B-DNA at non-imino proton positions is expected to be similar for both conformations. One of the DNA sequences chosen for these experiments was d(GGCGCC). This sequence has been studied in the B-DNA conformation in the absence of the M^{2+} that are of interest here (Vargason *et al.*, 2000) so that a point of comparison is available.

The ultimate goal of these crystallization experiments is to elucidate a detailed structural model for the M-DNA conformation. Under alkaline conditions precipitation of $[M(OH)_2(OH_2)_4]^0$ occurs readily and many DNA sequences do not crystallize. Therefore, to improve the chances of obtaining a crystal containing M-

DNA, another sequence containing the modified base 5FU was chosen because in this case, M-DNA forms under less alkaline conditions.

2.0 MATERIALS AND METHODS

2.1 Reagents, Supplies and Equipment

Table 2.1 lists the biological reagents, chemical reagents, supplies and equipment used in the experiments described along with their commercial suppliers. Table 2.2 details the companies and their addresses. Synthetic DNA sequences not listed in the table (Lee *et al.*, 1984) and the supercoiled plasmid DNA pKHa4PU (Hampel *et al.*, 1993) were gifts from Dr. J. S. Lee.

2.2 Effects of Ionizing and UV Radiation

2.2.1 Nucleic Acid Preparation

The DNA in this set of experiments included calf thymus DNA, bacterial DNA from *E. coli*, *C. perfringens* and *M. lysodiecticus*, the synthetic DNA sequences poly[d(TG)]•poly[d(CA)], poly[d(TC)]•poly[d(GA)], poly(dG)•poly(dC) and poly(dA)•poly(dT). The supercoiled plasmid DNA pKHa4PU was also studied.

DNA was first isolated from solution by ethanol precipitation (Sambrook *et al.*, 1989) using NaCl as the monovalent cation. All DNA was stored at –20 °C in 10 mM NaCl and 10 mM N-(2-hydroxyethyl)piperazine-N'-(2 ethanesulfonic acid) (HEPES), pH 7.5, TRIS (pH 7.5) or sodium borate (pH 9.0). Before use, the calf

Table 2.1. Biological reagents, chemical reagents, supplies and equipment.

Item	Supplier
Biological reagents	
Calf thymus DNA (type I: sodium salt)	Sigma
Clostridium perfringens DNA	Sigma
Escherichia coli DNA (type VIII: sodium salt)	Sigma
Micrococcus lysodiecticus DNA	Sigma
Synthetic d[GA(5FU)(5FU)AA(5FU)C]	Alpha DNA
Synthetic d(GGCGCC)	Alpha DNA
Chemical reagents	
Aqua sil – siliconizing agent	Hampton
Boric acid	Sigma
Cobalt Chloride hexahydrate ($CoCl_2 \bullet 6H_2O$)	Sigma
di-Potassium hydrogen orthophosphate (K_2HPO_4)	BDH
Ethidium Bromide	Sigma
Ethylenediaminetetraacetic acid disodium Salt (EDTA)	BDH
Glycerol	BDH
Hydrochloric acid (HCl)	BDH
Magnesium Chloride ($MgCl_2$)	EM Science
Manganous Chloride tetrahydrate ($MnCl_2 \bullet 4H_2O$)	Fisher, BDH
(±)-2-Methyl-2,4-pentanediol (MPD)	Fluka
N-(2-hydroxyethyl)piperazine-N'-(2-ethanesulfonic acid) sodium salt (HEPES)	Sigma
Nickel Chloride hexahydrate ($NiCl_2 \bullet 6H_2O$)	Sigma
Nitrogen (liquid)	Praxair
Poly(dG)•poly(dC)	Pharmacia
Potassium Phosphate, Tribasic (K_3PO_4)	Sigma
Sodium Chloride (NaCl)	Sigma, EM Science
Sodium Hydroxide (NaOH)	BDH
Spermine Tetrahydrochloride	ICN
Tris(hydroxymethyl)aminomethane (TRIS)	Sigma
N-Tris-(hydroxymethyl)methyl-3-aminopropanesulfonic acid, sodium salt (TAPS)	ICN

Zinc Chloride ($ZnCl_2$)	Sigma, BDH

Supplies and equipment

Absorbance Spectrophotometer 260	Gilford
Accumet Basic pH Meter	Fisher
ADSC Quantum 4 CCD Detector	Area Detector Systems
Cryoloops	Hampton
Dow Corning High Vacuum Grease	VWR
30 Gauge Needles	Becton Dickinson
F-2000 Fluorescence Spectrophotometer	Hitachi
Falcon Tubes	VWR
Gammacell 220	Atomic Energy Canada
Microcentrifuge Tubes	VWR
Micro Cover Glasses (No. 1, 22 mm square)	VWR
Nikon M-35 S Camera	Nikon
Nikon SMZ-2B/SMZ-10 Microscopes	Nikon
Quartz Cuvettes	Fisher
Silicon Graphics Indigo^2 Computer	SGI
Syringes	Becton Dickinson
TMAX Film for Black-and-White Prints	Kodak
UV Stratalinker 1800	Stratagene
24-Well VDX Plates	Hampton

Table 2.2. Names and addresses of suppliers.

Company	Address
Alpha DNA	Alpha DNA, Montreal, PQ, Canada.
Area Detector Systems	Area Detector Systems Corp., Poway, CA, USA.
Atomic Energy Canada	Atomic Energy of Canada Ltd., Mississauga, ON, Canada.
BDH	British Drug House, Saskatoon, SK, Canada.
Becton Dickinson	Becton Dickinson and Co., Franklin Lakes, NJ, USA.
EM Science	EM Science, Gibbstown, NJ, USA.
Fisher	Fisher Scientific, Winnipeg, MB, Canada.
Fluka	Sigma-Aldrich Canada Ltd., Oakville, ON, Canada.
Gilford	Gilford Instrument Laboratories Inc., Oberlin, OH, USA.
Hampton	Hampton Research, Laguna Niguel, CA, USA.
Hitachi	Hitachi Ltd., Tokyo, Japan
ICN	ICN Biomedical Canada Ltd., Saint Laurent, PQ, Canada.
Kodak	Eastman Kodak Company, Rochester, NY, USA.
Nikon	Nikon Corporation, Japan.
Pharmacia	Pharmacia Biotech Inc., Baie d'Urfe, PQ, Canada.
Praxair	Praxair, Saskatoon, SK, Canada.
SGI	Silicon Graphics Inc., Mountain View, CA, USA.
Sigma	Sigma Chemical Co., Saint Louis, MO, USA.
Stratagene	Stratagene, La Jolla, CA, USA.
VWR	VWR, Mississauga, ON, Canada.

thymus, bacterial and synthetic DNA sequences (but not the plasmid DNA) were sheared by passing through one-half inch 30 gauge needles five times in order to obtain fragments of uniform length (Pyeritz *et al.*, 1972). During this procedure, maximum thumb pressure was used to pass the DNA solution through the needle from a syringe.

2.2.2 Sample Preparation

The samples for these experiments were prepared as described here unless otherwise stated. For γ-irradiation experiments: 40 mM HEPES buffer (pH 7.5) or boric acid buffer (pH 9.0), 40 μM in base-pairs of DNA, 400 μM of M^{2+} chloride and 10 mM NaCl. For UV radiation experiments, conditions were the same except that TRIS buffer (pH 7.5) was used instead of HEPES. For γ-irradiations, the solutions were prepared and 20 μL aliquots for each time interval were transferred to 0.5 mL microcentrifuge tubes before exposure. In the case of UV irradiations the samples were prepared then transferred to 1 mL quartz cuvettes covered with thin plastic wrap to prevent evaporation during exposure. The DNA concentration was estimated from the absorbance at 260 nm with an extinction coefficient of 6600 cm^{-1} M^{-1}. Thus, 1.0 A_{260} is equivalent to 0.075 mM in base-pairs of DNA.

2.2.3 Radiation Exposure

Samples were γ-irradiated using a ^{60}Co source with an approximate dose rate of 1440 rad min^{-1}. A UV Stratalinker was used for UV exposure and contained five 8 W germicidal bulbs having a peak irradiance of 254 nm. In this case, a 20 μL sample was removed from the quartz cuvettes after each time interval. Following exposure, 2 μL of 200 mM EDTA, pH 8.0 was added to each 20 μL sample to remove the M^{2+} from their interactions with DNA.

2.2.4 Ethidium Fluorescence Assay

An alkaline ethidium fluorescence assay was used to investigate the induction of nicks and interstrand crosslinks in DNA upon exposure to radiation (Morgan *et al.*, 1979b). Aliquots of 18 μL, taken from the irradiated samples containing EDTA, were read in 2 mL of "pH 12 ethidium assay buffer" (0.5 μg mL^{-1} ethidium bromide, 20 mM potassium phosphate buffer, pH 11.8, and 0.5 mM EDTA) at an excitation wavelength of 525 nm and an emission wavelength of 600 nm in a fluorescence spectrophotometer. The pH of the ethidium assay buffer was adjusted with small amounts of alkali for different types of DNA since sequences with higher G•C content required more alkaline conditions for strand separation to occur on heating. Appropriate pH values were found by trial and error such that linear DNA gave a good fluorescence reading but denatured DNA would not. Calf thymus, *E. coli* and *C.*

perfringens DNA were analyzed at pH 11.8, while *M. lysodiecticus* DNA was analyzed at pH 12.2. The synthetic DNA sequences were analyzed at pH 11.9, except for poly(dG)•poly(dC) which was at pH 12.1 and poly(dA)•poly(dT) for which the assay buffer was pH 8 (5 mM TRIS-HCl, 0.5 μg mL^{-1} ethidium bromide and 0.5 mM EDTA).

The fluorescence values of the "before-heat" samples were recorded and the samples heated in a boiling water bath for 2 minutes followed by immersion in a room temperature water bath for at least 2 minutes. Fluorescence readings of the resulting samples gave the "after-heat" results. All results reported represent the mean of two independent experiments.

2.3 Proton Release During M-DNA Formation

2.3.1 Nucleic Acid Preparation

Calf thymus DNA was prepared by dissolving in water. Because of the high concentration of DNA, this did not result in denaturation as was evident from the observed ethidium fluorescence. The DNA was sheared using the same method described in Section 2.2.1.

2.3.2 Titration

Experiments were performed in a 10 mL glass beaker with calf thymus DNA. The titration was performed by adjusting the pH to the appropriate value with KOH then adding aliquots (4 μL) of 0.1 mM $NiCl_2$. Under conditions that favored M-DNA formation, a drop in pH was observed and this was adjusted back to the pH of the experiment by addition of KOH. After equilibration at each point for at least one minute, the amount of M-DNA was estimated by removal of a small aliquot (2 μL). Aliquots were added to 2 mL of the ethidium fluorescence assay buffer containing 5 mM TRIS-HCl, pH 8.0, 200 μM $ZnCl_2$ and 0.5 μg mL^{-1} ethidium bromide (Lee *et al.*, 1993). The experiment was terminated after precipitation was observed which happened at high concentrations of M^{2+}.

2.4 Crystal Structures of DNA-M^{2+} Complexes

2.4.1 Crystallization of Oligonucleotide-M^{2+} Complexes

Crystallization experiments were performed with various deoxyoligonucleotide sequences including d(GGCGCC), d[GA(5FU)(5FU)-AA(5FU)C], d[GG(5FU)ACC], d[GG(5BrU)ACC], d[A(5BrU)(5BrU)AA(5BrU)], d(GGCTAGCC) and d(CGTGTGCACACG). Additionally, two sequences containing inosine (I), the nucleoside of hypoxanthine, were tried: d[I(5BrU)A(5BrU)AC] and d(IICICC). All of these self-complementary deoxyoligonucleotides were synthesized

using the phosphoramidite method (Caruthers *et al.*, 1992) and purified using trityl-on reversed phase high performance liquid chromatography (Brown and Brown, 1992), followed by removal of the dimethoxytrityl groups and desalting by ethanol precipitation. These procedures were performed by the supplier. Once received, samples were dissolved in distilled autoclaved water and stored at –20 °C until use. All other chemical solutions were stored at 4 °C in plastic Falcon tubes and allowed to equilibrate to room temperature before setup of crystallization experiments for at least one-half hour.

Crystals were grown by vapour diffusion from hanging drops. Briefly, drops of volume 2-6 μL were placed on square glass microscope cover slips which had been treated with Aqua sil, a siliconizing agent that helps keep drops compact and uniform in size by providing a hydrophobic water repellent surface. Treatment of the cover slips involved rinsing them in the Aqua sil solution according to the manufacturer's directions followed by rinsing in distilled water and standing them to dry at room temperature for 24 hours. Once drops were placed on these cover slips, they were placed over reservoirs of a 24-well plate containing the reservoir solutions and sealed with vacuum grease. The reservoir solutions contained higher concentrations of 2-methyl-2,4-pentanediol (MPD) than the drops. MPD is a precipitant commonly used in crystallizing DNA oligonucleotides (Dock-Bregeon *et al.*, 1999). Slow equilibration allowed crystallization of the DNA-metal complexes because the

concentration of MPD in the drops increased as water diffused from the drop solutions to the reservoir solutions. All of the crystallization experiments were set up at room temperature and crystallization was allowed to proceed either at room temperature or at 4 °C. Observation of crystal growth was through an optical microscope and pictures were recorded using a camera mounted on the microscope.

Two of the sequences yielded crystals: d(GGCGCC) and d[GA(5FU)-(5FU)AA(5FU)C].

2.4.1.1 d(GGCGCC)-M^{2+} Complexes

Crystals of this sequence were grown from a modification of the protocol used by Vargason *et al.* (2000) but without the addition of spermine and changing the buffer from sodium cacodylate (pH 6) to N-Tris-[hydroxymethyl]methyl-3-aminopropanesulfonate (TAPS) so that a higher pH could be maintained. $MgCl_2$ was replaced by $CoCl_2$, $NiCl_2$ or $ZnCl_2$. Screening many conditions led to optimized conditions for growth of these crystals. Large crystals with little or no precipitate present in the drops at as high a pH as possible was selected for.

The Co^{2+} complex crystal was grown at room temperature in a 6 µL drop containing 2.0 mM hexamer, 50 mM TAPS-HCl (pH 8.1), 25 mM $CoCl_2$ and 2% (v/v) glycerol equilibrated against a 1 mL reservoir containing 50 mM TAPS-HCl (pH 8.1), 25 mM $CoCl_2$ and 20% (v/v) MPD. The Ni^{2+} complex crystal was grown at

4 °C in a 3 μL drop containing 2.0 mM hexamer, 40 mM TAPS-HCl (pH 8.0), 3.75 mM $NiCl_2$ and 10% (v/v) MPD equilibrated against a 0.4 mL reservoir containing 40 mM TAPS-HCl (pH 8.0), 3.75 mM $NiCl_2$ and 35% (v/v) MPD. The Zn^{2+} complex crystal was grown at 4 °C in a 2 μL drop containing 2.0 mM hexamer, 25 mM TAPS-HCl (pH 8.0), 2.25 mM $ZnCl_2$ and 1% (v/v) MPD equilibrated against a 0.4 mL reservoir containing 40 mM TAPS-HCl (pH 8.0), 2.25 mM $ZnCl_2$ and 30% (v/v) MPD. In some cases, $MgCl_2$ was added and an effect was observed on the crystal morphology. In these cases, the amounts are described in the appropriate result section and the same amount of the metal would have been added to both the drop and the reservoir.

2.4.1.2 d[GA(5FU)(5FU)AA(5FU)C]-Co^{2+} Complex

The conditions for growing crystals for this complex were elucidated by trial and error. The Co^{2+} complex was crystallized at 4 °C in a 2 μL drop containing 0.75 mM octamer, 40 mM TAPS-HCl (pH 8.5), 3 mM $CoCl_2$, 5% (v/v) MPD, 2% (v/v) glycerol and 2 mM spermine equilibrated against a 0.4 mL reservoir consisting of 40 mM TAPS-HCl (pH 8.5), 3 mM $CoCl_2$, 2% glycerol and 40% MPD.

2.4.2 Cryoprotection of Crystal Samples

Cryoprotectant solutions were made containing the components of the drops without DNA but with increased concentrations of MPD. MPD concentrations of 50%, 55%, 60% and 65% (v/v) were tried and in each case 55% yielded the best results. The temperatures of these solutions were brought to the same as that of the crystal growing conditions for each sample. Under a microscope, approximately 5 to 10 μL of the cryoprotectant solution was added to the drop containing the crystal of interest. After about 20 to 30 seconds, the crystal was transferred to another drop of pure cryoprotectant solution, mounted on a loop of the appropriate size then immediately submerged in liquid nitrogen. Crystals were stored on their loops under liquid nitrogen and transferred to the synchrotron radiation source in a dry shipper.

2.4.3 Data Collection and Processing

X-ray data were collected at BioCARS beamline 14-BMD of the Advanced Photon Source at Argonne National Laboratory (Argonne, IL, USA). Samples were placed in a nitrogen stream at a temperature of 110 K. Single crystal data were collected on a CCD detector with a 1° rotation about the omega axis per image. For the Co^{2+} complex, 180 images were collected. For the Ni^{2+} and Zn^{2+} samples, an additional 50 images were collected after rotating the kappa angle 45°. Data were

indexed, merged and scaled using the HKL package (Otwinowski and Minor, 1997). Data collection and processing parameters are given in Table 2.3.

2.4.4 Solution and Refinement of Structures

2.4.4.1 Initial Model

It was apparent that the d(GGCGCC)-M^{2+} complexes crystallized in a B-like conformation because strong stacking reflections were observed on the collected frames. These were present at approximately 3.4 Å resolution (see Section 3.4.3). The unit cell parameters were similar to those that were observed for a similar B-DNA structure (Nucleic Acid Database entry BD0040) of the same sequence in the absence of bound metal ions which had the same space group (Vargason *et al.*, 2000). This structure minus the spermine and water molecules was used as a starting model for refinement of all three structures described. The numbering of the residues was changed as follows: residues 7 to 12 were changed to residues 25 to 30, residues 13 to 18 were changed to residues 19 to 24, residues 19 to 24 were changed to residues 7 to 12 and residues 25 to 30 were changed to residues 13 to 18. The chain identifiers were changed accordingly such that residues 1 to 6 constituted chain A, residues 7 to 12 chain B, residues 13 to 18 chain C, residues 19 to 24 chain D and residues 25 to 30 chain E.

Table 2.3. Data collection and processing parameters.

Parameter	Complex Co^{2+}	Ni^{2+}	Zn^{2+}
Crystal to detector distance (mm)	120	110	110
X-ray wavelength (Å)	1.5088	0.9000	0.9000
Total reflections collected	138,163	180,742	133,922
Unique reflections	2731	3217	3115
Resolution range (Å)	100-3.0	50-2.9	50-2.9
Redundancy (outer shell)	5.9 (3.8)	8.9 (4.9)	7.2 (4.2)
R_{sym} (outer shell)	0.11(0.51)	0.09 (0.60)	0.11 (0.60)
Completeness (%) (outer shell)	94.8 (69.9)	96.9 (80.6)	97.5 (87.7)
Mosaicity (°)	0.84	0.58	0.53
I/σI (outer shell)	22.3 (1.0)	22.0 (1.8)	17.8 (1.8)
B-value from Wilson plot ($Å^2$)	20.8	47.9	42.4

2.4.4.2 Refinement Procedure

Refinement and map generation was carried out using the program X-PLOR version 3.851 (Brünger, 1992) using the nucleic acid specific parameter files that treat all hydrogen atoms explicitly (Nilsson and Karplus, 1986). Non-standard topology and parameter files for the metal ions and their associated water molecules as well as patch files for the metal N(7) interactions were manually written. In general, standard atomic masses and bond lengths from the International Tables for X-ray Crystallography (The International Union of Crystallography, 1968) were used. The topology input files are reproduced in Table 2.4, the parameter input files in Table 2.5 and the patch topology and parameter input files in Tables 2.6 and 2.7, respectively. Visualization of maps was with TURBO-FRODO (Roussel and Cambillau, 1992) and preparation of images was with Setor (Evans, 1993).

Overall, nine refinement steps were performed. In general, for each step the ideal weight for the x-ray term was calculated using the "check" procedure. This was followed by a "prepstage" of 200 cycles of conjugate gradient minimization and simulated annealing or positional refinement. The final stage of each refinement step was a B-factor refinement *via* conjugate gradient minimization methods for 20 steps. B-factors were refined by groups with a B_{min} limit of 10 because the B-factors were tending to fall unreasonably low for some of the base groups.

Table 2.4. X-PLOR topology input files for the M^{2+}-water complexes*.

```
REMARK  topology for zinc
REMARK  written November 2002    Shaun Labiuk

MASS TT          65.37      {atomic weight of Zn2+ (g mol-1)}
MASS O_2         15.99900   {atomic weight of water oxygen atom
MASS O_3         15.99900   (g mol-1)}
MASS O_4         15.99900
MASS O_5         15.99900
MASS O_6         15.99900
MASS HT           1.00800   {atomic weight of water hydrogen atom
                            (g mol-1)}
AUTOGENERATE ANGLES=TRUE END
!---------------------------------------------------------------
                            {defines the atoms of the M2+-
RESIdue TTT                  water complex}
 GROUp
  ATOM TT        TYPE=TT    CHARGE= 2.000   END
  ATOM OWA       TYPE=O_2   CHARGE=-0.834   END
  ATOM OWB       TYPE=O_3   CHARGE=-0.834   END
  ATOM OWC       TYPE=O_4   CHARGE=-0.834   END
  ATOM OWD       TYPE=O_5   CHARGE=-0.834   END
  ATOM OWE       TYPE=O_6   CHARGE=-0.834   END
  ATOM H1        TYPE=HT    CHARGE= 0.417   END
  ATOM H2        TYPE=HT    CHARGE= 0.417   END
  ATOM H3        TYPE=HT    CHARGE= 0.417   END
  ATOM H4        TYPE=HT    CHARGE= 0.417   END
  ATOM H5        TYPE=HT    CHARGE= 0.417   END
  ATOM H6        TYPE=HT    CHARGE= 0.417   END
  ATOM H7        TYPE=HT    CHARGE= 0.417   END
  ATOM H8        TYPE=HT    CHARGE= 0.417   END
  ATOM H9        TYPE=HT    CHARGE= 0.417   END
  ATOM H10       TYPE=HT    CHARGE= 0.417   END

BOND OWA TT                  {defines each of the M2+-
BOND OWB TT                  water oxygen bonds}
BOND OWC TT
BOND OWD TT
```

```
BOND OWE TT
BOND OWA H1                    {defines the oxygen-hydrogen
BOND OWA H2                    bonds for each water molecule
BOND OWB H3                    A, B, C, D and E}
BOND OWB H4
BOND OWC H5
BOND OWC H6
BOND OWD H7
BOND OWD H8
BOND OWE H9
BOND OWE H10

IMPROPER TT OWA OWB OWC

ACCEPTOR OWA TT
ACCEPTOR OWB TT
ACCEPTOR OWC TT
ACCEPTOR OWD TT
ACCEPTOR OWE TT

END {* TTT *}
```

---

* For Co^{2+} and Ni^{2+}, the value for MASS TT was replaced with 58.933 and 58.69 respectively. Descriptive comments are in bold rounded brackets.

Table 2.5. X-PLOR parameter input files for the M^{2+}-water complexes*.

```
REMARK  parameters for zinc
REMARK  written November 2002  Shaun Labiuk

BOND O_2 TT 450.0 2.10          {describe the restraint weights along
BOND O_3 TT 450.0 2.10          with the bond lengths (Å) for each bond}
BOND O_4 TT 450.0 2.10
BOND O_5 TT 450.0 2.10
BOND O_6 TT 450.0 2.10
BOND HT O_2 450.0 0.9572
BOND HT O_3 450.0 0.9572
BOND HT O_4 450.0 0.9572
BOND HT O_5 450.0 0.9572
BOND HT O_6 450.0 0.9572
BOND HT HT 0.0 1.5139

ANGLE O_2 TT O_3 55.0 90        {describe the restraint weights along
ANGLE O_2 TT O_4 55.0 180       with the bond angles (°) for each bond
ANGLE O_2 TT O_5 55.0 90        angle}
ANGLE O_2 TT O_6 55.0 90
ANGLE O_3 TT O_4 55.0 90        {idealized octahedral geometry is
ANGLE O_3 TT O_5 55.0 180       imposed}
ANGLE O_3 TT O_6 55.0 90
ANGLE O_4 TT O_5 55.0 90
ANGLE O_4 TT O_6 55.0 90
ANGLE O_5 TT O_6 55.0 90
ANGLE HT O_2 HT 55.0 104.52
ANGLE HT O_3 HT 55.0 104.52
ANGLE HT O_4 HT 55.0 104.52
ANGLE HT O_5 HT 55.0 104.52
ANGLE HT O_6 HT 55.0 104.52
ANGLE TT O_2 HT 55.0 109.5
ANGLE TT O_3 HT 55.0 109.5
ANGLE TT O_4 HT 55.0 109.5
ANGLE TT O_5 HT 55.0 109.5
ANGLE TT O_6 HT 55.0 109.5

IMPROPER TT O_2 O_3 O_4 750.0 0 0.000
```

NONBONDED TT 0.01 1.568 0.01 1.568	**{describe bonding**
NONBONDED O_2 0.1591 2.8509 0.1591 2.8509	**parameters for interactions**
NONBONDED O_3 0.1591 2.8509 0.1591 2.8509	**not fully described**
NONBONDED O_4 0.1591 2.8509 0.1591 2.8509	**by the restraints above}**
NONBONDED O_5 0.1591 2.8509 0.1591 2.8509	
NONBONDED O_6 0.1591 2.8509 0.1591 2.8509	
NONBONDED HT 0.0498 1.4254 0.0498 1.4254	

---

* For Co^{2+} and Ni^{2+}, the value for the water oxygen-M^{2+} distance (BOND O_2 TT) was replaced with 2.13 and 2.085 respectively. The values for NONBONDED were taken from standard X-PLOR input files. Descriptive comments are in bold rounded brackets.

Table 2.6. X-PLOR topology input files for the M^{2+}-N(7) patch*.

```
REMARK  topology for zinc patch
REMARK  written November 2002  Shaun Labiuk

 presidue LIG
  group
   modify atom 1N7  type=NB  charge=-0.250   END     {defines the atoms
   modify atom 1C5  type=CB  charge= 0.020   END     whose parameters will
   modify atom 1C8  type=CE  charge= 0.195   END     be directly affected by
  group                                              coordination with M2+}
   modify atom 2N7  type=NB  charge=-0.250   END
   modify atom 2C5  type=CB  charge= 0.020   END
   modify atom 2C8  type=CE  charge= 0.195   END
  group
   modify atom 3N7  type=NB  charge=-0.250   END
   modify atom 3C5  type=CB  charge= 0.020   END
   modify atom 3C8  type=CE  charge= 0.195   END
  group
   modify atom 4N7  type=NB  charge=-0.250   END
   modify atom 4C5  type=CB  charge= 0.020   END
   modify atom 4C8  type=CE  charge= 0.195   END
group
   modify atom 5N7  type=NB  charge=-0.250   END
   modify atom 5C5  type=CB  charge= 0.020   END
   modify atom 5C8  type=CE  charge= 0.195   END

  add bond 1N7 6TT                                   {bonds between
  add bond 2N7 7TT                                   M2+ and the N(7)
  add bond 3N7 8TT                                   of bases are added}
  add bond 4N7 9TT
  add bond 5N7 aTT

  add angle 1C5 1N7 6TT     add angle 2C5 2N7 7TT    {all of the affected
  add angle 3C5 3N7 8TT     add angle 4C5 4N7 9TT    angles are described}
  add angle 5C5 5N7 aTT
```

```
add angle 1C8 1N7 6TT      add angle 2C8 2N7 7TT
add angle 3C8 3N7 8TT      add angle 4C8 4N7 9TT
add angle 5C8 5N7 aTT

add angle 1N7 6TT 6OWA     add angle 2N7 7TT 7OWA
add angle 3N7 8TT 8OWA     add angle 4N7 9TT 9OWA
add angle 5N7 aTT aOWA

add angle 1N7 6TT 6OWB     add angle 2N7 7TT 7OWB
add angle 3N7 8TT 8OWB     add angle 4N7 9TT 9OWB
add angle 5N7 aTT aOWB

add angle 1N7 6TT 6OWC     add angle 2N7 7TT 7OWC
add angle 3N7 8TT 8OWC     add angle 4N7 9TT 9OWC
add angle 5N7 aTT aOWC

add angle 1N7 6TT 6OWD     add angle 2N7 7TT 7OWD
add angle 3N7 8TT 8OWD     add angle 4N7 9TT 9OWD
add angle 5N7 aTT aOWD

add angle 1N7 6TT 6OWE     add angle 2N7 7TT 7OWE
add angle 3N7 8TT 8OWE     add angle 4N7 9TT 9OWE
add angle 5N7 aTT aOWE

END
```

---

* This file is the same for Co^{2+} and Ni^{2+}. Descriptive comments are in bold rounded brackets.

Table 2.7. X-PLOR parameter input files for the M^{2+}-N(7) patch*.

REMARK parameters for zinc patch	
REMARK written November 2002 Shaun Labiuk	
bonds NB TT 600.0 2.1	**{describes the restraint weights along with the bond lengths (Å) for the base N(7)-metal bonds}**
angles CB NB TT 50.0 120	
angles CE NB TT 50.0 120	
angles NB TT O_2 700 90	**{describe the restraint weights along with the bond angles (°) for each bond angle}**
angles NB TT O_3 700 90	
angles NB TT O_4 700 90	
angles NB TT O_5 700 90	
angles NB TT O_6 700 180	

* For Co^{2+}, the value for the guanine N(7)-metal distance (bonds NB TT) was replaced with 2.13. Descriptive comments are in bold rounded brackets.

The diffraction data were first separated into a working set containing approximately 90% of the reflections and a reference set with approximately 10%. Step one was a rigid body refinement, the groups being two duplexes and one single strand. It was necessary to increase the number of cycles to 150 for convergence indicating a substantial difference between the placement of the helices within the unit cell between the model structure and the metal complex structures. This was followed by 150 cycles of rigid body refinement with each single strand of DNA being considered a group (step two).

Step three consisted of a simulated annealing protocol. Here, B-DNA restraints for base planarity, sugar pucker and Watson-Crick hydrogen bonding were imposed. The annealing procedure consisted of a slowcooling stage with an initial temperature of 2000 K and decreasing to 300 K over steps of 50 K. This was followed by 120 cycles of conjugate gradient energy minimization.

Inspection of both SIGMAA weighted F_O-F_C and $2F_O$-F_C electron density maps showed large spherical regions of density adjacent to the N(7) positions of each of the five terminal G residues. The distance between the N(7) atom of each of the concerned G residues and the center of the spherical region was reasonable for a nitrogen-metal ion interaction. For step four of refinement, a Co^{2+}, Ni^{2+} or Zn^{2+} cation was placed in the center of each spherical region, depending on the complex. This was followed by energy minimization of the model that included the M^{2+}. The

resulting difference electron density maps showed extra densities around metal ions. This was interpreted to be due to water atoms in the metals' coordination spheres. Because of the limited resolution of the data, it was not possible to determine the placement of water molecules and octahedral coordination for the metal atoms was assumed. Step five involved placing five water molecules around each M^{2+} with idealized octahedral geometry followed by energy minimization and B-group refinement with the hydration shell considered as a group.

Step six was a fitting round followed by positional refinement. This and all further steps imposed resolution-dependent weighting and a bulk solvent correction. In step seven, another fitting round was performed followed by energy minimization. Steps eight and nine were energy minimization steps without Watson-Crick hydrogen bonding restraints. It was not deemed justifiable to add additional water molecules due to the low resolution of the data.

After completion of each structure, the metal sites were verified by removing them (and their associated water molecules) then running a simulated annealing protocol imposing a bulk solvent correction followed by B-group refinement. The annealing procedure consisted of a slowcooling stage with an initial temperature of 500 K, decreasing to 300 K over steps of 50 K, followed by 120 cycles of conjugate gradient energy minimization. An increase in R-factor and strong density in both F_O-F_C and $2F_O$-F_C maps indicated a correct placement of the original M^{2+}.

2.4.5 Structure Analysis

After the structures had been refined, the coordinates for each double helix consisting of six base-pairs were isolated. Because there are two and one half duplexes per asymmetric unit, base-pair and base-pair step parameters were calculated for three duplexes of each complex separately (two duplexes plus the single strand with its symmetry mate) then averaged. Helical parameters were calculated using FREEHELIX98 (Dickerson, 1998).

3.0 RESULTS

3.1 Effects of Ionizing Radiation on DNA with M^{2+}

To investigate the responses of B-DNA and M-DNA to ionizing radiation, DNA was exposed to γ-radiation at pH 7.5 or 9.0 in the presence of Co^{2+}, Ni^{2+} or Zn^{2+}. At pH 9.0, these samples have the M-DNA conformation but at pH 7.5 they remain in the B-DNA conformation. Additionally, Mg^{2+} and Mn^{2+} were used as controls because neither promote the M-DNA conformation at either pH. An additional control was exposure without any M^{2+} present. Damage was estimated from changes in ethidium fluorescence assays (Morgan *et al.*, 1979b).

Normally, the fluorescence of bound ethidium is proportional to the concentration of duplex DNA because ethidium does not bind to single-stranded regions. Similarly ethidium does not bind to pyrimidine dimers or hydrated bases so that a loss of fluorescence can be correlated with DNA damage (Prütz, 1996). Crosslinking of DNA can also be included under this category of "general DNA damage" since if many crosslinks are present, the topology of the DNA might be restrained in such a way that ethidium binding is inhibited. However, crosslinking of the DNA duplex can be measured after a heating and cooling step performed at pH 12. Upon heating, the duplex denatures and on cooling at this high pH no duplex

reforms so that all of the ethidium fluorescence is lost. However, if a crosslink is present, it acts as a nucleation site to overcome the repulsion between strands and the duplex will re-anneal on cooling resulting in a complete return of fluorescence.

Finally, DNA strand breaks can be assayed with covalently closed circular plasmid DNA. Upon heating at pH 12 the two strands normally cannot separate so that the fluorescence returns on cooling. However, if a strand break occurs two effects are observed. First, the fluorescence before heating increases by as much as 40% because an open circular DNA can bind more ethidium than a topologically constrained circular DNA. Second, the fluorescence after heating and cooling is eliminated since even one strand break is sufficient to allow strand separation. All of these assays can also be used to assess damage to M-DNA as long as the measurements are performed after conversion to B-DNA by the addition of EDTA.

Results for this section will be presented under the subheadings of supercoiled plasmid DNA, calf thymus DNA, microbial and synthetic DNA followed by the effects of a free radical scavenger and EDTA.

3.1.1 Supercoiled Plasmid DNA

For plasmid DNA at pH 7.5 the fluorescence before heating increased with dose of ionizing radiation for all of the samples (Figure 3.1). Before any irradiation, the after-heat fluorescence was less than the before-heat fluorescence. This means

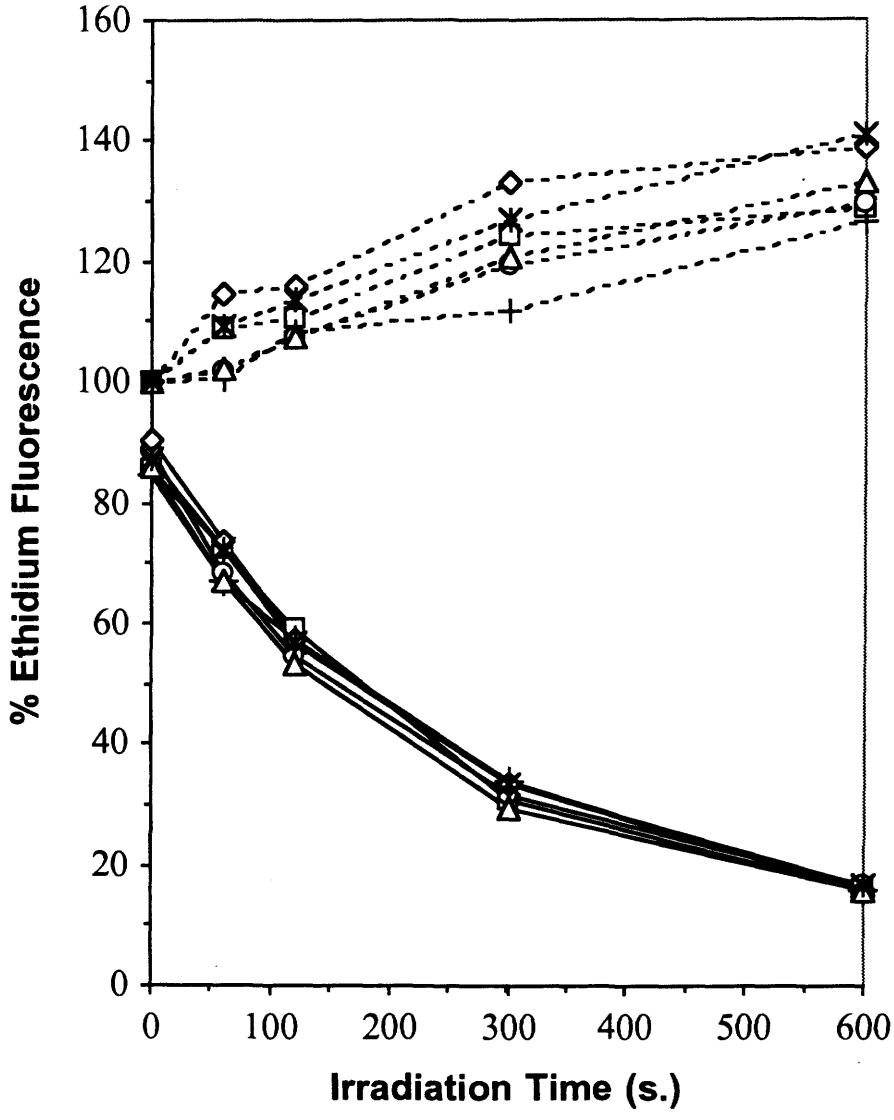

Figure 3.1. Gamma irradiation of plasmid DNA at pH 7.5 in the presence of M^{2+}. Samples contained Co^{2+} (diamonds), Ni^{2+} (circles), Zn^{2+} (triangles), Mg^{2+} (squares), Mn^{2+} (crosses) or no M^{2+} (stars). Dashed lines represent before-heat readings and solid lines represent after-heat readings.

that some of the plasmid DNA was already in the open circular form. The increase in before-heat fluorescence can be attributed to nicking of the DNA since the open circular form of the plasmid binds more ethidium. This interpretation was confirmed by the after-heat measurements since in this case nicking leads to loss of fluorescence. As can be seen on Figure 3.1, the results were almost identical in the presence of all of the M^{2+} and these in turn were virtually identical to the results with no M^{2+} present.

The results at pH 9.0 were slightly more complex (Figure 3.2). For all of the samples, the rate of nicking was more rapid than at pH 7.5 because the before-heat fluorescence increased more rapidly. Also, except in the case of Co^{2+}, there was a corresponding faster decrease in the fluorescence after heat at pH 9.0. After the initial rapid increase in the before-heat fluorescence there was generally a slow decrease with increasing exposure time. This may be attributed to general DNA damage. In the presence of Co^{2+} at pH 9.0 under M-DNA conditions, the after-heat fluorescence returned to near maximal values throughout the experiment, indicating crosslink formation even at short exposure times. That this effect was due to crosslink formation was verified making use of calf thymus DNA.

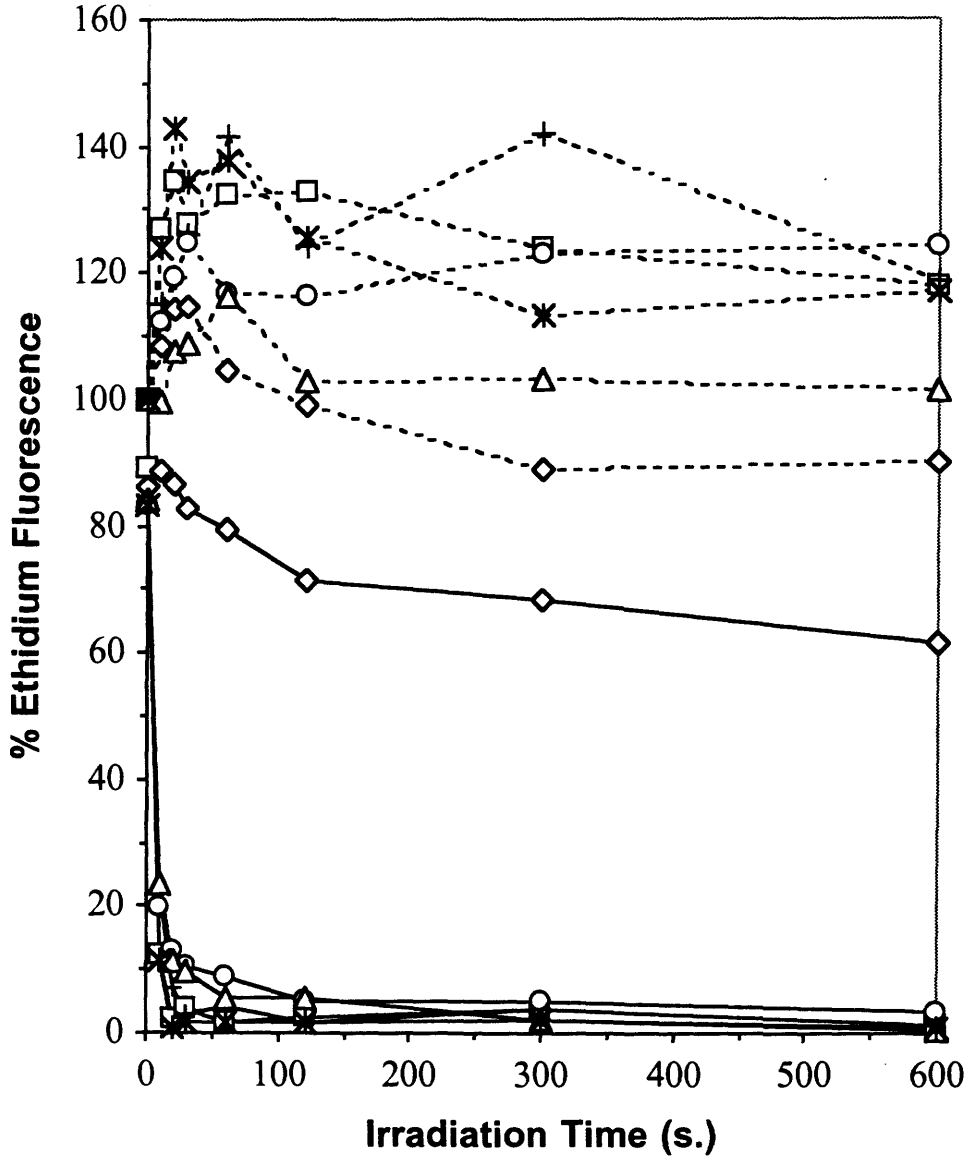

Figure 3.2. Gamma irradiation of plasmid DNA at pH 9.0 in the presence of M^{2+}. Samples contained Co^{2+} (diamonds), Ni^{2+} (circles), Zn^{2+} (triangles), Mg^{2+} (squares), Mn^{2+} (crosses) or no M^{2+} (stars). Dashed lines represent before-heat readings and solid lines represent after-heat readings.

3.1.2 Calf Thymus DNA

For calf thymus DNA at pH 7.5 (Figure 3.3) there was no loss of fluorescence with increasing dose demonstrating that overall damage that would prevent ethidium binding to the DNA was minimal. Similarly there was no increase in fluorescence after heating and cooling showing that no crosslinks were being formed under any of the conditions tested. As in the case of the plasmid DNA at pH 7.5, all of the results were virtually identical.

For calf thymus DNA at pH 9.0 (Figure 3.4) the pattern again became more complex. The general trend was a decrease in the before-heat fluorescence with increasing dose so that damage was being inflicted on the DNA that prevented ethidium from binding. This was less apparent in the samples containing Mn^{2+} and Ni^{2+} but was nevertheless still present. No crosslinking occurred in any of the samples except with Co^{2+} because there was no return of fluorescence after heating. Conversely, in the presence of Co^{2+} the fluorescence after heating increased to nearly 50% at short exposure times so that considerable crosslinking must have been occurring in the M-DNA. After 30 seconds of exposure, the return in fluorescence decreased, indicating that general DNA damage was starting to dominate. Without any radiation exposure, all of the samples showed similar before-heat ethidium fluorescence, indicating that the DNA had not become single stranded in the presence of M^{2+} at pH 9.0.

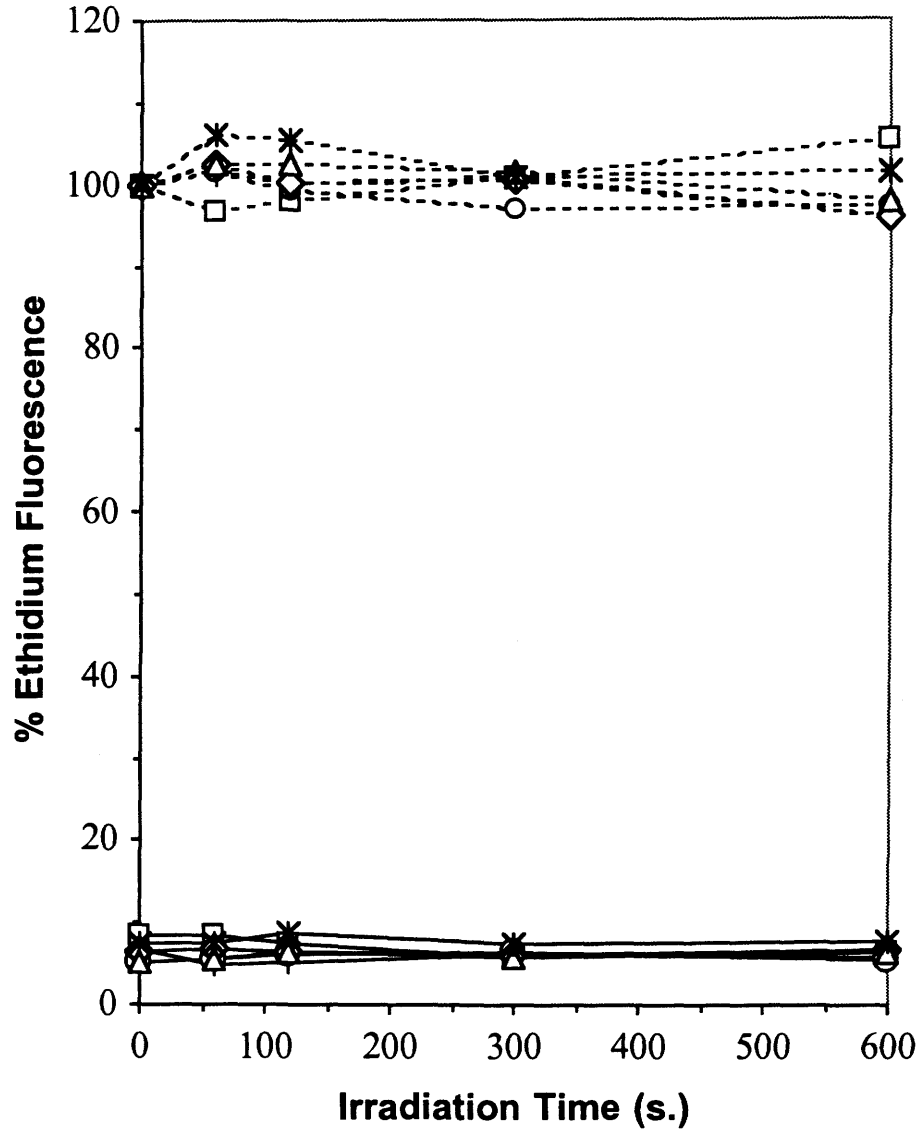

Figure 3.3. Gamma irradiation of calf thymus DNA at pH 7.5 in the presence of M^{2+}. Samples contained Co^{2+} (diamonds), Ni^{2+} (circles), Zn^{2+} (triangles), Mg^{2+} (squares), Mn^{2+} (crosses) or no M^{2+} (stars). Dashed lines represent before-heat readings and solid lines represent after-heat readings.

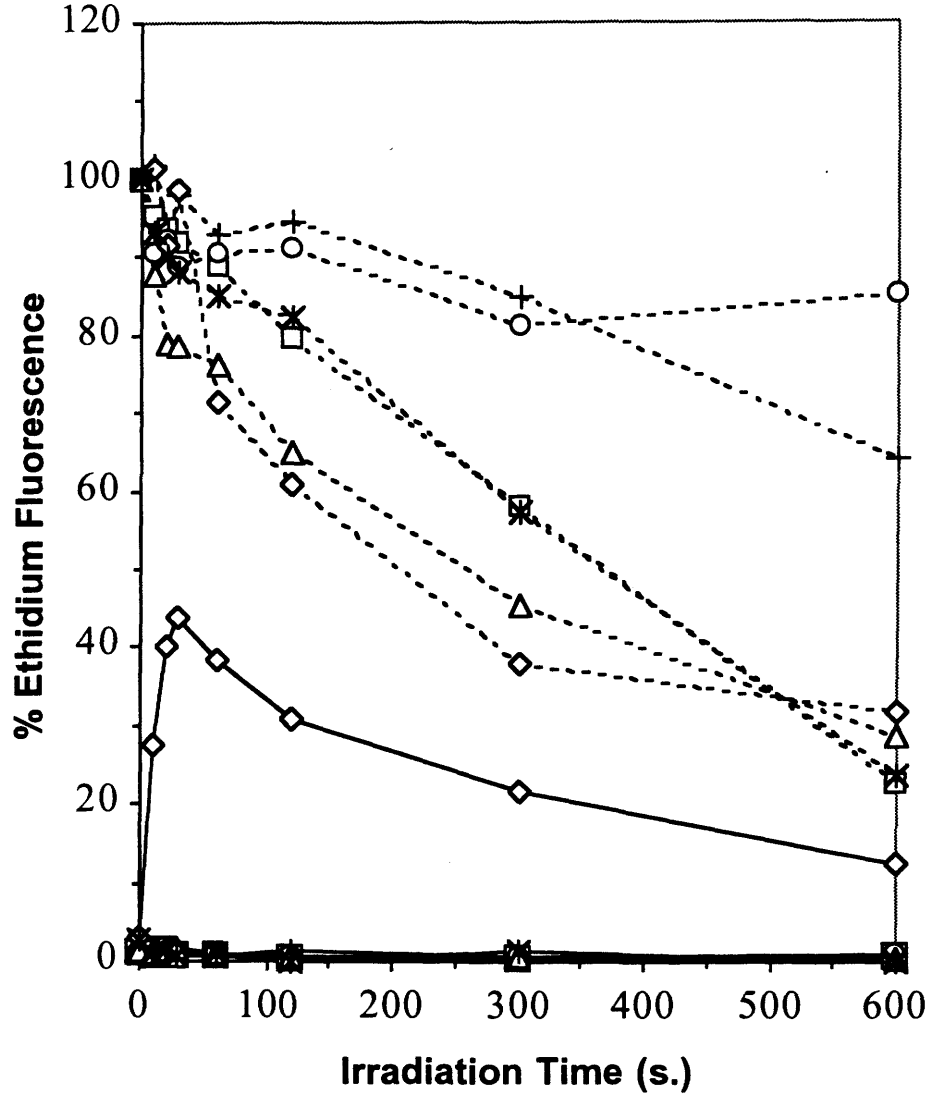

Figure 3.4. Gamma irradiation of calf thymus DNA at pH 9.0 in the presence of M^{2+}. Samples contained Co^{2+} (diamonds), Ni^{2+} (circles), Zn^{2+} (triangles), Mg^{2+} (squares), Mn^{2+} (crosses) or no M^{2+} (stars). Dashed lines represent before-heat readings and solid lines represent after-heat readings.

To estimate the dependence of crosslinking on the ratio of [calf thymus DNA]:[Co^{2+}], the experiment at pH 9.0 was repeated using various concentrations of the metal chloride such that this ratio varied between 1 : 1 and 1 : 15 (figure 3.5). The maximum before-heat fluorescence suppression and after-heat fluorescence increase were considered for each ratio. These values both increased steadily between [DNA] : [Co^{2+}] ratios of 1 : 1 and 1 : 5 after which they reached a plateau corresponding to an approximate 60% before-heat fluorescence decrease and 25% after-heat fluorescence increase.

3.1.3 Microbial and Synthetic DNA Sequences

Having demonstrated interstrand crosslinking in the Co^{2+} form of M-DNA upon exposure to γ-radiation, it was of interest to determine whether the observed reaction was dependent on the DNA composition. *C. perfringens*, *E. coli* and *M. lysodiecticus* bacterial DNAs were chosen because they contain G•C contents of 27%, 50% and 72%, respectively. All three samples followed a similar pattern to that of calf thymus DNA in the presence of Co^{2+}. There was no return of after-heat fluorescence at pH 7.5 (Figure 3.6), neither was there any loss of before-heat fluorescence. There was a similar return in after-heat fluorescence at pH 9.0 in all cases (Figure 3.7) that was accompanied by a decrease in before-heat fluorescence.

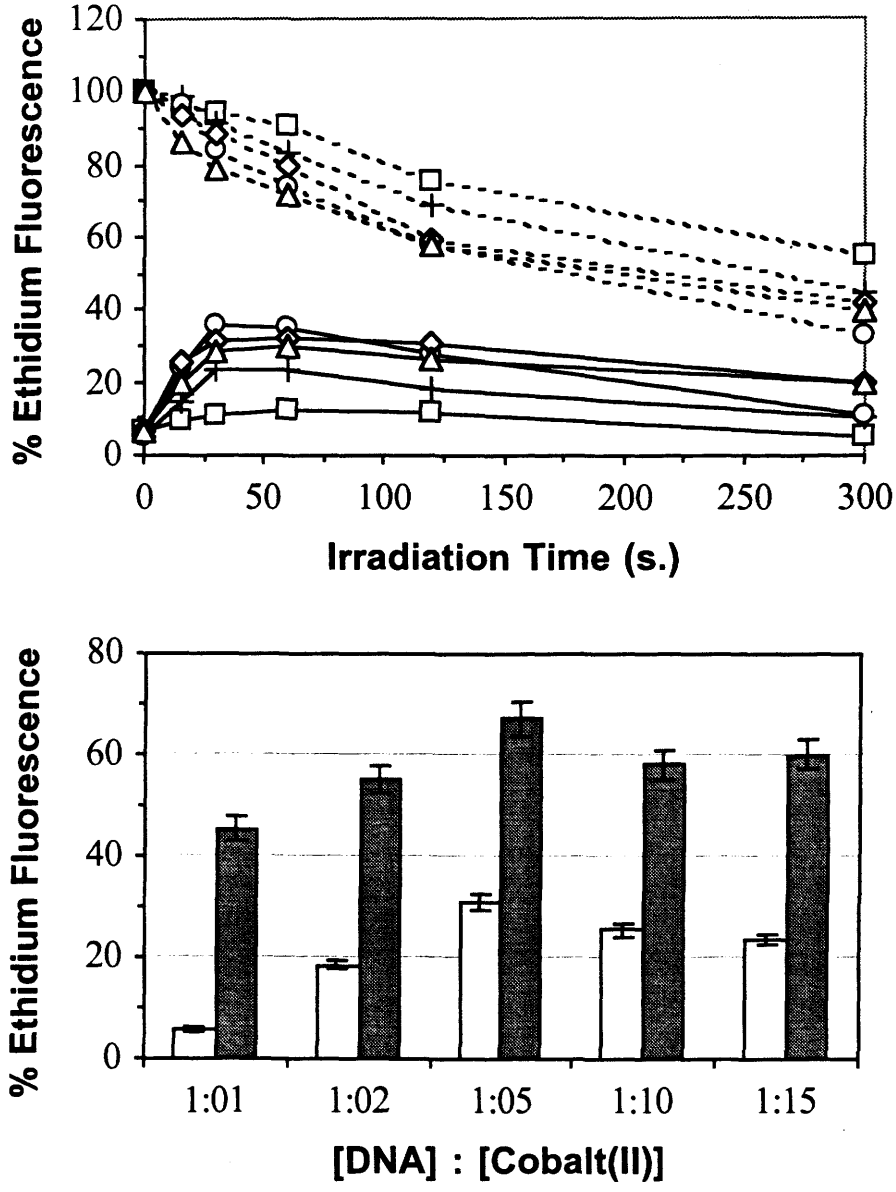

Figure 3.5. Dependence of γ-radiation-induced crosslinking on the [DNA] : [Co^{2+}] ratio. (Top) Samples of calf thymus DNA at pH 9.0 having a [DNA] : [Co^{2+}] ratio of 1 : 1 (squares), 1 : 2 (crosses), 1 : 5 (triangles), 1 : 10 (diamonds) or 1 : 15 (circles) were irradiated. Dashed lines represent before-heat readings and solid lines represent after-heat readings. (Bottom) The maximal increase in after-heat fluorescence (white) and the maximal decrease in before-heat fluorescence (grey) are shown against the [DNA] : [Co^{2+}] ratio.

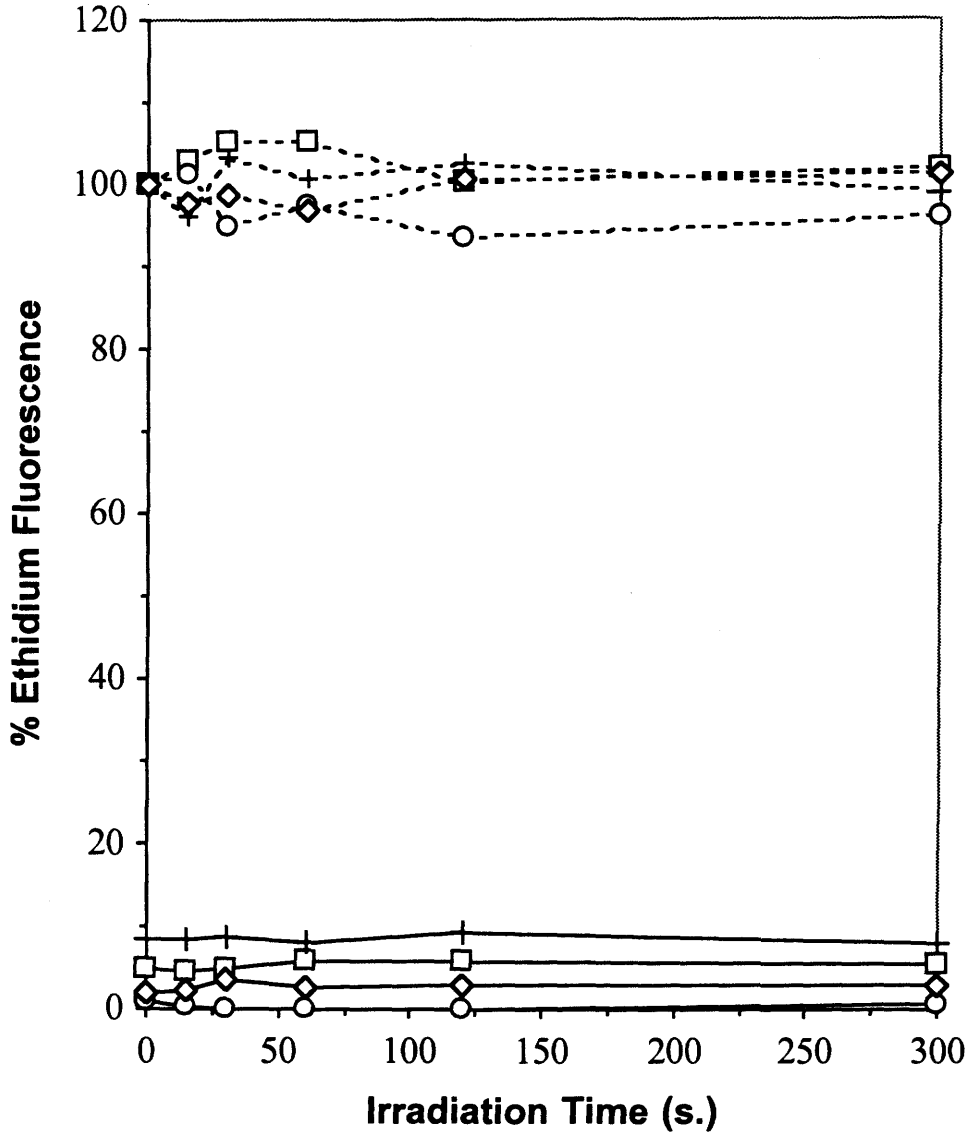

Figure 3.6. Gamma irradiation of bacterial DNA at pH 7.5 in the presence of Co^{2+}. DNA samples were from calf thymus (squares), *E. coli* (crosses), *C. perfringens* (circles) and *M. lysodiecticus* (diamonds). Dashed lines represent before-heat readings and solid lines represent after-heat readings.

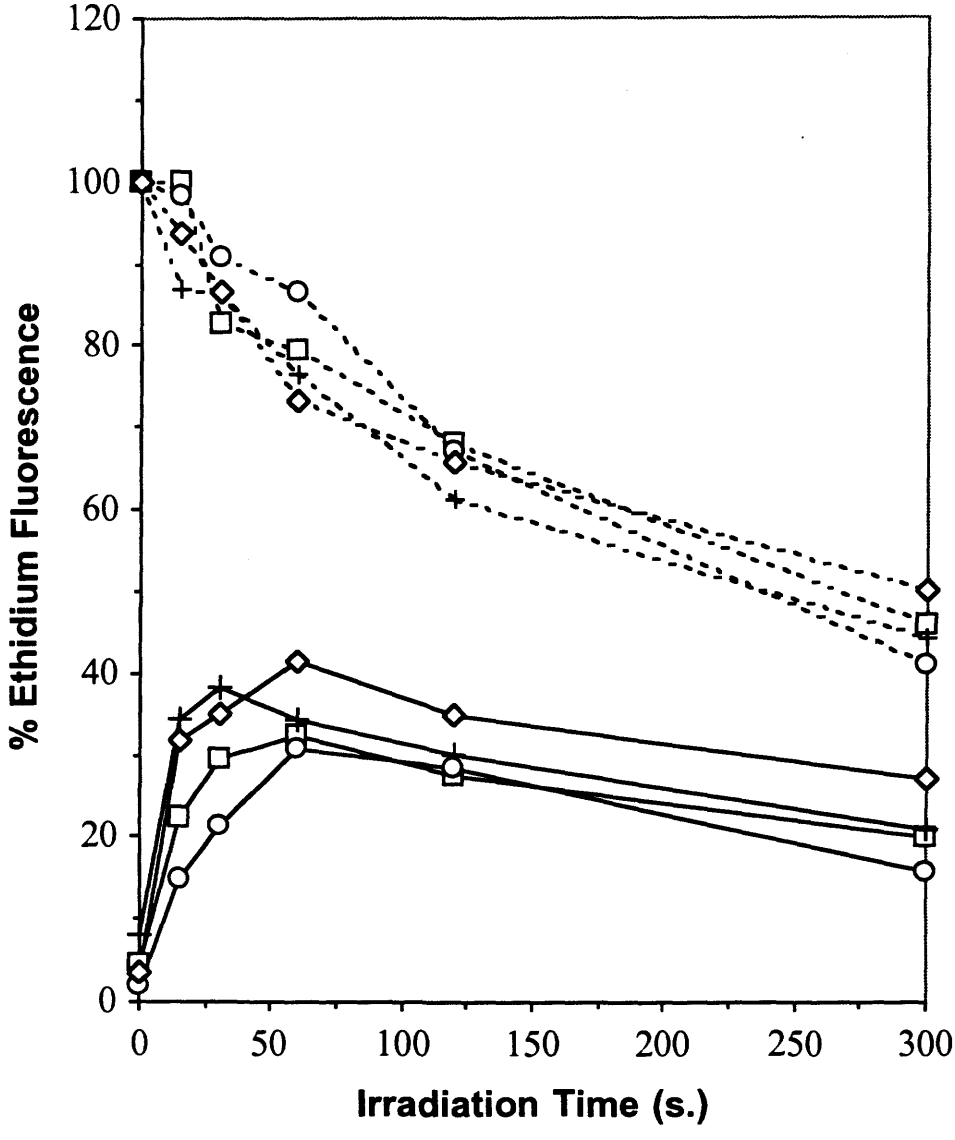

Figure 3.7. Gamma irradiation of bacterial DNA at pH 9.0 in the presence of Co^{2+}. DNA samples were from calf thymus (squares), *E. coli* (crosses), *C. perfringens* (circles) and *M. lysodiecticus* (diamonds). Dashed lines represent before-heat readings and solid lines represent after-heat readings.

To determine whether formation of the interstrand crosslinks are dependent on sequence considerations, the experiments were repeated using various synthetic DNA sequences. These assays showed no increase in after-heat fluorescence and before-heat fluorescence showed little or no decrease at pH 7.5 in the presence of Co^{2+} (Figure 3.8). At pH 9.0 (Figure 3.9) there was an increase in after-heat fluorescence with all samples tested, poly[d(TG)]•poly[d(CA)] being the highest followed by poly[d(TC)]•poly[d(GA)], poly(dG)•poly(dC) and poly(dA)•poly(dT). At pH 9.0, this was also accompanied by a decrease in before-heat fluorescence with radiation dose, which again demonstrated general DNA damage. This effect became dominant after 30 to 60 seconds resulting in a decrease in after-heat fluorescence after these times.

3.1.4 Effects of a Free Radical Scavenger and EDTA

Because much of the DNA damage caused by ionizing radiation results from the formation of $^{\bullet}OH$ radicals (Breen and Murphy, 1995), it was of interest to determine whether this is also the cause of interstrand crosslink formation. After-heat fluorescence was completely suppressed when the calf thymus pH 9.0 Co^{2+} sample was γ-irradiated in the presence of the $^{\bullet}OH$ scavenger TRIS-HCl (Figure 3.10). The decrease in before-heat fluorescence for this sample was also abolished so that when

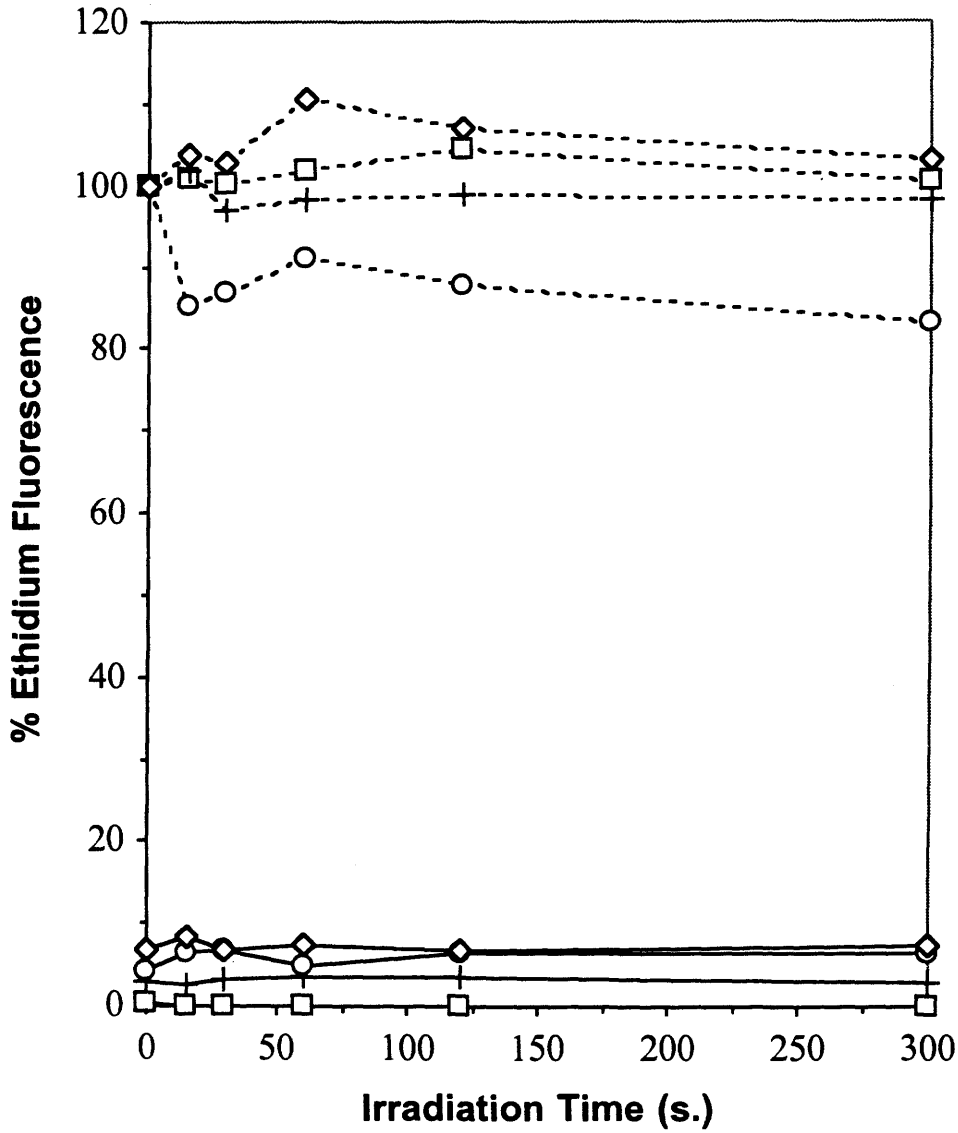

Figure 3.8. Gamma irradiation of synthetic DNA sequences at pH 7.5 in the presence of Co^{2+}. Samples were poly[d(TC)]•poly[d(GA)] (squares), poly(dA)•poly(dT) (crosses), poly[d(TG)]•poly[d(CA)] (circles) and poly(dG)•poly(dC) (diamonds). Dashed lines represent before-heat readings and solid lines represent after-heat readings.

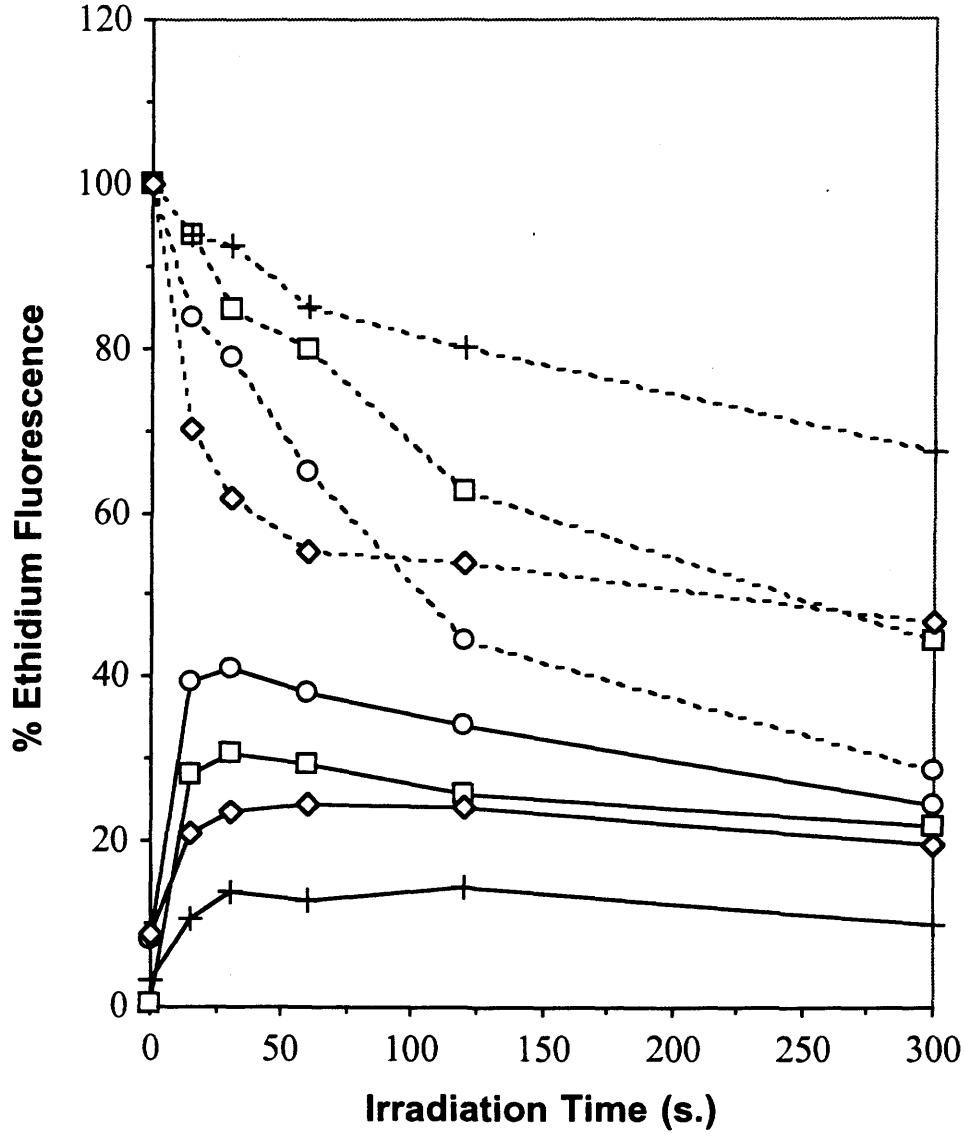

Figure 3.9. Gamma irradiation of synthetic DNA sequences at pH 9.0 in the presence of Co^{2+}. Samples were poly[d(TC)]•poly[d(GA)] (squares), poly(dA)•poly(dT) (crosses), poly[d(TG)]•poly[d(CA)] (circles) and poly(dG)•poly(dC) (diamonds). Dashed lines represent before-heat readings and solid lines represent after-heat readings.

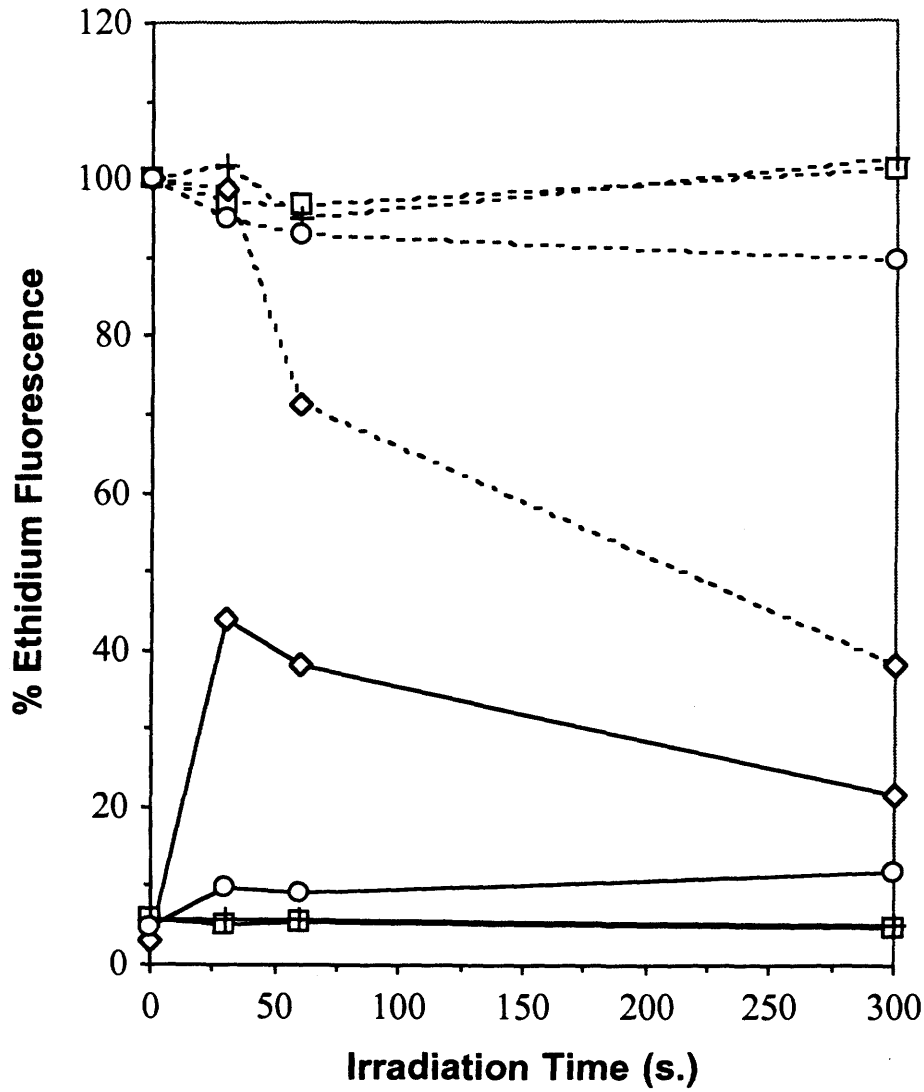

Figure 3.10. Suppression of γ-radiation-induced crosslinking by TRIS-HCl in calf thymus DNA. Samples containing Co^{2+} at pH 7.5 (crosses) and 9.0 (diamonds) are compared to those containing Co^{2+} at pH 7.5 in TRIS-HCl (squares) and pH 9.0 with 1 mM TRIS-HCl (circles). Dashed lines represent before-heat readings and solid lines represent after-heat readings.

TRIS was present, the results were similar to those at pH 7.5. The same suppression of γ-radiation-induced crosslinking was observed with plasmid DNA (Figure 3.11). In this case, however, the decrease in after-heat fluorescence for the sample containing TRIS-HCl was not complete, nor was it as rapid as would have been observed normally for plasmid DNA at pH 9.0 (compare with Figure 3.2). Thus, much of the nicking of plasmid DNA was caused by free radical formation, which was inhibited in the presence of TRIS-HCl.

An almost identical pattern was seen when 1 mM EDTA was present during irradiation of calf thymus DNA in the presence of Co^{2+} (Figure 3.12). Samples containing EDTA showed no decrease in before-heat fluorescence and no increase in after-heat fluorescence, having been virtually identical with samples containing EDTA at pH 7.5 or samples at pH 7.5 containing no EDTA (compare to figure 3.10). This would be expected if the crosslinking was dependent on the nucleic acid having the M-DNA conformation, which would have been abolished in the presence of EDTA.

3.2 Effects of UV Radiation on DNA with M^{2+}

Damage to DNA resulting from UV radiation is known to be different than that resulting from γ-radiation (Douki and Cadet, 1995; Douki *et al.*, 1997). Therefore, samples similar to those described above were also exposed to UV

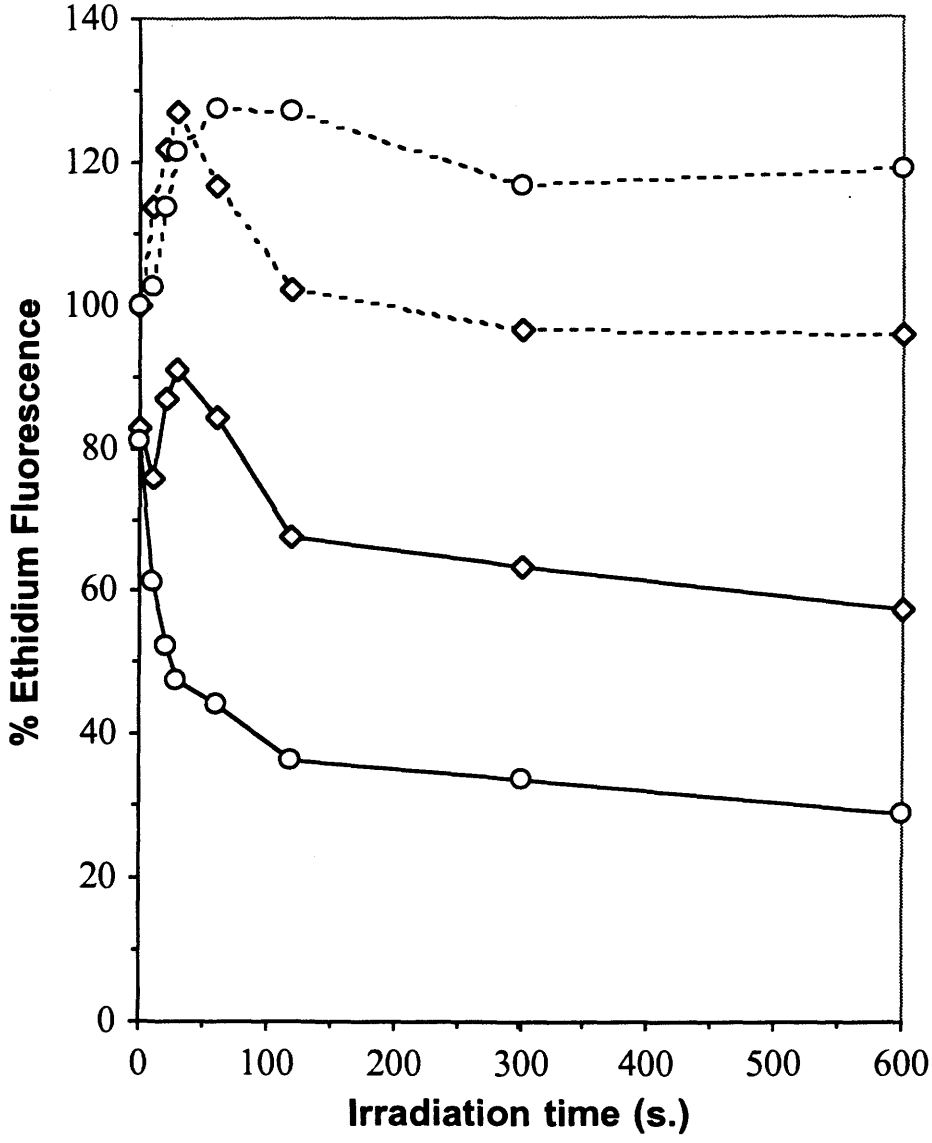

Figure 3.11. Suppression of γ-radiation-induced crosslinking by TRIS-HCl in plasmid DNA. Samples containing Co^{2+} at pH 9.0 alone (diamonds) are compared to those containing Co^{2+} and 1 mM TRIS-HCl (circles). Dashed lines represent before-heat readings and solid lines represent after-heat readings.

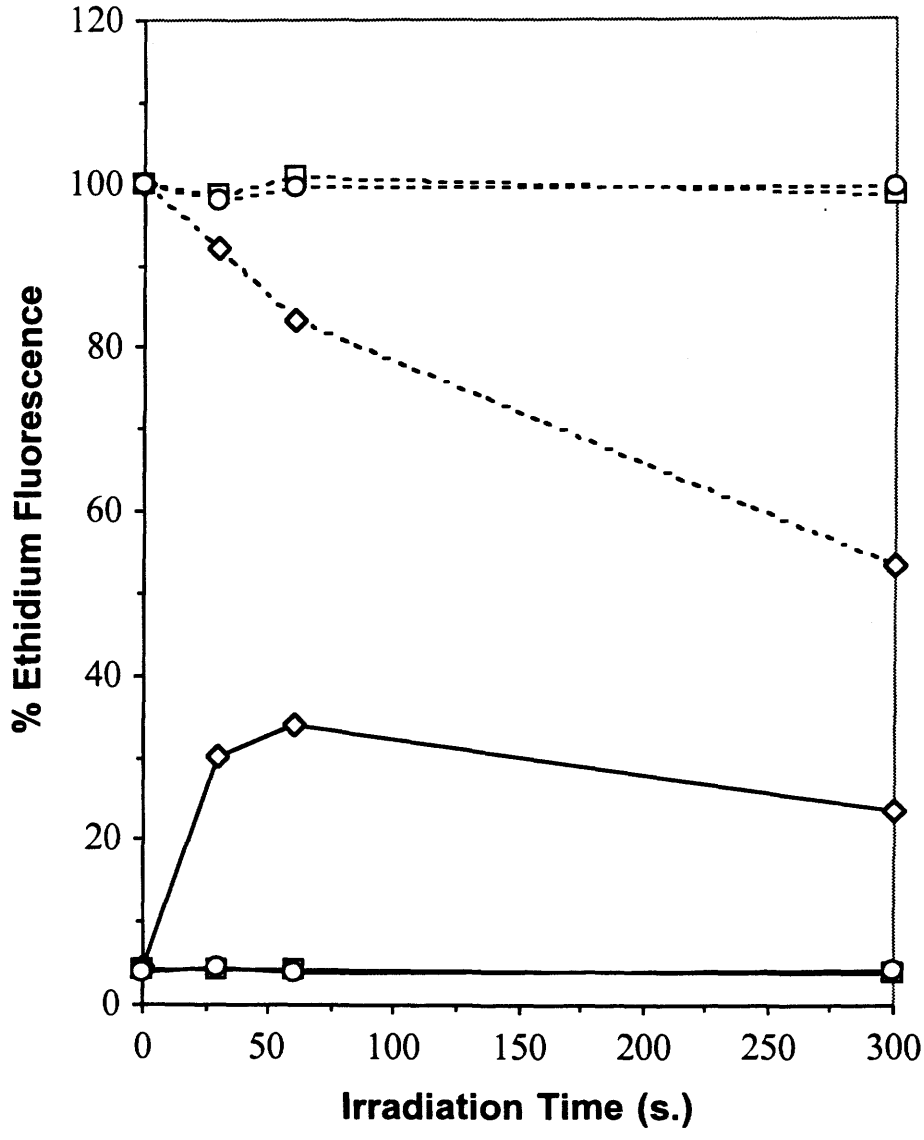

Figure 3.12. Suppression of γ-radiation-induced crosslinking by EDTA. Samples of calf thymus DNA containing Co^{2+} were irradiated at pH 9.0 alone (diamonds), in the presence of 1 mM EDTA (circles) or at pH 7.5 in the presence of 1 mM EDTA (squares). Dashed lines represent before-heat readings and solid lines represent after-heat readings.

radiation. It was expected that M-DNA might show a different response to UV radiation than B-DNA. Damage and interstrand crosslinking were assessed using the same fluorescence assays and the results are again described in the same order.

3.2.1 Supercoiled Plasmid DNA

Exposure of plasmid DNA to UV radiation at pH 7.5 (Figure 3.13) resulted in nicking because in general the fluorescence before heat increased and the fluorescence after heat decreased. At longer exposure times crosslinking of the DNA began to dominate and the return of after-heat fluorescence leveled off for all of the samples with M^{2+} present.

For the Co^{2+} and Ni^{2+} samples at pH 9.0 the rate of crosslinking exceeded the rate of nicking because at short exposure times the fluorescence after heat actually increased (Figure 3.14). For the other samples, there was a decrease in after-heat fluorescence with exposure time similar to the case at pH 7.5. The Zn^{2+} sample showed a small increase in after-heat fluorescence but only at exposure times of less than 2 minutes. Again, before-heat fluorescence generally increased indicating nicking. However, for the Co^{2+} and Ni^{2+} samples there was either a decrease in before-heat fluorescence or an initial increase followed by a decrease after 10 minutes of exposure, respectively.

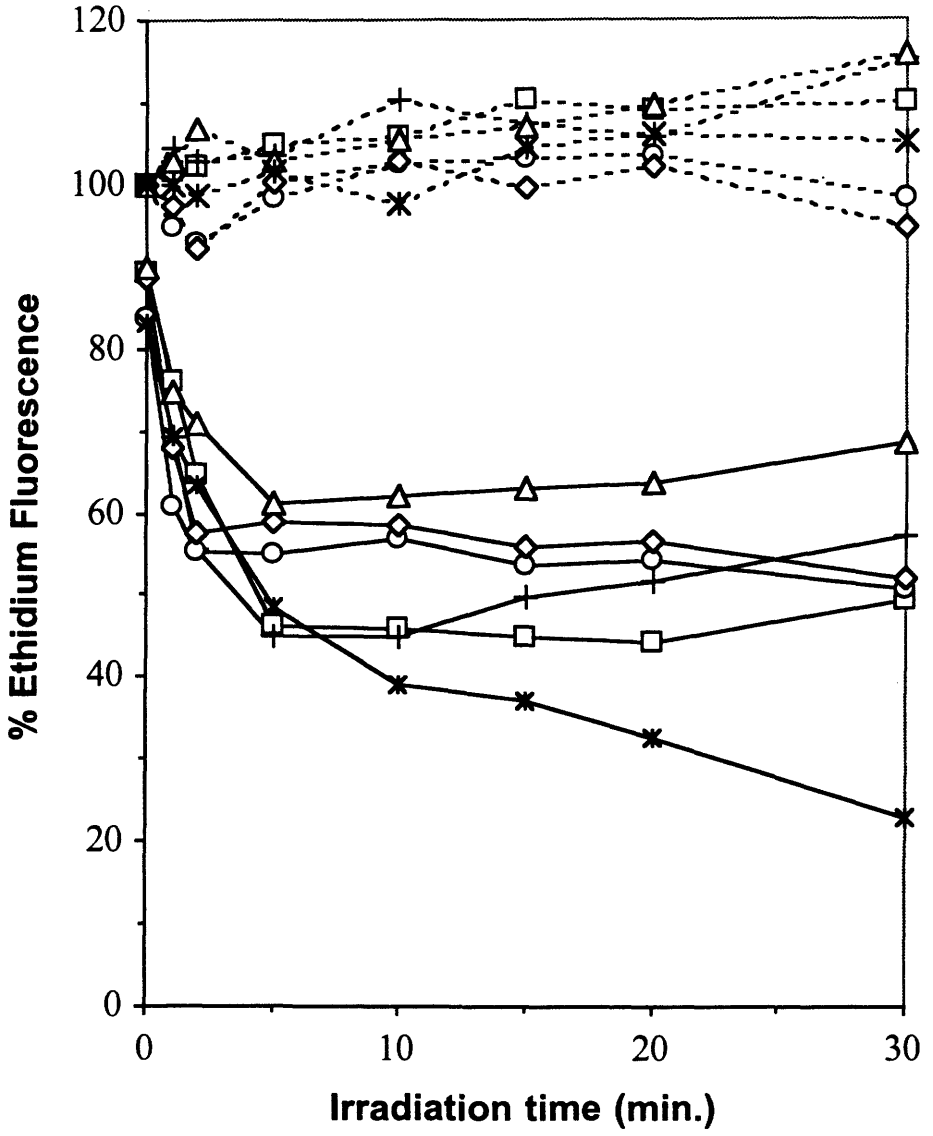

Figure 3.13. UV irradiation of plasmid DNA at pH 7.5 in the presence of M^{2+}. Samples contained Co^{2+} (diamonds), Ni^{2+} (circles), Zn^{2+} (triangles), Mg^{2+} (squares), Mn^{2+} (crosses) or no M^{2+} (stars). Dashed lines represent before-heat readings and solid lines represent after-heat readings.

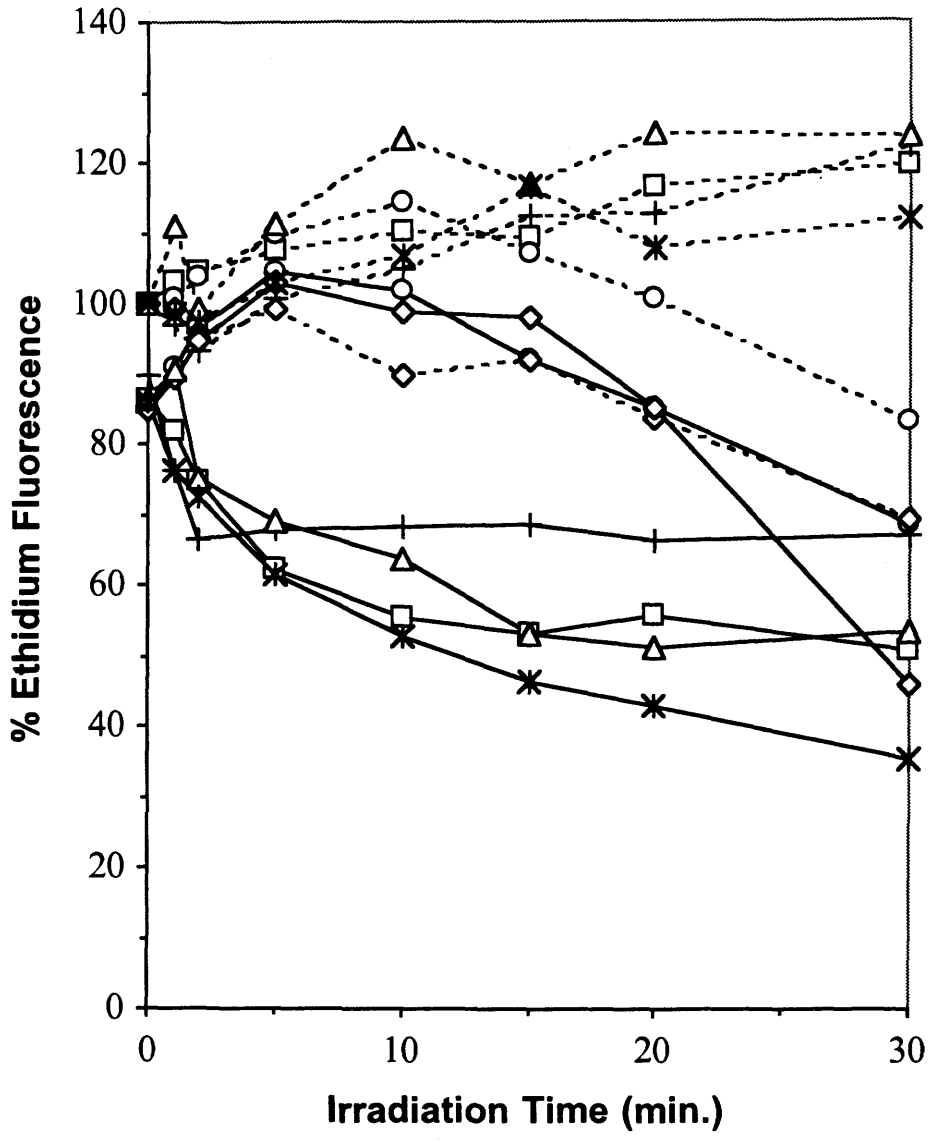

Figure 3.14. UV irradiation of plasmid DNA at pH 9.0 in the presence of M^{2+}. Samples contained Co^{2+} (diamonds), Ni^{2+} (circles), Zn^{2+} (triangles), Mg^{2+} (squares), Mn^{2+} (crosses) or no M^{2+} (stars). Dashed lines represent before-heat readings and solid lines represent after-heat readings.

3.2.2 Calf Thymus DNA

Exposure of calf thymus DNA to UV radiation at pH 7.5 was undertaken in order to asses the extent of interstrand crosslinking. Results indicated a decrease in the fluorescence before heat and an increase in fluorescence after heat for all samples (Figure 3.15). Therefore, both general DNA damage and crosslinking were occurring simultaneously.

For calf thymus DNA at pH 9.0 several differences were apparent (Figure 3.16). For samples containing Co^{2+}, Ni^{2+} or Zn^{2+} the amount of crosslinking increased compared to pH 7.5. Those containing Co^{2+} or Ni^{2+} reached maximal values of after-heat fluorescence after about 10 minutes of exposure but those containing Zn^{2+} reached this point after only 1 minute of exposure. The Zn^{2+} samples, however, did not show crosslinking to the same extent as the Co^{2+} or Ni^{2+} forms, the maximum return in ethidium fluorescence having been only about 30% compared to nearly 50% for Co^{2+} or Ni^{2+}. There was a correspondingly more pronounced decrease in before-heat fluorescence for samples containing Co^{2+}, Ni^{2+} or Zn^{2+}.

3.2.3 Synthetic DNA Sequences

In general, the synthetic sequences showed only a small increase in after-heat fluorescence accompanied by a small decrease in before-heat fluorescence at pH 7.5 in the presence of Co^{2+} (Figure 3.17), although this effect was less pronounced than

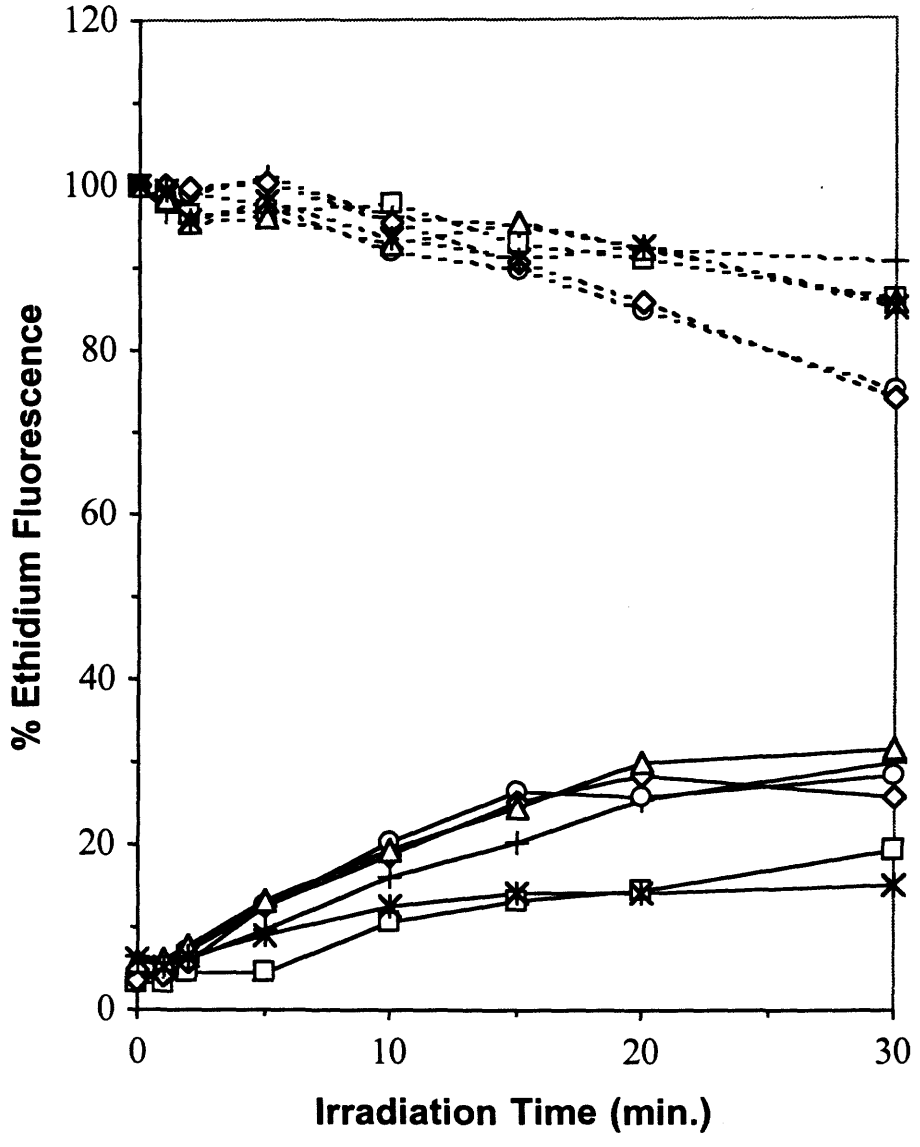

Figure 3.15. UV irradiation of calf thymus DNA at pH 7.5 in the presence of M^{2+}. Samples contained Co^{2+} (diamonds), Ni^{2+} (circles), Zn^{2+} (triangles), Mg^{2+} (squares), Mn^{2+} (crosses) or no M^{2+} (stars). Dashed lines represent before-heat readings and solid lines represent after-heat readings.

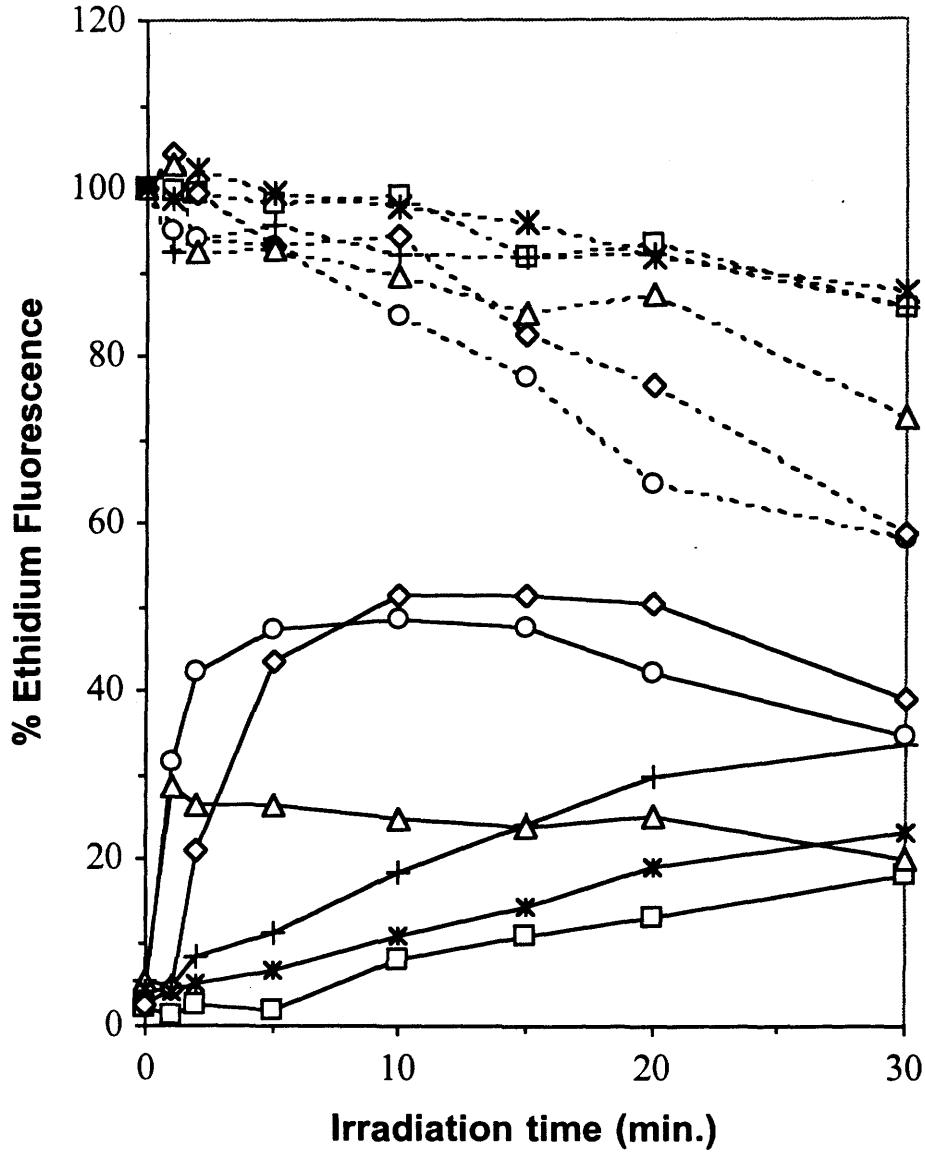

Figure 3.16. UV irradiation of calf thymus DNA at pH 9.0 in the presence of M^{2+}. Samples contained Co^{2+} (diamonds), Ni^{2+} (circles), Zn^{2+} (triangles), Mg^{2+} (squares), Mn^{2+} (crosses) or no M^{2+} (stars). Dashed lines represent before-heat readings and solid lines represent after-heat readings.

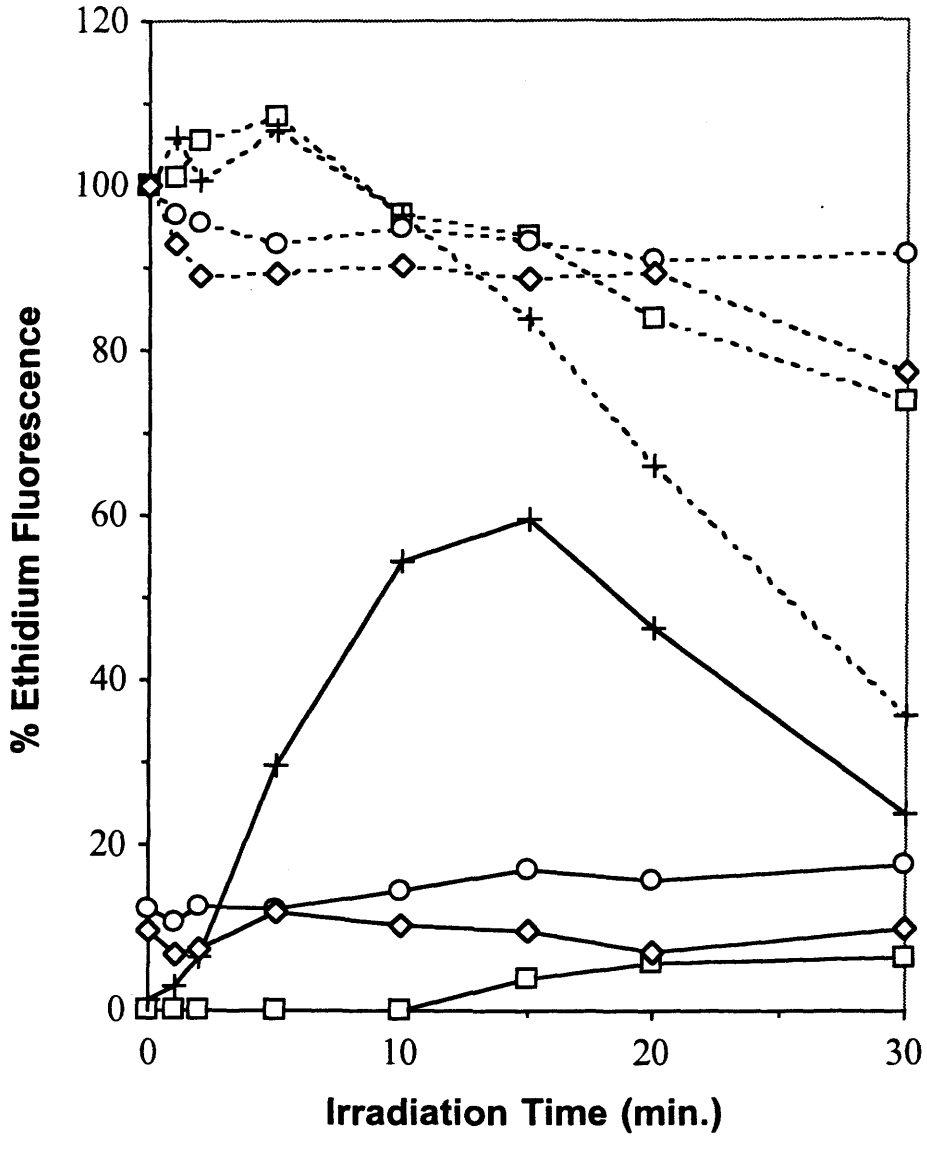

Figure 3.17. UV irradiation of synthetic DNA sequences at pH 7.5 in the presence of Co^{2+}. Samples contained poly[d(TC)] • poly[d(GA)] (squares), poly(dA) • poly(dT) (crosses), poly[d(TG)] • poly[d(CA)] (circles) and poly(dG) • poly(dC) (diamonds). Dashed lines represent before-heat readings and solid lines represent after-heat readings.

with calf thymus DNA. Poly(dA)•poly(dT) showed a strong decrease in before-heat fluorescence (less than 40% after 30 minutes of exposure) that can at least partially be explained by the formation of cyclobutyl pyrimidine dimers (Douki and Cadet, 1995). Surprisingly, there was also a strong increase in after-heat fluorescence (about 60% after 15 minutes of exposure). This was completely different from exposure with ionizing radiation and indicated a different mechanism of crosslink formation.

As in the case of γ-radiation, UV radiation caused increased crosslinking with all of the synthetic DNA sequences assayed in the presence of Co^{2+} at pH 9.0 (Figure 3.18). Compared to pH 7.5, poly[d(TC)]•poly[d(GA)] showed the greatest increase followed by poly[d(TG)]•poly[d(CA)] and poly(dG)•poly(dC). Poly(dA)•poly(dT) showed only a small increase compared to pH 7.5, the return in after-heat fluorescence being unexpectedly high in both cases.

Unlike exposure to γ-radiation, exposure to UV radiation resulted in crosslinking under all conditions tested with calf thymus DNA, even when only Mg^{2+} ions were present in the samples. It was therefore decided to perform additional experiments, exposing the synthetic DNA sequences to UV radiation in the presence of Mg^{2+}. At pH 7.5 (Figure 3.19), the overall pattern was very similar to the one seen in the presence of Co^{2+}. However, there was a greater decrease in before-heat fluorescence in the case of poly[d(TC)]•poly[d(GA)] and poly(dG)•poly(dC) and a

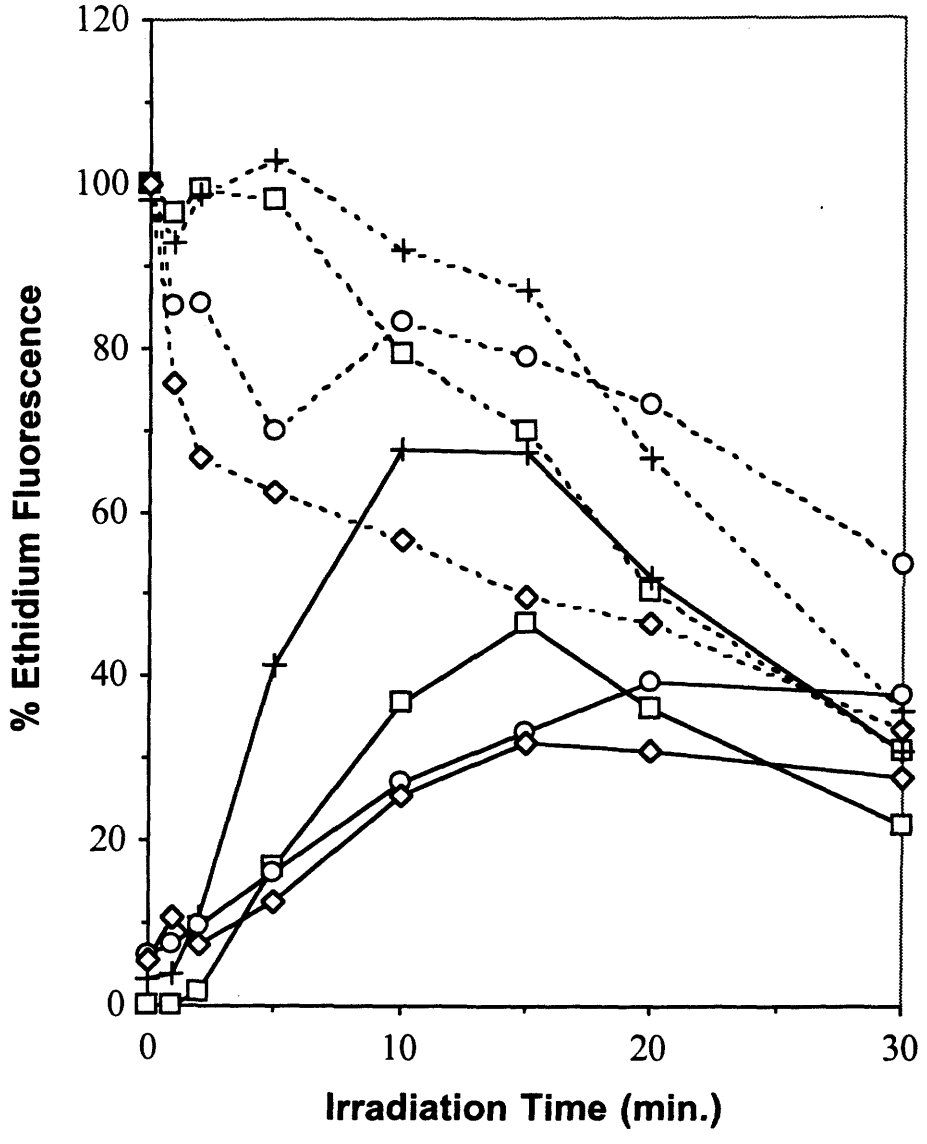

Figure 3.18. UV irradiation of synthetic DNA sequences at pH 9.0 in the presence of Co^{2+}. Samples contained poly[d(TC)] • poly[d(GA)] (squares), poly(dA) • poly(dT) (crosses), poly[d(TG)] • poly[d(CA)] (circles) and poly(dG) • poly(dC) (diamonds). Dashed lines represent before-heat readings and solid lines represent after-heat readings.

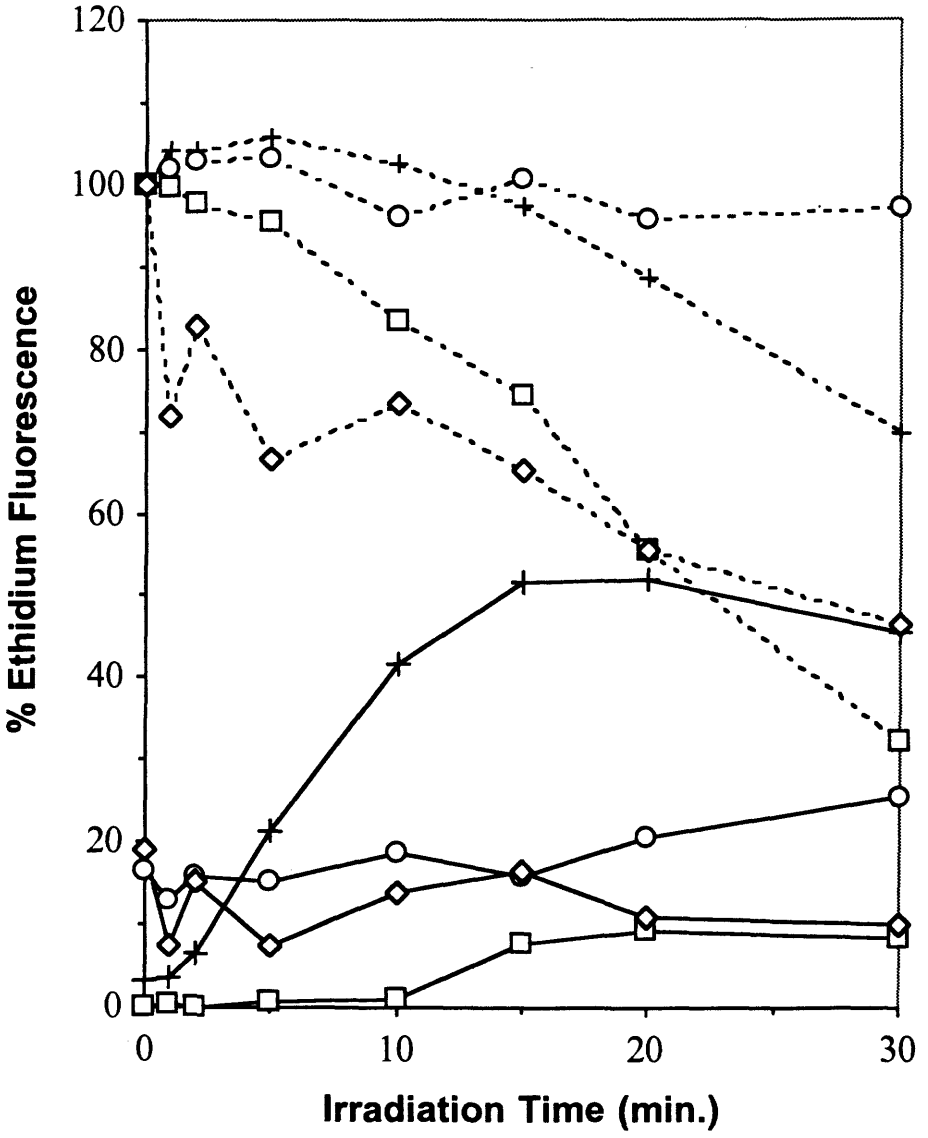

Figure 3.19. UV irradiation of synthetic DNA sequences at pH 7.5 in the presence of Mg^{2+}. Samples contained poly[d(TC)]•poly[d(GA)] (squares), poly(dA)•poly(dT) (crosses), poly[d(TG)]•poly[d(CA)] (circles) and poly(dG)•poly(dC) (diamonds). Dashed lines represent before-heat readings and solid lines represent after-heat readings.

lesser decrease in before-heat fluorescence in the case of poly(dA)•poly(dT). The after-heat readings were very similar with poly(dA)•poly(dT) reaching about 50% after 15 minutes.

At pH 9.0, there was no induction of crosslink formation by Mg^{2+} for any of the synthetic DNA sequences (Figure 3.20). This correlates well with the observation that Mg^{2+} did not induce increased crosslink formation in calf thymus DNA (compare Figures 3.15 and 3.16). The before-heat fluorescence results showed that there was general DNA damage being inflicted to an extent similar to that seen in the presence of Co^{2+} (compare with Figure 3.18), except in the case of poly[d(TG)]•poly[d(CA)].

3.2.4 Effects of a Free Radical Scavenger and EDTA

In contrast to the γ-irradiations, the after-heat fluorescence was not suppressed when the pH 9.0 Co^{2+} sample was UV irradiated in the presence of TRIS-HCl (Figure 3.21). After 2 minutes of exposure to UV radiation, for example, it was observed that the after-heat fluorescence values for samples containing Co^{2+} or Co^{2+} with TRIS-HCl were almost identical, being just above 20% in both cases. At pH 7.5, the corresponding after-heat fluorescence values were less than half. For pH 7.5, samples were prepared in both HEPES and TRIS buffers to verify that performing the pH 7.5 control experiments in TRIS buffer was justified in the case of UV radiation.

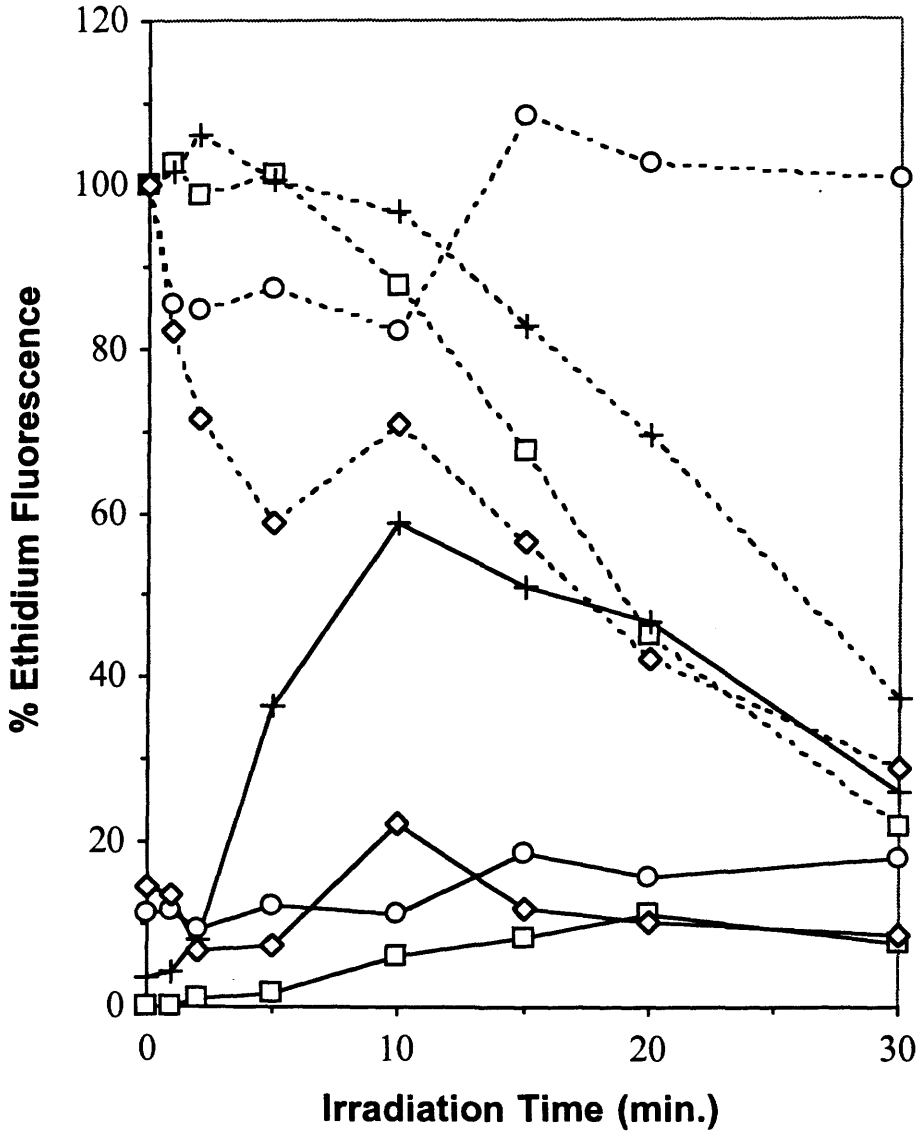

Figure 3.20. UV irradiation of synthetic DNA sequences at pH 9.0 in the presence of Mg^{2+}. Samples contained poly[d(TC)]•poly[d(GA)] (squares), poly(dA)•poly(dT) (crosses), poly[d(TG)]•poly[d(CA)] (circles) and poly(dG)•poly(dC) (diamonds). Dashed lines represent before-heat readings and solid lines represent after-heat readings.

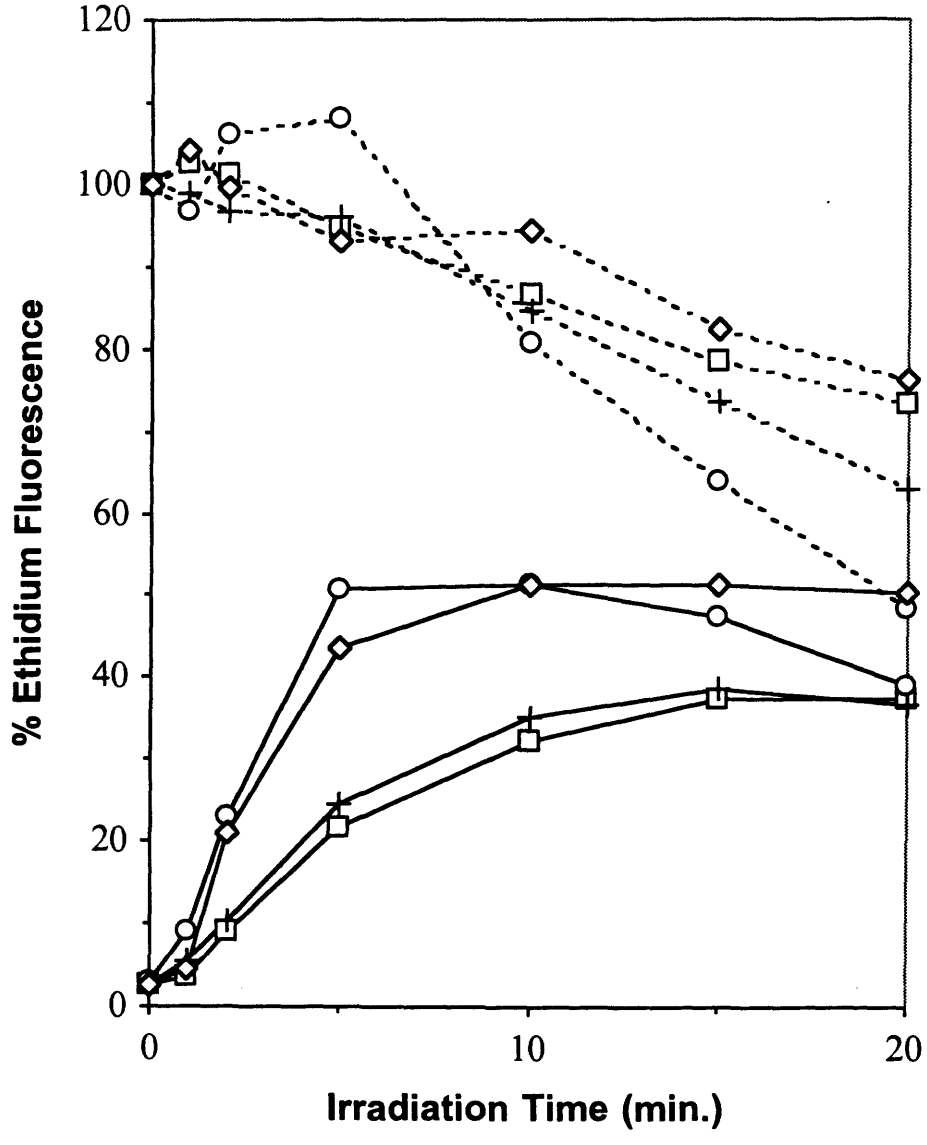

Figure 3.21. No suppression of UV radiation-induced crosslinking by TRIS-HCl. Samples of calf thymus DNA containing Co^{2+} at pH 7.5 in HEPES (crosses) and 9.0 (diamonds) are compared to those containing Co^{2+} at pH 7.5 in TRIS-HCl (squares) and pH 9.0 with 1 mM TRIS-HCl (circles). Dashed lines represent before-heat readings and solid lines represent after-heat readings.

The addition of EDTA (Figure 3.22) resulted in suppression of UV radiation-induced crosslinking in the same manner as that described for the γ-irradiations. The only difference was that there was an approximate 20% to 30% loss of before-heat fluorescence and an approximate 10% to 20% increase in after-heat fluorescence in the pH 7.5 samples. This was expected since DNA damage and interstrand crosslinking occur upon exposure to UV radiation even when the conformation is not that of M-DNA.

3.3 Proton Release During M-DNA Formation

The results discussed thus far are consistent with the proposal that, in the M-DNA conformation, the M^{2+} is intimately associated with duplex DNA. As discussed in Section 1.3, evidence suggests that in the M-DNA conformation, the M^{2+} replaces the imino protons of G and T residues. The current experiment was performed in order to measure the release of protons during M-DNA formation.

When Ni^{2+} was added to 0.1 mM in base-pairs of calf thymus DNA at pH 9.5, a decrease in pH was observed so that a basic solution of KOH could be added to retain a constant pH (Figure 3.23). Accompanying this effect was a loss of ethidium fluorescence, which indicated M-DNA formation. Significant decrease in pH did not occur until the Ni^{2+} concentration reached 0.02 mM. According to the ethidium fluorescence assay, nearly complete M-DNA formation occurred with a concentration

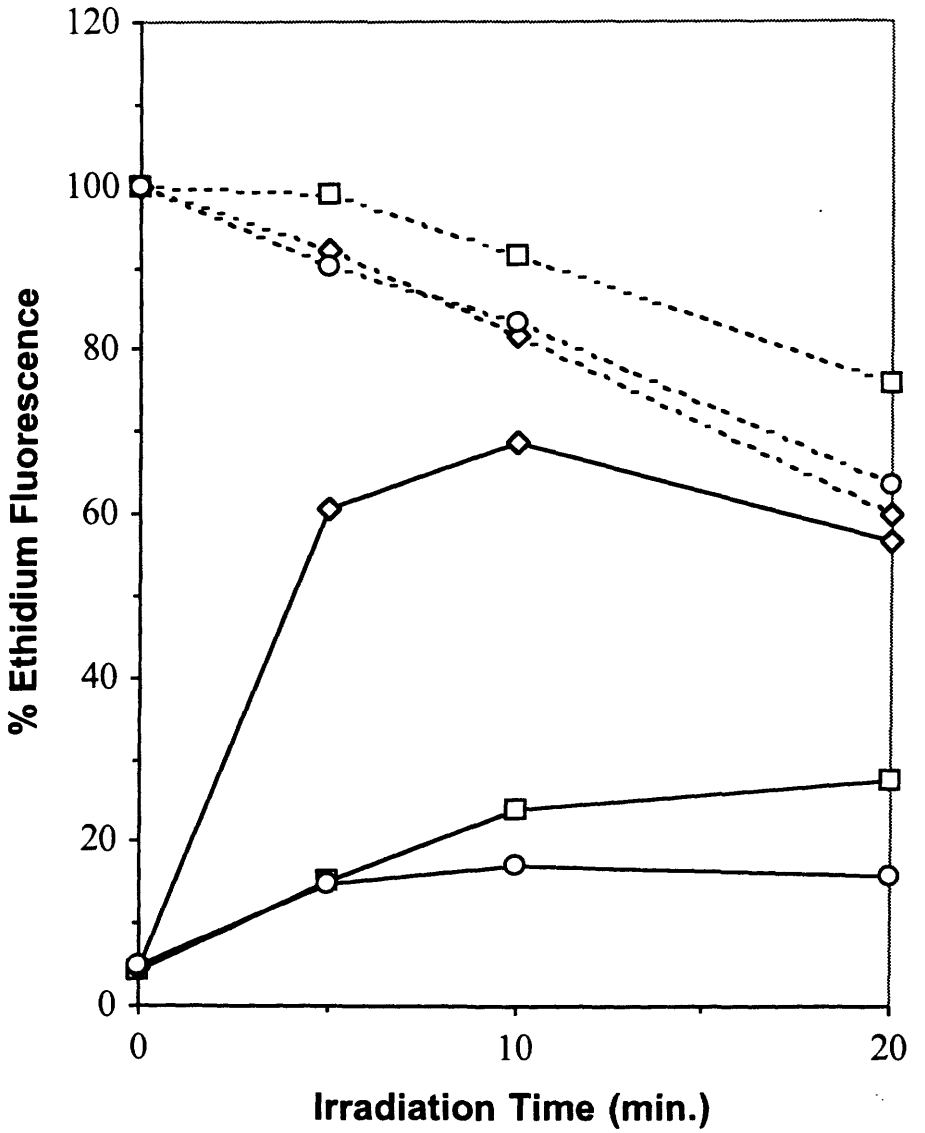

Figure 3.22. Suppression of UV radiation-induced crosslinking by EDTA. Samples of calf thymus DNA contained Co^{2+} at pH 9.0 alone (diamonds), in the presence of 1 mM EDTA (circles) or at pH 7.5 in the presence of 1 mM EDTA (squares). Dashed lines represent before-heat readings and solid lines represent after-heat readings.

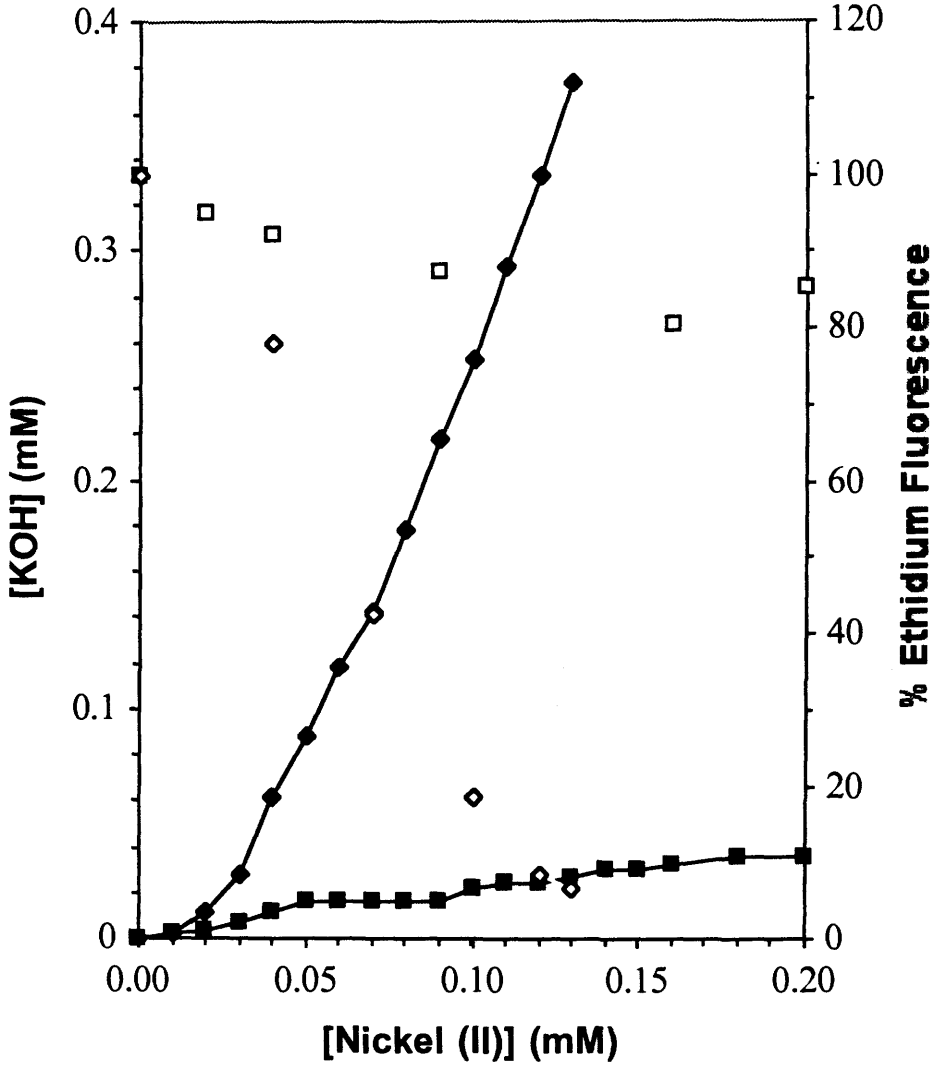

Figure 3.23. Titration experiments at pH 7.5 and 9.5 with calf thymus DNA and Ni^{2+}. The DNA concentration was 0.1 mM in base pairs. Filled squares represent the amount of KOH added to retain a pH of 7.5 and filled diamonds represent the amount of KOH added to retain a pH of 9.5. Hollow squares and diamonds represent the % ethidium fluorescence at pH 7.5 and 9.5 respectively.

of 0.12 mM Ni^{2+}. Thus, 0.1 mM of Ni^{2+} were incorporated into M-DNA during the period of proton release. During this period, a total of nearly 0.4 mM KOH were consumed to retain a constant pH. For the same sample at pH 7.5, there was little loss of ethidium fluorescence with addition of Ni^{2+}. At best, a 20% decrease was observed. Correspondingly, there was an insignificant decrease in pH.

At pH 9.5, the denaturation of DNA can be a concern. Thus, the experiment was repeated at pH 8.5 with a higher DNA concentration (Figure 3.24). A higher DNA concentration was used because the pH differences observed were small. Even with the 0.1 mM DNA used in the previous experiments, pH decreases were on the order of under 0.1 pH units. With 1.1 mM DNA, the pH decreases were on the order of between 0.1 and 0.3 pH units. At pH 8.5 with 1.1 mM in base-pairs of calf thymus DNA, significant pH decrease began with a Ni^{2+} concentration of 0.6 mM and precipitation was observed with a Ni^{2+} concentration of 1.8 mM. Ethidium fluorescence indicated at least 60% M-DNA formation at this stage. It should be noted that once the DNA started precipitating at these high concentrations, the ethidium fluorescence assay became unreliable since the readings became unstable. It was assumed that once precipitate was observed, the DNA has bound all of the M^{2+} possible and formation of M-DNA was complete. Thus, approximately 1.2 mM of Ni^{2+} was incorporated into M-DNA while approximately 1.1 mM of KOH was consumed.

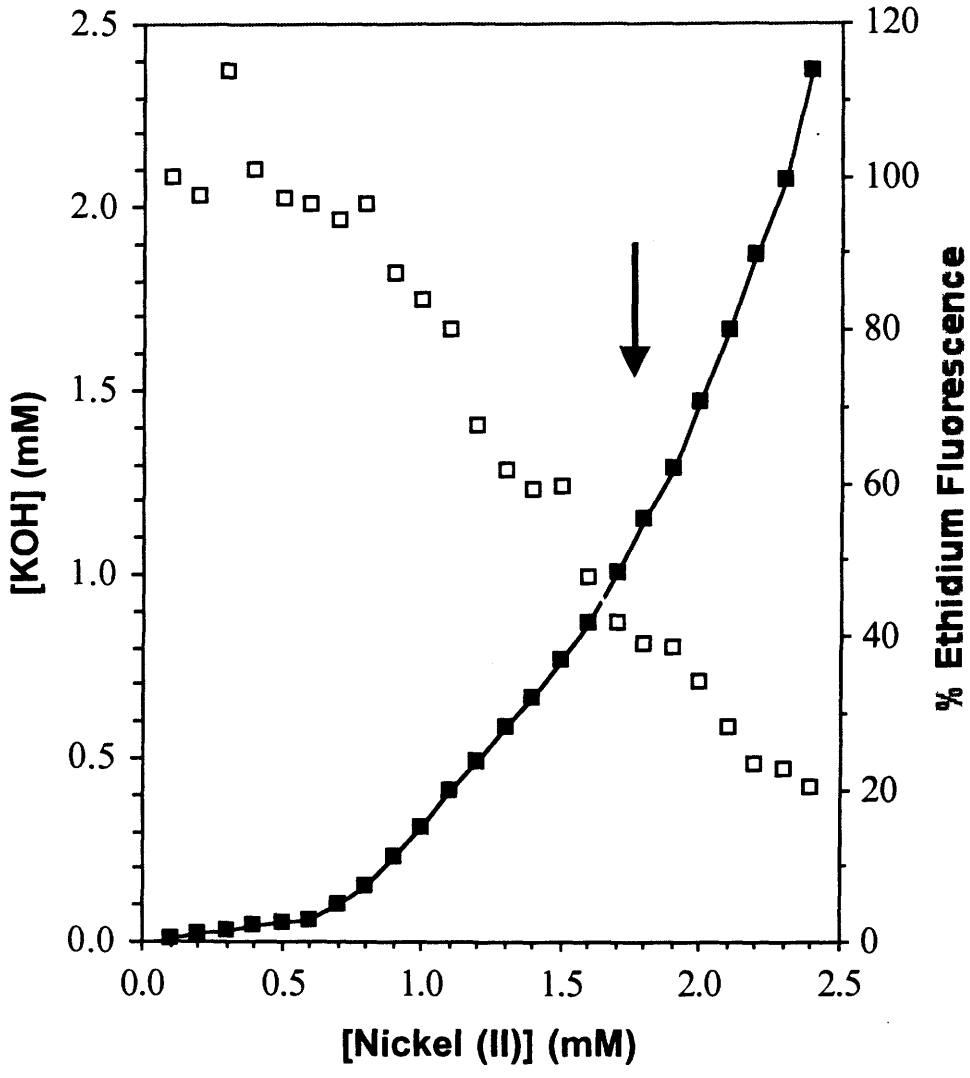

Figure 3.24. Titration experiment at pH 8.5 with calf thymus DNA and Ni^{2+}. The DNA concentration was 1.1 mM in base pairs. Filled squares represent the amount of KOH added to retain a pH of 8.5. Unfilled squares represent the % ethidium fluorescence. The arrow indicates the point at which precipitate became visible.

3.4 Crystal Structures of d(GGCGCC) With Co^{2+}, Ni^{2+} and Zn^{2+}

Having described the results of some of the experiments involving the M-DNA conformation, as well as the B-DNA conformation in the presence of various M^{2+}, we next turn to the results of several experiments aimed at obtaining crystal structures for some of these DNA-M^{2+} complexes.

3.4.1 Observations During Crystallization

Crystals were grown according to the method outlined in Section 2.4.2. Originally, crystals of the Co^{2+} complex were obtained at room temperature and it was unexpected that the Ni^{2+} and Zn^{2+} forms would not grow under similar conditions, even though many screening experiments were performed. Eventually, it was discovered that these forms would grow under similar conditions but at a lower temperature. The Ni^{2+} and Zn^{2+} forms were finally grown reproducibly at 4 °C. The crystals grew over a period of three to six days as square prisms having either one or both ends shaped as square pyramids in the case of Co^{2+} (Figure 3.25) and Zn^{2+} (Figure 3.26), or football shapes having four sides in the case of Ni^{2+} (Figure 3.27). Dimensions were typically about 0.2 X 0.2 X 0.4 mm^3, the largest axis sometimes being longer.

Initially, crystals with Co^{2+} were grown under higher concentrations of the metal cation than was later found to be necessary. The crystal used for data collection,

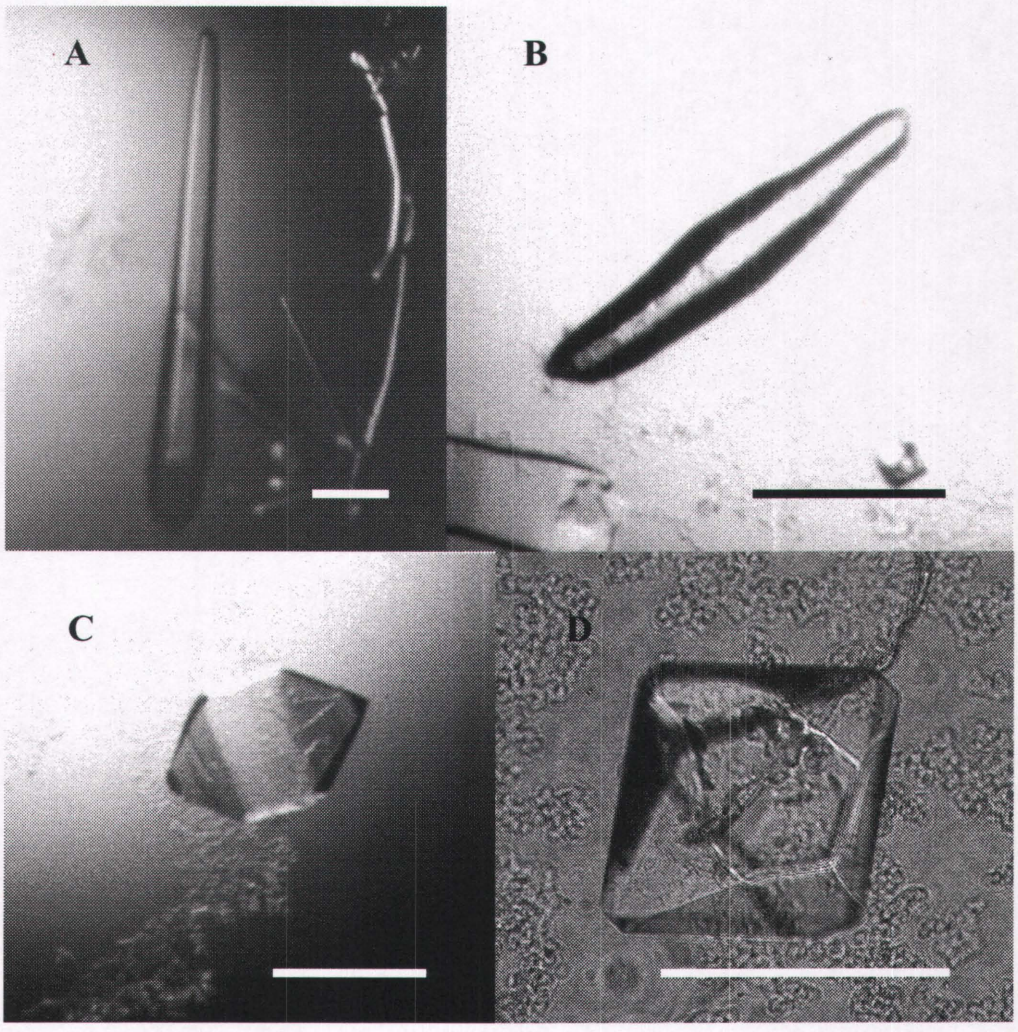

Figure 3.25. Crystals of d(GGCGCC) grown in the presence of Co^{2+}. Crystals were grown without Mg^{2+} (A) or in the presence of 10, 22.5 and 32.5 mM Mg^{2+} (B to D respectively). The scale bar in each photograph corresponds to a distance of approximately 0.2 mm.

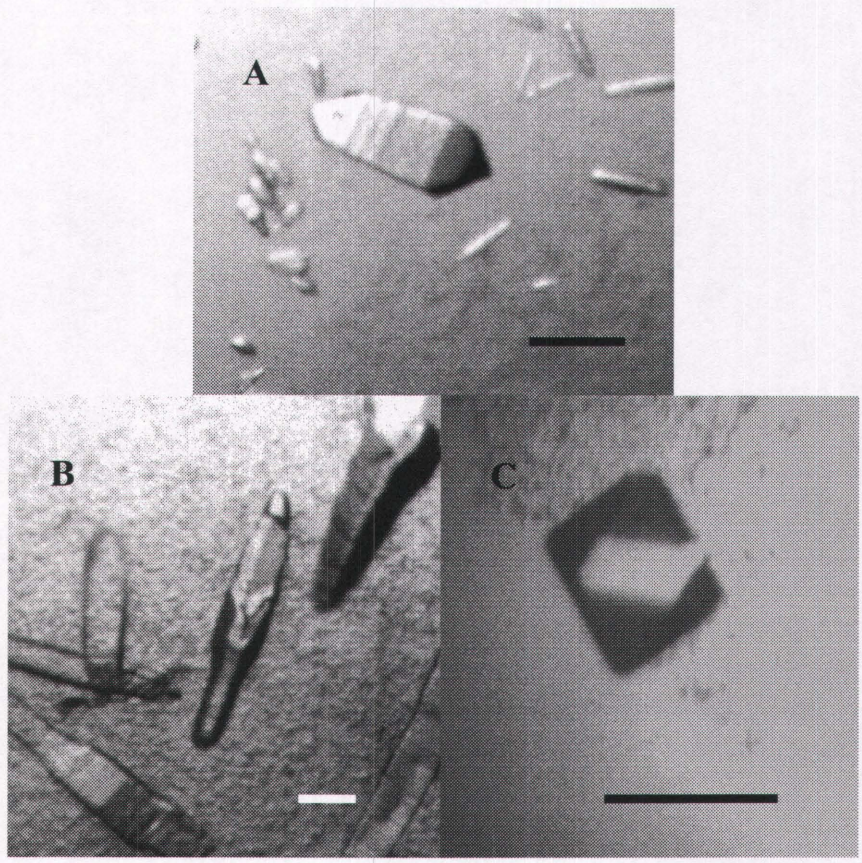

Figure 3.26. Crystals of d(GGCGCC) grown in the presence of Zn^{2+}. Crystals were grown in the presence of 0 (A), 20 (B) and 70 (C) mM Mg^{2+}. The image of the crystal grown without Mg^{2+} was taken after one month in order to demonstrate the pattern of cracking observed once crystals become aged. The scale bars represent distances of approximately 0.2 mm.

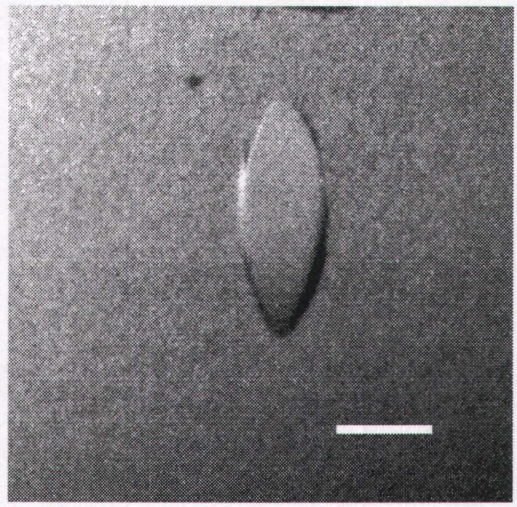

Figure 3.27. Crystal of d(GGCGCC) grown in the presence of Ni^{2+}. The scale bar represents a distance of approximately 0.2 mm.

for example, was grown in 25 mM $CoCl_2$ whereas it was later found to grow in a concentration under 10 mM. Although growth in this lower concentration of Co^{2+} resulted in little or no precipitate in the drops, the diffraction quality of the crystals was not enhanced so that new data sets were not collected with these. Crystals grown in the presence of Ni^{2+} and Zn^{2+} at 4 °C required metal chloride concentrations of only 3.75 mM and 2.25 mM respectively; higher concentrations did not result in better crystals but only precipitate.

Many different buffers were made use of during the crystallization experiments. These included TAPS, TRIS, HEPES and N,N-bis(2-hydroxyethyl)glycine (BICINE). Whereas TRIS always resulted in crystals and considerable precipitate, HEPES did not give satisfactory crystals and BICINE gave salt crystals in the presence of M^{2+}. Overall, TAPS gave the best results with regularly formed crystals and little or no precipitate. Like every other component, the buffer concentration as well as pH was optimized for each of the complexes. It was found that a buffer concentration of 50 mM was best for the Co^{2+} complex whereas 40 mM and 25 mM were best for the Ni^{2+} and Zn^{2+} complexes, respectively. Screens for pH typically used increments of 0.1 pH units. For Co^{2+}, a pH of 8.1 was ideal whereas for the Ni^{2+} and Zn^{2+} forms, pH 8.0 was best. The ideal pH values had a surprisingly small range. In general, pH values more than 0.2 pH units above ideality gave either no crystals or crystals that were very small or deformed. A pH more than about 0.2

pH units below ideality typically gave very large, fast growing crystals too fragile to mount for data collection. Testing the pH of the final drops with pH strips revealed that the pH was held constant except for the Co^{2+} form which was lowered to approximately 7.9. This is presumably due to the high concentration of the metal chloride that was used in this setup.

Like the crystals grown with Ni^{2+} or Zn^{2+}, those grown with Co^{2+} would also grow with MPD in the drop solution, which is the more usual procedure. They would also grow without MPD being present in the drop. Interestingly, the crystals with Co^{2+} also grew in the presence of glycerol in such a way that the concentration of Co^{2+} necessary for good crystal growth was found to be dependent on glycerol concentration (Figure 3.28). If too much of the metal chloride was present relative to glycerol concentration, the crystals grew very quickly but were fragile and cracked easily, being unusable for diffraction experiments. Conversely, if the metal chloride concentration was too low relative to the glycerol concentration, no crystals would grow. Although glycerol was not necessary for crystal growth, it was used because it acts as a cryoprotectant. It was thought that this would help during the cryoprotection procedure, but this was not found to be necessary in these experiments and glycerol was not used for growing crystals with Ni^{2+} or Zn^{2+}.

In an effort to improve diffraction quality, many different additives were added to the crystallization drops. These additives included sodium chloride, calcium

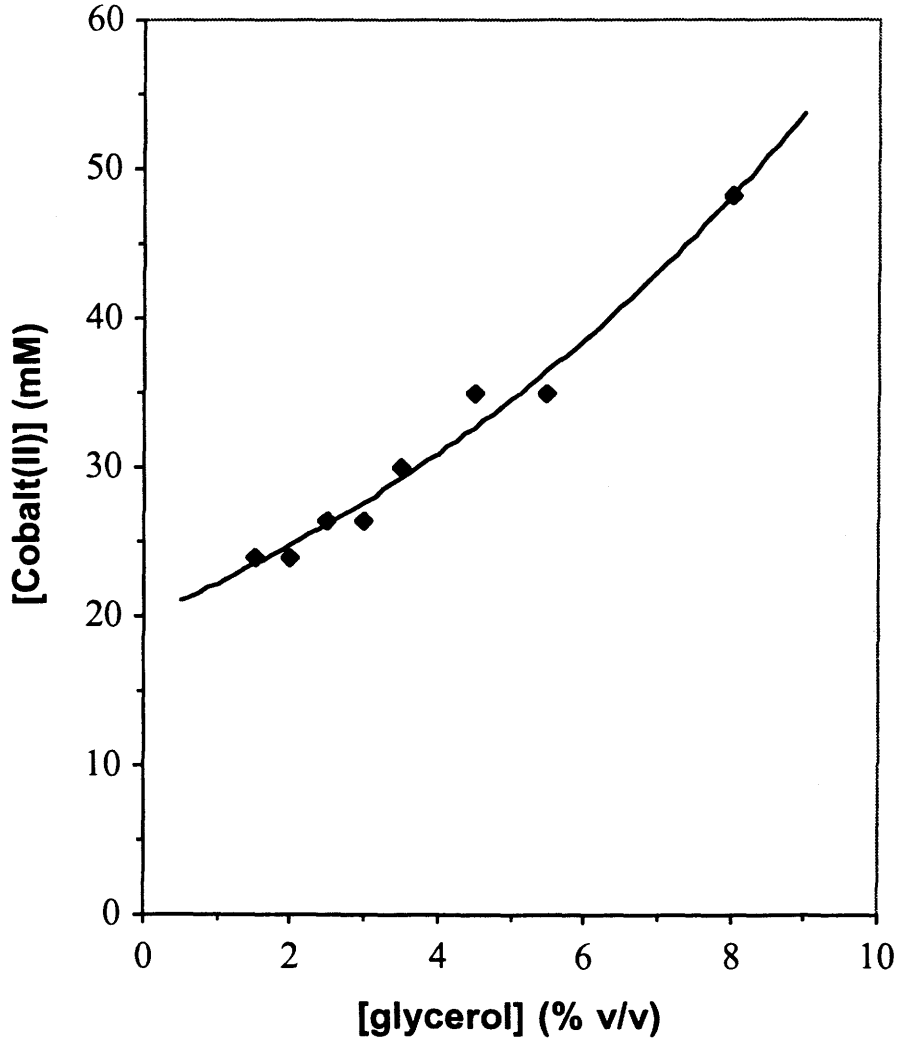

Figure 3.28. Dependence of Co^{2+} concentration on glycerol concentration for crystal growth. The trend line follows the equation $y = 19.9e^{0.11x}$ with $R^2 = 0.97$.

chloride, magnesium chloride, glucose, sucrose, potassium sulfate, sodium carbonate, spermine, spermidine, ethylene glycol, polyethylene glycol of various molecular weights, serinol, and various organic solvents including acetone, ethanol, propanol, butanol and methanol. These additives were added in concentrations of 1 mM or 5% (v/v) to the crystallization drops. In general, none of these additives visibly improved the crystal quality. There was one significant exception: the addition of magnesium chloride.

It was found that for the crystals grown in the presence of Co^{2+} or Zn^{2+}, Mg^{2+} addition resulted in crystals that were shaped more uniformly (see Figure 3.25 B to D and Figure 3.26 B and C). Without Mg^{2+}, crystals with these metal cations tended to grow very long, having one dimension sometimes more than 5 times longer than the shortest dimension. However, the longer dimensions of the crystals grown in the presence of Co^{2+} and Zn^{2+} shrunk when grown in increasing concentrations of Mg^{2+}. All dimensions became roughly proportional for both the Co^{2+} and Zn^{2+} complexes with 32.5 mM and 70 mM Mg^{2+}, respectively. For crystals grown in the presence of Ni^{2+}, the addition of Mg^{2+} did not have this effect but rather inhibited crystal growth entirely.

It was surprising that a diffraction experiment with a crystal grown in the presence of both Co^{2+} and Mg^{2+} resulted in no improvement of diffraction quality. Both the unit cell and the resolution limits were similar to those of the complex with

Co^{2+} alone. Because of this and because the presence of Mg^{2+} might also bind to the DNA or interfere with binding of the transition metal cations, it was decided to restrict further data collection to crystals grown without added Mg^{2+}.

3.4.2 Observations During Cryoprotection

Cryoprotection of the crystal samples was straightforward for crystals grown in the presence of any of the three M^{2+}. An MPD concentration of 55% in the cryoprotectant solution was found to give the best results. Concentrations lower than this would give an opaque appearance when dipped in liquid nitrogen whereas higher concentrations more often caused cracking of the crystals. If crystals were left sitting in the cryoprotectant solution for more than about 5 minutes, they would start to crack and appear opaque. Thus, transfer to liquid nitrogen was performed quickly (usually under 1 minute). If crystals that had been cooled in liquid nitrogen were warmed again by dipping into fresh cryoprotectant solution, they appeared clear with no cracking. If crystals that underwent this annealing procedure were re-cooled, no increase in diffraction quality was obtained.

3.4.3 Diffraction

Diffraction experiments gave similar results in all three cases. The observed diffraction pattern for the crystal grown in the presence of Ni^{2+} is shown as an

example (Figure 3.29). Simulated precession images were calculated from the diffraction data using the CCP4 program HKLVIEW (CCP4, 1994). Representations of the 0kl and hk0 planes are shown for the crystal grown in the presence of Co^{2+} (Figure 3.30). These images were very similar for crystals grown in the presence of any one of the three M^{2+}. It is apparent that the reflections 00l with l = 4n, 0k0 with k = 2n and h00 with h = 2n are present. This limits the possible space groups to $P4_12_12$ or $P4_32_12$. Rigid body refinement procedures did not result in a solution using the latter, but they did in $P4_12_12$, meaning that this is the correct space group for all three of the samples. Note also the strong stacking reflections between 3.7 and 2.8 Å.

3.4.4 Description of the Overall Structures

Refinement statistics are given in Table 3.1 and the R-factor at each refinement step in Table 3.2. All three structures have five single strands of DNA in the asymmetric unit giving the unit cell a total of 20 double helices. Stereo diagrams are shown for the Co^{2+} complex (Figure 3.31), the Ni^{2+} complex (Figure 3.32) and the Zn^{2+} complex (Figure 3.33). Note that one of the single strands in each asymmetric unit lies such that its complementary strand is generated by a crystallographic two-fold axis. Each duplex has six Watson-Crick base-pairs with no bases being extra-helical. The duplexes are stacked end-to-end into continuous columns with negative twist at the interhelical base-pair step. The columns are arranged diagonally within

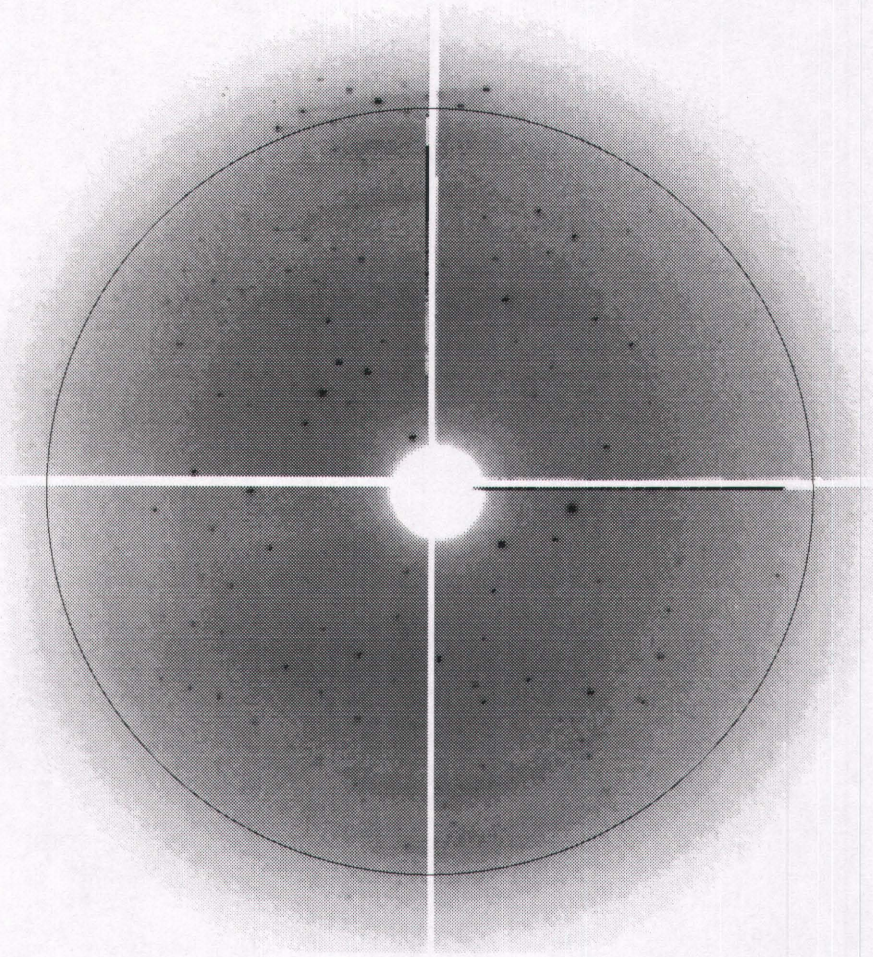

Figure 3.29. Diffraction observed for the d(GGCGCC) crystal grown in the presence of Ni^{2+}. This is a snapshot taken before data collection and is characterized by intense peaks at moderate to low resolution with a sharp drop in intensity at about 3 Å resolution. Crystals grown in the presence of Co^{2+} or Zn^{2+} gave diffraction patterns with similar characteristics. The circle shows an approximate resolution boundary of 3.5 Å.

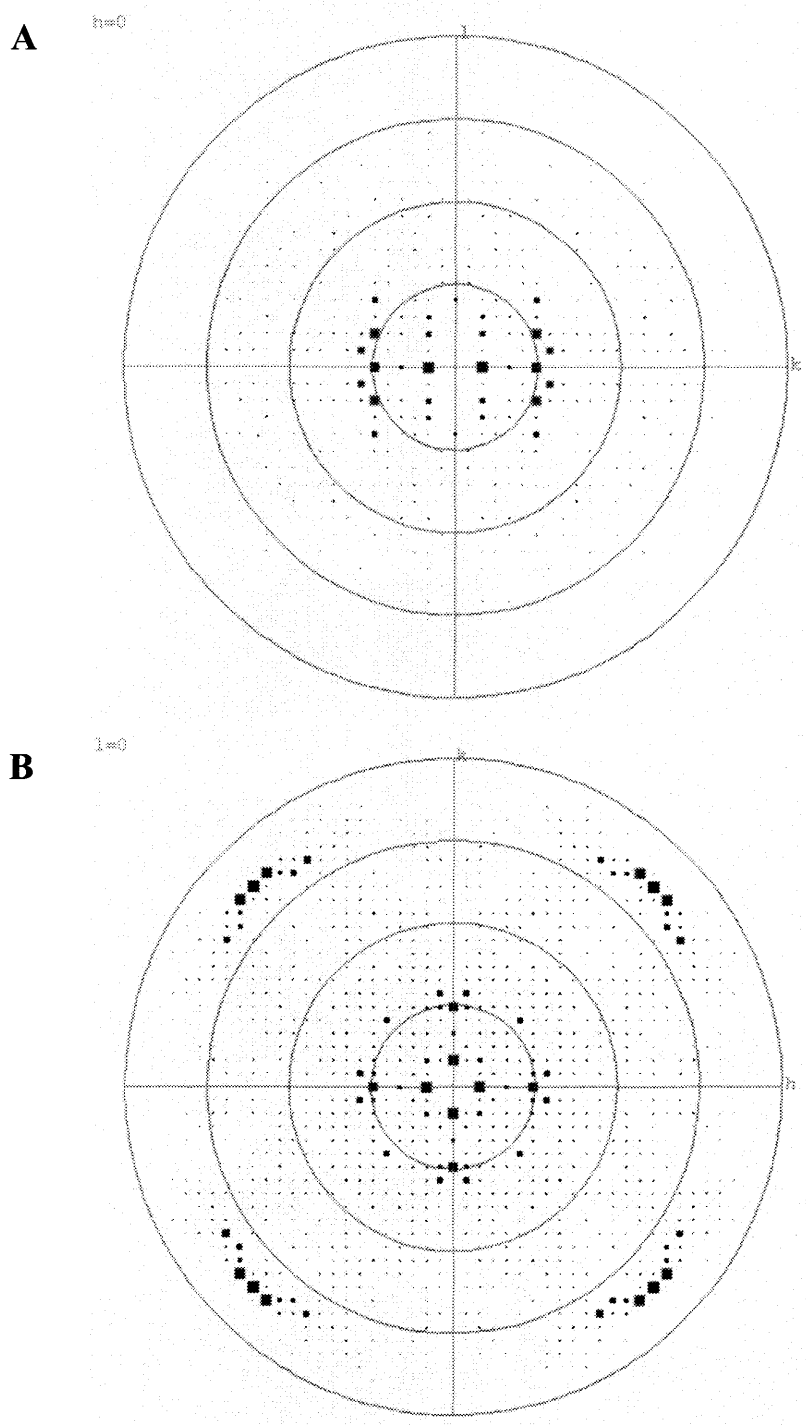

Figure 3.30. Simulated precession images calculated from the diffraction data for the crystal grown in the presence of Co^{2+}. Shown are the 0kl (A) and hk0 (B) planes. The circles show resolution boundaries of 2.8, 3.7, 5.6 and 11.2 Å (outside toward centre).

Table 3.1. Crystallographic and refinement parameters.

Parameter	Complex Co^{2+}	Ni^{2+}	Zn^{2+}
Crystallographic data			
Cell constants (Å)	a=68.94	a=68.99	a=68.80
	c=55.27	c=56.18	c=55.28
Solvent Content (%)	66.7	67.3	66.6
Refinement results			
Resolution range	15.0-3.0	15.0-2.9	15.0-2.9
Reflections in workset (F>2σ)	2021	2445	2350
Reflections in R_{free} set (F>2σ)	206	261	258
R_{work} (R_{free})	0.227 (0.286)	0.223 (0.276)	0.210 (0.264)
R-value over all reflections (F>0)	0.233	0.228	0.215
R.m.s.d. in bond lengths (Å)	0.013	0.016	0.015
R.m.s.d. in bond angles (°)	3.83	4.00	3.93
R.m.s.d in dihedral angles (°)	32.1	32.7	32.3
R.m.s.d in improper angles (°)	1.28	1.31	1.14
Mean B-factors ($Å^2$)			
All atoms	37.9	29.4	25.6
DNA atoms	37.7	29.1	25.0
Metal cations	49.7	36.4	32.5
Water oxygen atoms	39.7	34.5	38.7

Table 3.2. Progress of refinement.

Step	R_{work} (R_{free}) for complex Co^{2+}	Ni^{2+}	Zn^{2+}
1	0.424 (0.406)	0.447 (0.460)	0.462 (0.454)
2	0.419 (0.397)	0.445 (0.453)	0.456 (0.448)
3	0.306 (0.407)	0.333 (0.417)	0.331 (0.403)
4	0.281 (0.357)	0.288 (0.373)	0.286 (0.350)
5	0.255 (0.298)	0.261 (0.339)	0.273 (0.319)
6	0.249 (0.291)	0.247 (0.297)	0.236 (0.272)
7	0.243 (0.292)	0.231 (0.278)	0.214 (0.257)
8	0.231 (0.292)	0.223 (0.278)	0.209 (0.263)
9	0.227 (0.286)	0.223 (0.276)	0.210 (0.264)

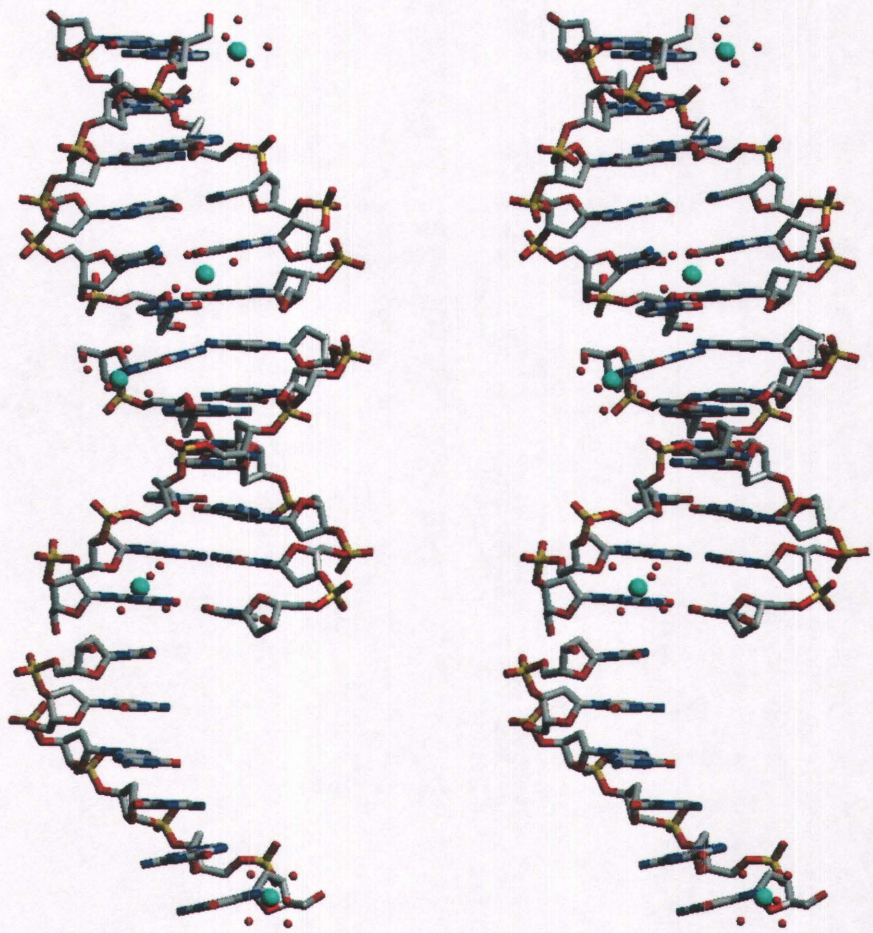

Figure 3.31. Stereo diagram of the asymmetric unit of the Co^{2+} complex. Co^{2+} cations are colored green, oxygen atoms red, phosphorus atoms yellow and carbon atoms gray. Starting from the bottom, Co^{2+} are bound to G residues G1, G7, G13, G19 and G25.

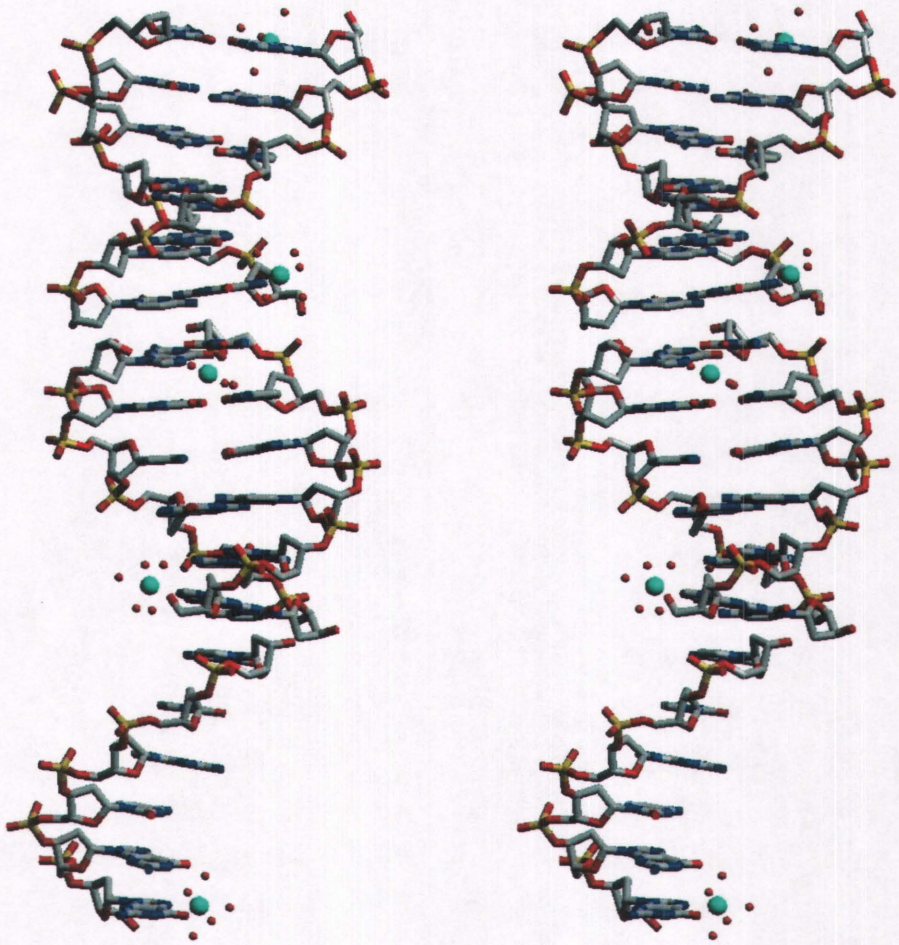

Figure 3.32. Stereo diagram of the asymmetric unit of the Ni^{2+} complex. See legend of Figure 3.31 for color scheme and numbering.

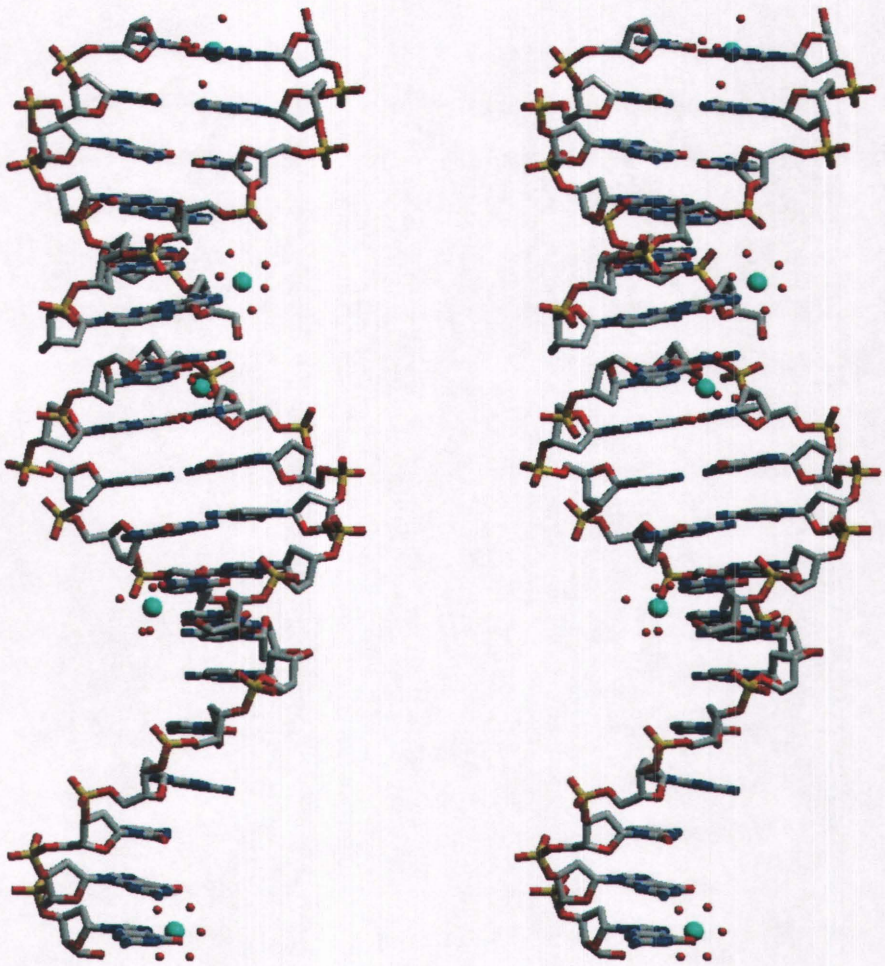

Figure 3.33. Stereo diagram of the asymmetric unit of the Zn^{2+} complex. See legend of Figure 3.31 for color scheme and numbering.

the *a-b* plane. When viewed along the *c* axis, the helices are observed to interact with each other at 90-degree angles with the phosphate backbone of one duplex interacting, *via* the metal complex, with the major groove of the other duplex (Figure 3.34). Overall, this arrangement is similar to the structure of the same sequence reported by Vargason *et al.* (2000) that was crystallized in the presence of spermine.

3.4.5 Description of M^{2+} Sites

In each of the three structures, five M^{2+} were located per asymmetric unit. Five water molecules surround each metal cation for a total of 25 in each asymmetric unit. These metal cations are bound to the N(7) positions of each terminal G residue (Figure 3.35). There are hydrogen bond interactions between water molecules and phosphate oxygen atoms from neighboring DNA strands (Figure 3.36 and Figure 3.37). This is the case with metal cations coordinated at positions G1, G7, G19 and G25. The other metal cation at position G13 does not come into close enough contact with any neighboring helices and therefore these interactions are absent. In each case, there is a hydrogen bond interaction between a water molecule from the metal ion's hydration sphere and the O(6) atom of the same G residue. The average bond distance for this interaction over all samples is 2.51 Å ± 0.08 Å (n = 15).

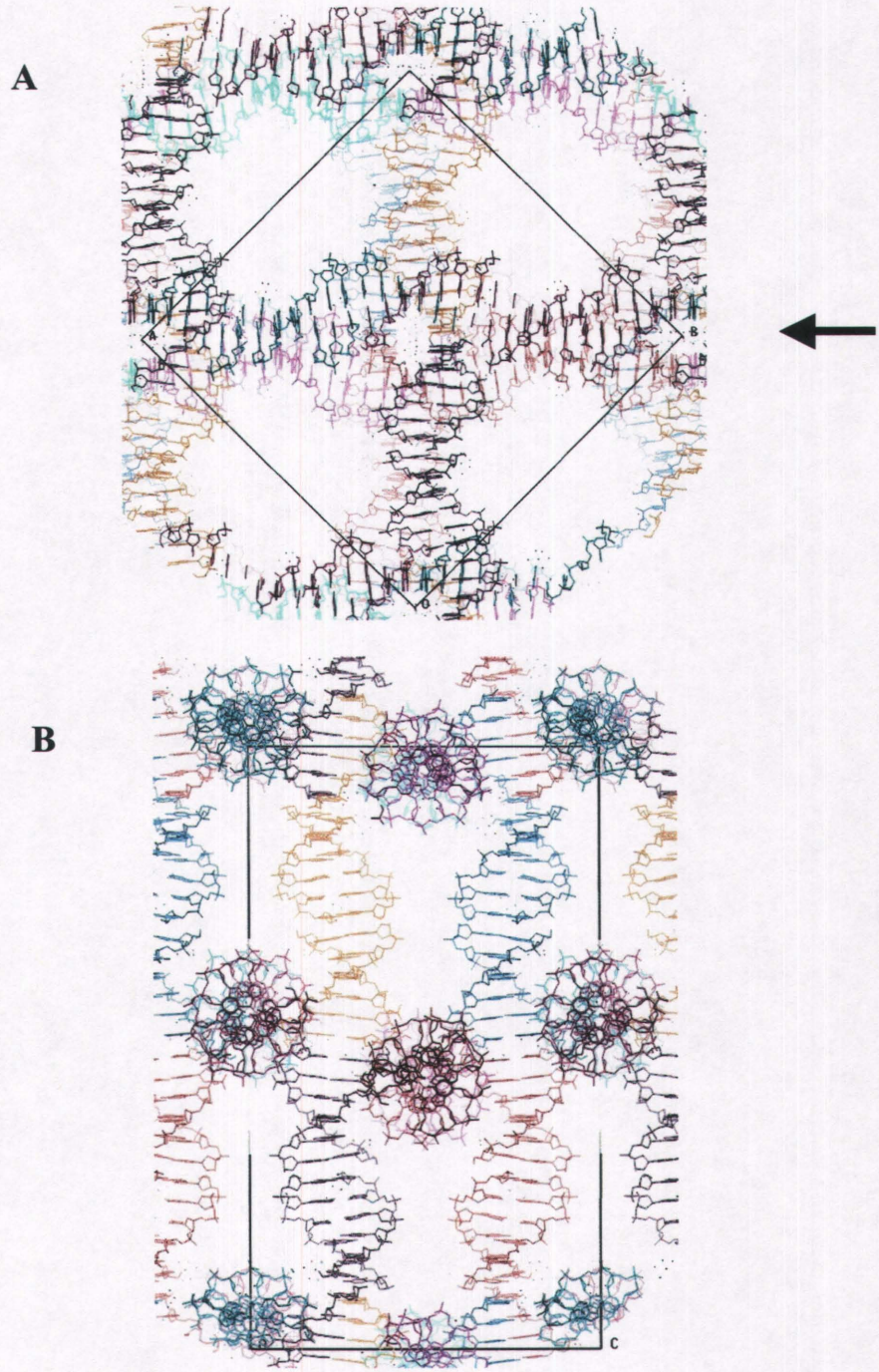

Figure 3.34. Packing of the DNA helices in the unit cell. (A) A unit cell of the Ni^{2+} complex structure is depicted as viewed along the *c*-axis. If the observer views the unit cell along the displayed arrow, the view is as shown in (B).

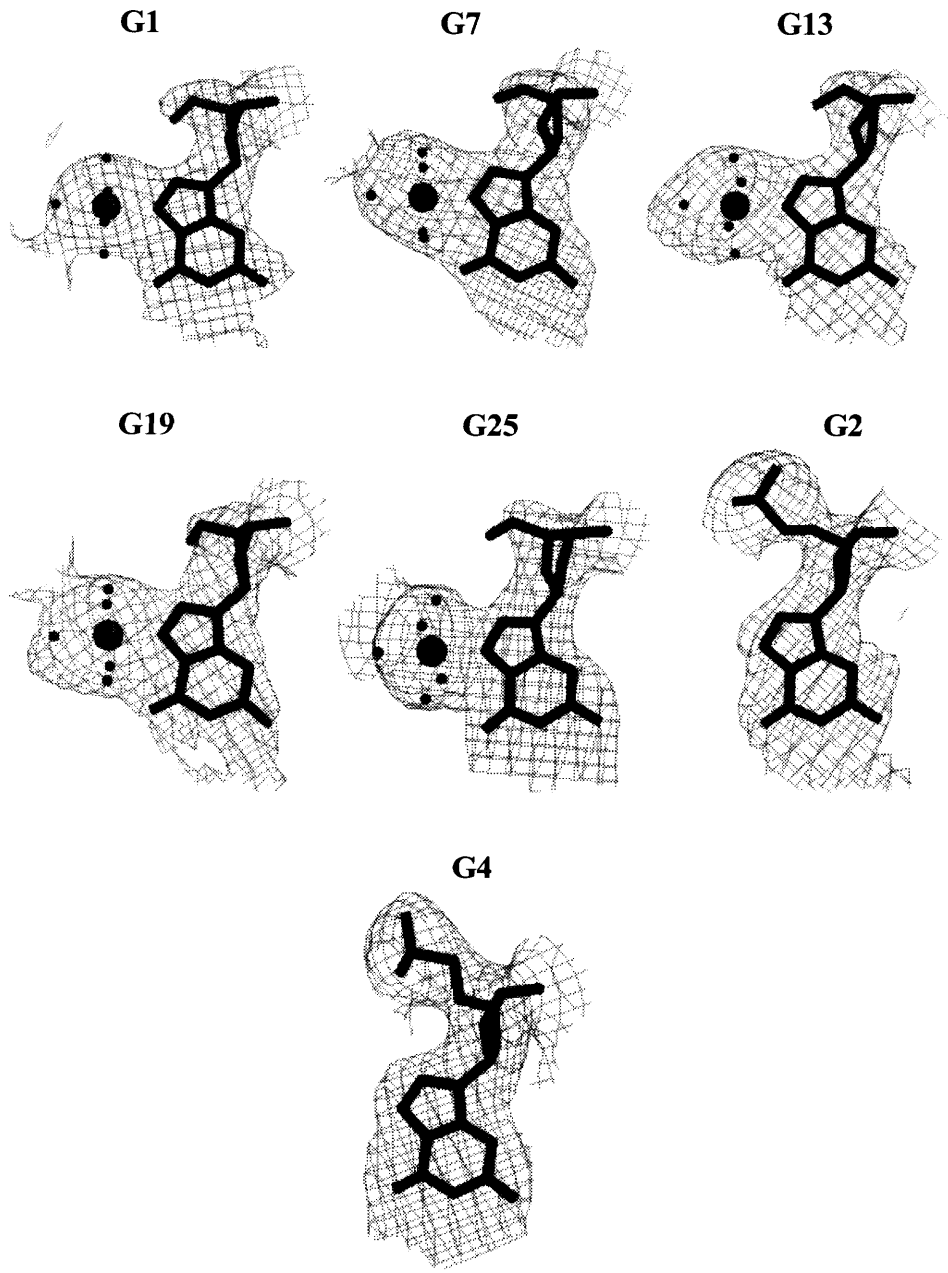

Figure 3.35. Electron density maps contoured around G residues to which M^{2+} are bound. Ni^{2+} cations are represented by large spheres while the associated water molecules are represented by the smaller spheres. Residue numbers are depicted above each image. Two G residues that do not bind M^{2+} (G2 and G4) are also given, showing no extra electron density next to N(7) positions. The $2F_O$-F_C electron density maps are contoured at 1σ.

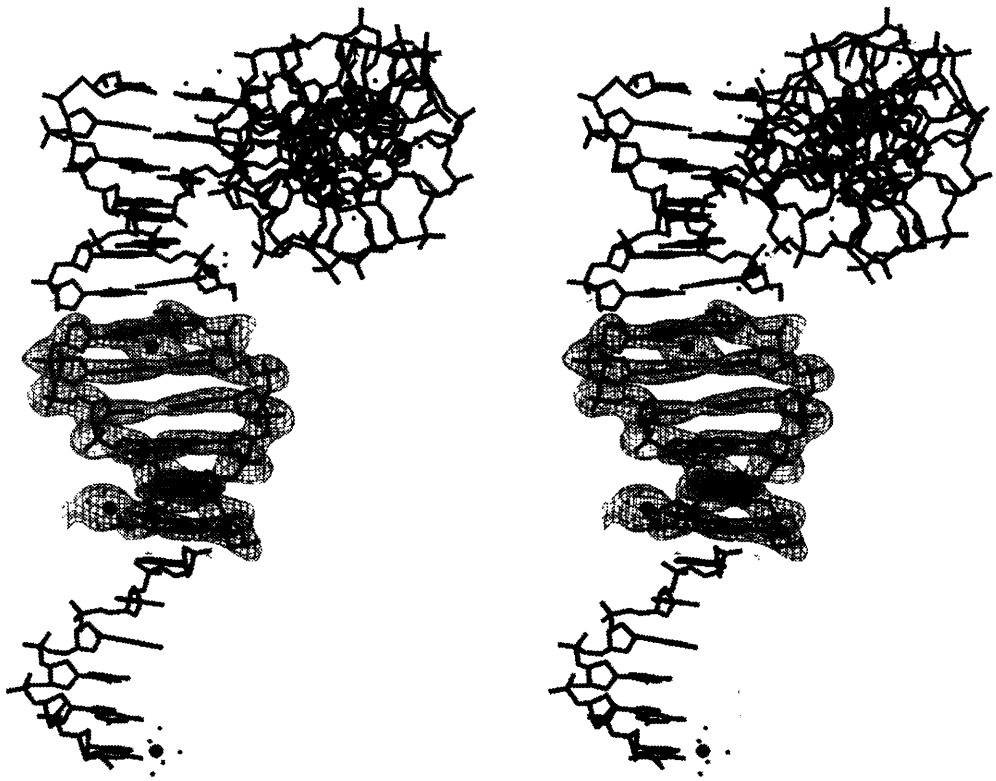

Figure 3.36. Interaction between duplexes in the crystal. An M^{2+} coordinated to G at position N(7) in the major groove of one duplex interacts with phosphate oxygen atoms of the other duplex *via* the cation's hydration sphere. Here, the atoms of the asymmetric unit of the Ni^{2+} complex are shown in a stereo view along with a neighboring symmetry-related duplex. A $2F_O$-F_C electron density map contoured at 1σ is shown for the central duplex (residues G7 to G18) in order to give some idea of the quality of the map.

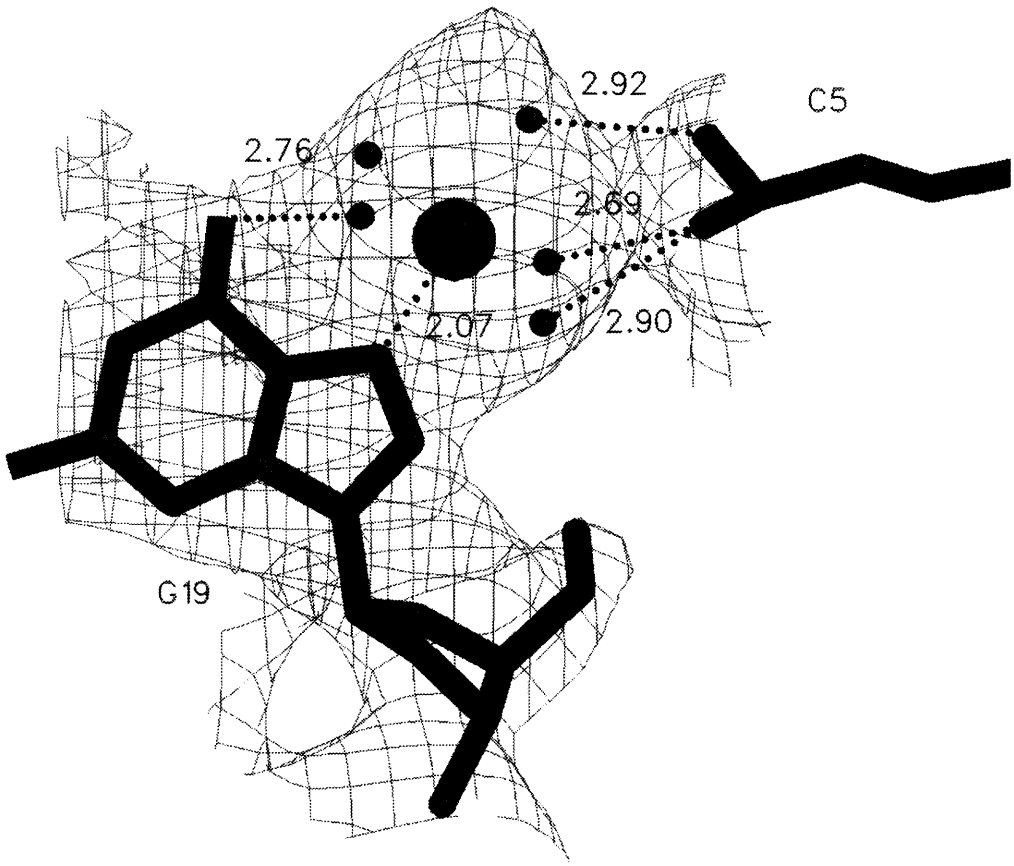

Figure 3.37. Close-up view of the interaction between a metal complex and a neighboring phosphate group. The M^{2+} is coordinated to the N(7) atom of residue G19 and interacts with neighboring phosphate oxygen atoms of residue C5 *via* the hydration sphere. Distances are given in Ångstroms between atoms that are involved in hydrogen bonding. The large sphere represents a nickel atom while the smaller spheres represent the oxygen atoms of water molecules. The $2F_O$-F_C electron density map is contoured at 1σ.

Analysis of the metal cation-N(7) bond distances (Table 3.3) reveals a range that falls within the expected values based on the x-ray crystallographic studies performed on nucleosides and nucleotides (Section 1.2.4).

3.4.6 Verification of M^{2+} Position Assignments

In all cases, the metal ion locations were positively verified. Removal of the metal cations along with their associated water molecules from the model, followed by the simulated annealing protocol resulted in an increase in both R_{work} and R_{free} in each case (Table 3.4). As well, both $2F_O$-F_C and F_O-F_C electron density maps showed strong density where the metal cations had been removed (Figure 3.38).

3.4.7 Quality of the Models

Because there are two and one half duplexes per asymmetric unit, helical parameters were calculated for three duplexes separately (two duplexes plus the single strand with its symmetry mate), then averaged. The base-pair parameters analyzed included tip (Table 3.5), inclination (Table 3.6), propeller twist (Table 3.7), buckle (Table 3.8), x-displacement (Table 3.9) and y-displacement (Table 3.10). The base-pair step parameters that were analyzed included tilt (Table 3.11), roll (Table 3.12), slide (Table 3.13) and twist (Table 3.14). For definitions of these terms and for typical values for B- and A-DNA see Figure 1.6 and Table 1.1, respectively. In each

Table 3.3. N(7)-M^{2+} bond lengths.

Residue	Bond length for complex (Å) Co^{2+}	Ni^{2+}	Zn^{2+}
G1	2.10	2.12	2.10
G7	2.09	2.06	2.08
G13	2.10	2.10	2.09
G19	2.09	2.07	2.10
G25	2.16	2.11	2.12
Mean	2.11	2.09	2.10

Table 3.4. Verification of the metal binding sites.

Sites tested	R_{work} (R_{free}) for complex Co^{2+}	Ni^{2+}	Zn^{2+}
G1 + G13	0.272 (0.304)	0.277 (0.327)	0.257 (0.299)
G7 + G19	0.273 (0.312)	0.277 (0.321)	0.259 (0.304)
G13 + G25	0.264 (0.297)	0.272 (0.317)	0.251 (0.300)

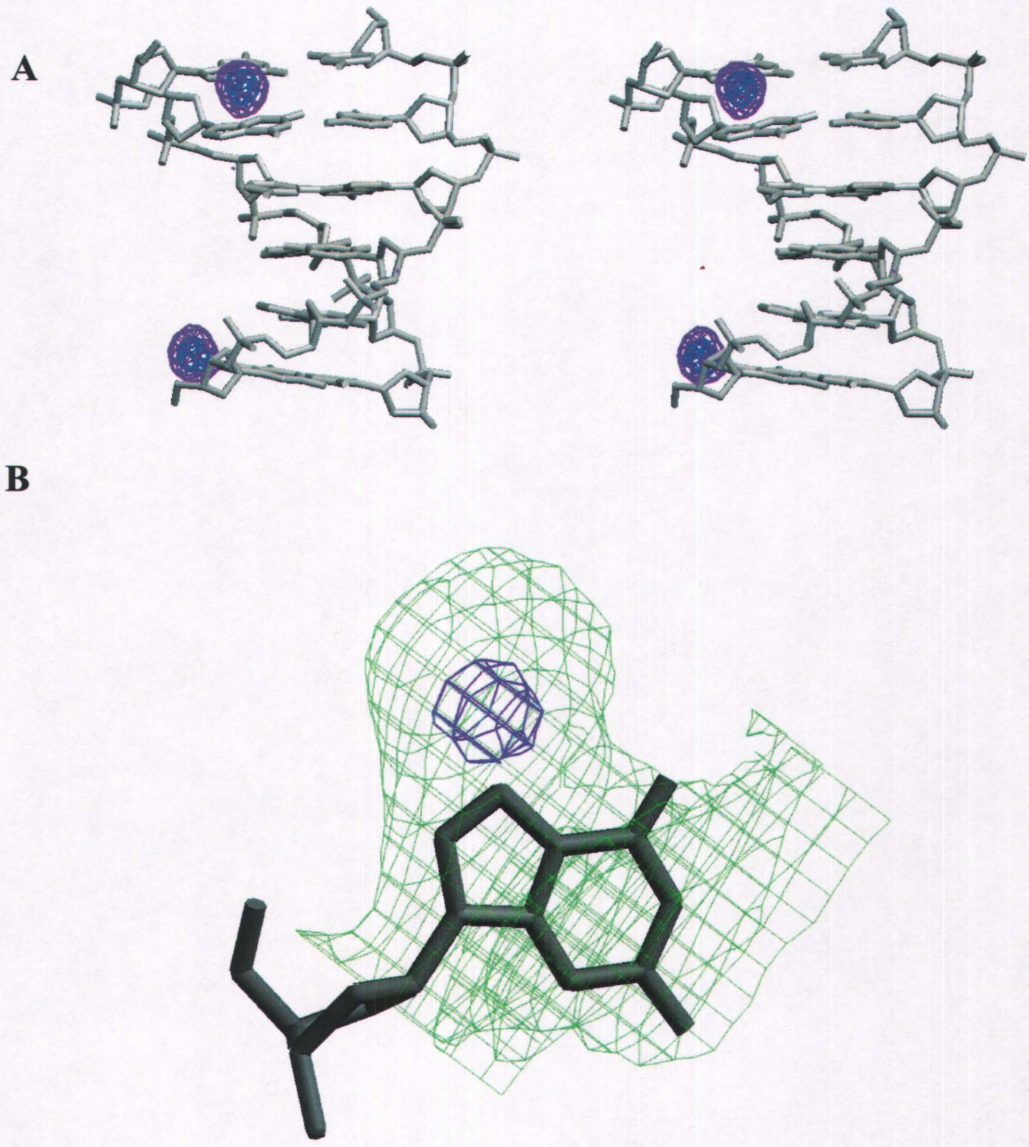

Figure 3.38. Verification of the M^{2+} positions. (A) The single strand of DNA that lies on the two-fold crystallographic axis is shown along with its symmetry mate. Removal of the M^{2+} was followed by a simulated annealing protocol and difference maps unambiguously confirm the location of the M^{2+} bound to residue G1. (B) Close-up view of residue G13 after the same procedure. The $2F_O$-F_C electron density map is contoured at 1σ and is depicted in green. The F_O-F_C electron density maps are contoured at 5σ and 7σ and are depicted in violet and dark blue, respectively.

Table 3.5. Analysis of tip for each base-pair*.

Helix	Tip for base-pair (°) 1	2	3	4	5	6
Co^{2+} structure						
AA	-0.49	-2.21	-0.08	0.09	2.21	0.49
BC	3.37	-2.76	-1.34	-3.12	-5.72	1.97
DE	-1.46	-3.31	1.00	2.08	4.15	0.13
Mean	0.47	-2.76	-0.14	-0.32	0.21	0.86
Ni^{2+} structure						
AA	2.45	0.33	-0.58	0.57	-0.34	-2.46
BC	0.70	-0.40	-0.40	-1.17	-4.48	-0.66
DE	-4.59	-1.27	-0.50	-0.12	-0.36	-3.39
Mean	-0.48	-0.45	-0.49	-0.24	-1.73	-2.17
Zn^{2+} structure						
AA	3.19	-0.49	-0.39	0.33	0.46	-3.19
BC	0.94	1.25	-0.89	-2.49	-4.86	-2.97
DE	-1.69	-0.51	1.42	-1.13	1.04	-1.55
Mean	0.81	0.08	0.05	-1.10	-1.12	-2.57
Average tip over all Co^{2+}, Ni^{2+} and Zn^{2+} samples						
Base-pairs with no M^{2+}:	-0.67 ± 2.01 (n=36)					
Base-pairs with M^{2+}:	-0.51 ± 2.35 (n=18)					

* In all of these analysis tables, the helix is defined by the strands of which it is composed. Thus helix AA refers to the double helix composed of strand A and its crystallographic symmetry mate. Similarly, helix BC refers to the helix composed of strand B and strand C. The base-pairs are listed from the 5' end to the 3' end of the first strand for each helix. The global helix axis was generated using C1' and N9 of purines, and C1' and N1 of pyrimidines. Mean values are given with sample standard deviations.

Table 3.6. Analysis of inclination for each base-pair.

Helix	Inclination for base-pair (°) 1	2	3	4	5	6
Co^{2+} structure						
AA	10.50	9.39	8.57	8.58	9.40	10.50
BC	8.71	6.59	8.90	9.07	7.85	9.58
DE	5.34	4.79	6.87	7.23	6.19	8.15
Mean	8.18	6.92	8.11	8.29	7.81	9.41
Ni^{2+} structure						
AA	9.28	9.12	7.99	7.99	9.12	9.25
BC	8.25	5.61	8.07	9.20	6.95	8.25
DE	9.04	6.71	6.59	7.21	6.14	6.33
Mean	8.86	7.15	7.55	8.13	7.40	7.94
Zn^{2+} structure						
AA	10.40	10.67	10.47	10.45	10.61	10.32
BC	8.07	8.27	9.40	9.76	7.80	9.41
DE	6.91	6.00	7.67	8.72	6.18	7.86
Mean	8.46	8.31	9.18	9.64	8.20	9.20

Average inclination over all Co^{2+}, Ni^{2+} and Zn^{2+} samples

Base-pairs with no M^{2+}:	8.06 ± 1.53	(n=36)
Base-pairs with M^{2+}:	8.68 ± 1.45	(n=18)

Table 3.7. Analysis of propeller twist for each base-pair.

Helix	Propeller twist for base-pair (°) 1	2	3	4	5	6
Co^{2+} structure						
AA	-4.95	-3.60	9.14	9.12	-3.70	-5.07
BC	-3.82	-0.68	2.39	-1.30	0.27	-11.73
DE	0.44	9.53	-8.37	-1.71	6.63	0.04
Mean	-2.78	1.75	1.05	2.04	1.07	-5.59
Ni^{2+} structure						
AA	-5.06	-3.18	-0.76	-0.83	-3.39	-5.33
BC	-11.89	-4.99	-2.28	-0.52	-3.50	-6.09
DE	-9.53	-0.32	-4.75	-2.29	5.56	-3.86
Mean	-8.83	-2.83	-2.60	-1.21	-0.44	-5.09
Zn^{2+} structure						
AA	-5.54	-3.64	-8.04	-8.07	-3.69	-5.60
BC	-4.98	-2.28	-4.35	-3.76	-3.28	-6.21
DE	-2.29	-2.26	-0.63	-0.80	6.02	-5.76
Mean	-4.27	-2.73	-4.34	-4.21	-0.32	-5.86

Average propeller twist over all Co^{2+}, Ni^{2+} and Zn^{2+} samples

Base-pairs with no M^{2+}: -1.06 ± 4.60 (n=36)

Base-pairs with M^{2+}: -5.40 ± 3.25 (n=18)

Table 3.8. Analysis of buckle for each base-pair.

Helix	Buckle for base-pair (°) 1	2	3	4	5	6
Co^{2+} structure						
AA	-10.52	1.77	9.92	-10.03	-1.86	10.52
BC	3.76	2.55	3.70	-6.19	-5.47	13.87
DE	7.68	2.35	-4.30	-0.52	4.66	-3.28
Mean	0.31	2.22	3.11	-5.58	-0.89	7.04
Ni^{2+} structure						
AA	2.85	-4.90	1.37	-1.64	4.73	-2.89
BC	-2.07	2.12	3.66	-6.50	-0.04	10.03
DE	-0.50	-1.32	-2.89	-0.68	-1.12	1.42
Mean	0.09	-1.37	0.71	-2.94	1.19	2.85
Zn^{2+} structure						
AA	-0.02	-1.73	2.72	-2.76	1.70	0.01
BC	0.81	3.72	4.16	-2.46	-2.28	10.37
DE	-2.87	-0.96	2.78	-4.57	-0.39	-1.08
Mean	-0.69	0.34	3.22	-3.26	-0.32	3.10
Average buckle over all Co^{2+}, Ni^{2+} and Zn^{2+} samples						
Base-pairs with no M^{2+}:	-0.30 ± 3.97	(n=36)				
Base-pairs with M^{2+}:	2.12 ± 6.22	(n=18)				

Table 3.9. Analysis of x-displacement for each base-pair.

Helix	X-displacement for base-pair (Å) 1	2	3	4	5	6
Co^{2+} structure						
AA	-1.12	-1.19	-1.55	-1.55	-1.19	-1.12
BC	-1.18	-1.29	-0.64	-0.72	-1.17	-0.71
DE	-0.22	-1.07	-0.69	-0.67	-1.58	-1.48
Mean	-0.84	-1.18	-0.96	-0.98	-1.31	-1.10
Ni^{2+} structure						
AA	-1.05	-0.90	-1.38	-1.38	-0.90	-1.05
BC	-1.02	-1.21	-0.76	-0.42	-1.08	-0.94
DE	-0.44	-1.16	-0.63	-0.50	-1.09	-1.08
Mean	-0.84	-1.09	-0.92	-0.77	-1.02	-1.02
Zn^{2+} structure						
AA	-1.25	-1.01	-1.49	-1.49	-1.01	-1.25
BC	-1.12	-1.20	-0.83	-0.59	-1.19	-0.71
DE	-0.54	-1.42	-0.86	-0.75	-1.36	-1.45
Mean	-0.97	-1.21	-1.06	-0.94	-1.19	-1.14
Average x-displacement over all Co^{2+}, Ni^{2+} and Zn^{2+} samples						
Base-pairs with no M^{2+}:	-1.05 ± 0.33 (n=36)					
Base-pairs with M^{2+}:	-0.99 ± 0.34 (n=18)					

Table 3.10. Analysis of y-displacement for each base-pair.

Helix	Y-displacement for base-pair (Å) 1	2	3	4	5	6
Co^{2+} structure						
AA	0.03	0.14	-0.09	0.09	-0.14	-0.03
BC	0.39	0.27	-0.27	0.35	0.47	-0.22
DE	-0.57	-0.66	-0.22	-0.48	-0.50	-0.49
Mean	-0.05	-0.08	-0.19	-0.01	-0.06	-0.25
Ni^{2+} structure						
AA	0.15	-0.09	-0.17	0.17	0.10	-0.15
BC	0.18	0.09	-0.25	0.14	0.19	0.01
DE	-0.25	-0.11	-0.08	-0.47	-0.10	0.00
Mean	0.03	-0.04	-0.17	-0.05	0.06	-0.05
Zn^{2+} structure						
AA	0.20	0.06	-0.35	0.35	-0.05	-0.20
BC	0.27	0.12	-0.20	0.23	-0.13	-0.33
DE	-0.40	-0.42	0.06	-0.33	-0.57	-0.09
Mean	0.02	-0.08	-0.16	0.08	-0.25	-0.21
Average y-displacement over all Co^{2+}, Ni^{2+} and Zn^{2+} samples						
Base-pairs with no M^{2+}:	-0.08 ± 0.28 (n=36)					
Base-pairs with M^{2+}:	-0.08 ± 0.27 (n=18)					

Table 3.11. Analysis of tilt for each base-pair step.

Helix	Tilt for base-pair step (°) 1	2	3	4	5
Co^{2+} structure					
AA	-0.10	0.11	0.01	-0.10	0.10
BC	-2.24	2.51	1.93	1.73	1.92
DE	1.03	2.25	-0.49	-2.74	0.89
Mean	-0.44	1.62	0.48	-0.37	0.97
Ni^{2+} structure					
AA	-0.95	-0.72	0.02	0.74	0.93
BC	-2.44	2.38	1.72	-0.47	2.56
DE	-0.60	0.52	0.84	-0.91	1.23
Mean	-1.33	0.73	0.86	-0.21	1.57
Zn^{2+} structure					
AA	-0.50	0.27	-0.02	-0.30	0.48
BC	-0.55	0.85	1.62	0.02	3.88
DE	-0.01	1.30	0.93	-2.50	1.75
Mean	-0.35	0.81	0.84	-0.93	2.04
Average tilt over all Co^{2+}, Ni^{2+} and Zn^{2+} samples					
Base-steps with no M^{2+}:	0.43 ± 1.32	(n=27)			
Base-steps with M^{2+}:	0.41 ± 1.58	(n=18)			

Table 3.12. Analysis of roll for each base-pair step.

Helix	Roll for base-pair step (°) 1	2	3	4	5
Co^{2+} structure					
AA	4.34	6.46	5.44	6.47	4.36
BC	-0.91	5.80	4.38	2.92	12.30
DE	1.36	7.67	5.26	6.15	-0.42
Mean	1.60	6.64	5.03	5.18	5.41
Ni^{2+} structure					
AA	2.84	4.17	5.66	4.19	2.86
BC	3.38	4.21	4.59	1.70	8.24
DE	7.39	4.86	4.20	3.68	0.61
Mean	4.54	4.41	4.82	3.19	3.90
Zn^{2+} structure					
AA	2.36	5.73	7.09	5.72	2.34
BC	5.35	3.16	4.75	2.44	6.14
DE	4.79	6.10	2.43	6.08	1.52
Mean	4.17	5.00	4.76	4.75	3.33
Average roll over all Co^{2+}, Ni^{2+} and Zn^{2+} samples					
Base-steps with no M^{2+}:	4.86 ± 1.50	(n=27)			
Base-steps with M^{2+}:	3.83 ± 3.27	(n=18)			

Table 3.13. Analysis of slide for each base-pair step.

Helix	Slide for base-pair step (Å) 1	2	3	4	5
Co^{2+} structure					
AA	-0.08	-0.41	-0.28	-0.41	-0.08
BC	-0.44	-0.60	0.65	-0.02	-0.74
DE	-0.18	0.28	-0.22	-0.37	-0.32
Mean	-0.23	-0.24	0.05	-0.27	-0.38
Ni^{2+} structure					
AA	-0.19	-0.26	0.04	-0.26	-0.19
BC	-0.40	-0.52	0.50	0.05	-0.39
DE	0.13	-0.16	-0.29	0.27	-0.16
Mean	-0.15	-0.31	0.08	0.02	-0.25
Zn^{2+} structure					
AA	-0.14	-0.46	0.40	-0.47	-0.14
BC	-0.41	-0.38	0.50	-0.33	-0.22
DE	-0.22	0.10	-0.36	-0.37	0.07
Mean	-0.26	-0.25	0.18	-0.39	-0.10
Average slide over all Co^{2+}, Ni^{2+} and Zn^{2+} samples					
Base-steps with no M^{2+}:	-0.13 ± 0.35	(n=27)			
Base-steps with M^{2+}:	-0.23 ± 0.20	(n=18)			

Table 3.14. Analysis of twist for each base-pair step.

Helix	Twist for base-pair step (°) 1	2	3	4	5
Co^{2+} structure					
AA	34.46	27.82	36.64	27.87	34.56
BC	35.93	29.64	41.36	36.51	29.93
DE	36.04	33.39	35.53	34.85	28.02
Mean	35.48	30.28	37.84	33.08	30.84
Ni^{2+} structure					
AA	30.79	32.36	35.65	32.48	30.93
BC	35.86	34.09	37.62	34.24	34.28
DE	31.03	35.45	33.16	33.64	33.30
Mean	32.56	33.97	35.48	33.45	32.84
Zn^{2+} structure					
AA	32.57	30.05	36.61	30.00	32.48
BC	35.98	32.61	40.38	30.28	30.17
DE	32.24	36.20	34.32	31.22	33.84
Mean	33.60	32.95	37.10	30.50	32.16
Average twist over all Co^{2+}, Ni^{2+} and Zn^{2+} samples					
Base-steps with no M^{2+}:	33.85 ± 3.38 (n=27)				
Base-steps with M^{2+}:	32.91 ± 2.40 (n=18)				

case, values are given for each base-pair or base-pair step for each of the three structures. A mean value is given for each of the base-pairs or base-pair steps. Each table also contains the mean value for the base-pair or base-pair step either when complexed to a metal cation or not.

In general, there were only minor differences between the three structures and that of the Vargason *et al.* (2000) model that was used as a starting point and all of the values fall within the normal range for B-DNA (Table 1.1) except propeller twist, which has a somewhat less negative value. The Co^{2+}, Ni^{2+} and Zn^{2+} structures have 10.60, 10.61 and 10.65 residues per turn, respectively. These values are slightly larger than that of the Vargason *et al.* (2000) structure with spermine which has approximately 10.38 residues per turn when calculated in the same manner. It should be noted, however, that the data for the crystals with the metal cations were collected at 110 K, whereas the data of the structure with spermine were collected at room temperature.

Another significant feature is the hydrogen bond interaction of the metal cation-bound water with the O(6) atom of the G residue 3' to the one to which the cation is coordinated (Figure 3.39). For this interaction, the bond lengths are 3.09 Å ± 0.36 Å (n=15). Although this represents relatively weak hydrogen bonding, it seems to stabilize a mean propeller twist of –5.40° ± 3.25° (n=18, mean taken over all base-pairs having a coordinated M^{2+}). The base-pairs with no coordinated metal cations

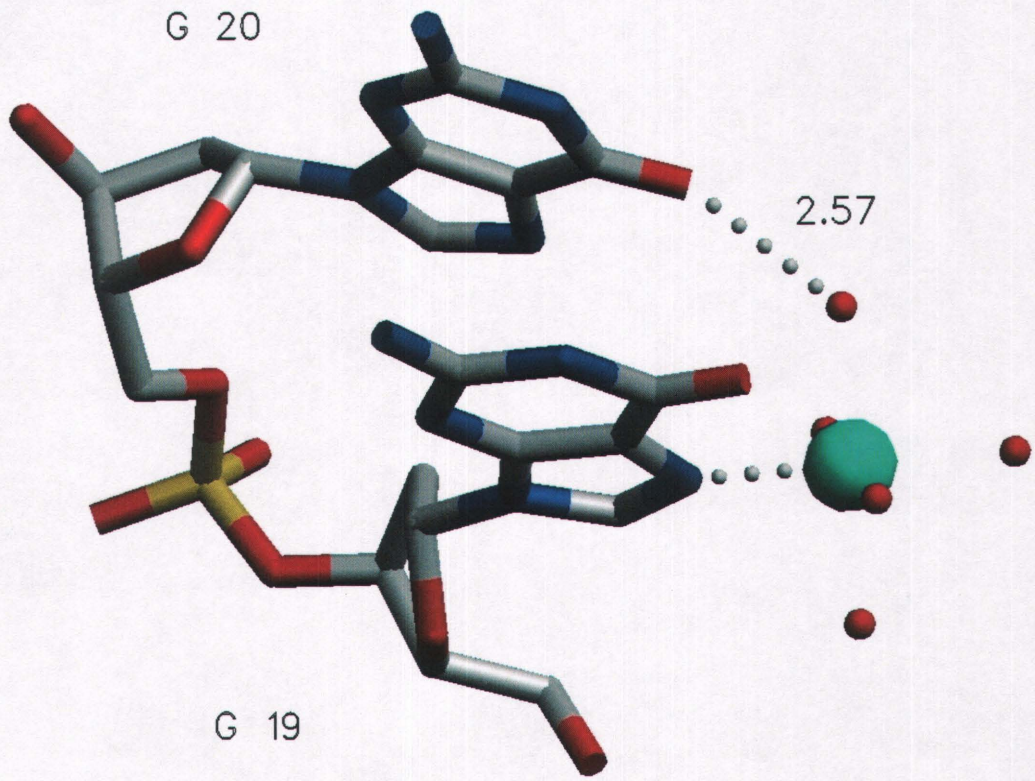

Figure 3.39. The interaction of the M^{2+} with O(6) of the G residue on the 3' side. Here, water molecules coordinated to a Ni^{2+} cation bound to residue G19 are within hydrogen bonding distance to O(6) of residue G20. See Figure 3.31 for color scheme. The bond length distance is given in Ångstroms.

show a mean propeller twist of −1.06° ± 4.60° (n=36). Analysis of the hydrogen bonding distances between Watson-Crick base-pairs reveals the distribution shown in Figure 3.40. The mean values are 2.79 Å ± 0.22 Å, 2.68 Å ± 0.14 Å and 2.74 Å ± 0.14 Å (n = 54 for each) for the Co^{2+}, Ni^{2+} or Zn^{2+} samples, respectively. These values fall within the range expected for DNA base-pairs (Saenger, 1984).

3.5 Crystallization of d[GA(5FU)(5FU)AA(5FU)C] with Co^{2+}

Crystals of d[GA(5FU)(5FU)AA(5FU)C] grew at 4°C as described in Section 2.4.3 in the presence of Co^{2+} (Figure 3.41). They grew over a period of about one week as rectangular prisms having approximate maximum dimensions of 0.1 X 0.08 X 0.03 mm^3. A diffraction experiment on a cryoprotected crystal showed only weak diffraction (Figure 3.42) with intensity peaks indicating at least one relatively long unit cell axis. The maximum resolution observed was approximately 7 Å. Additional data were not collected on these samples because the intensity peaks could not be indexed and a unit cell could not be calculated.

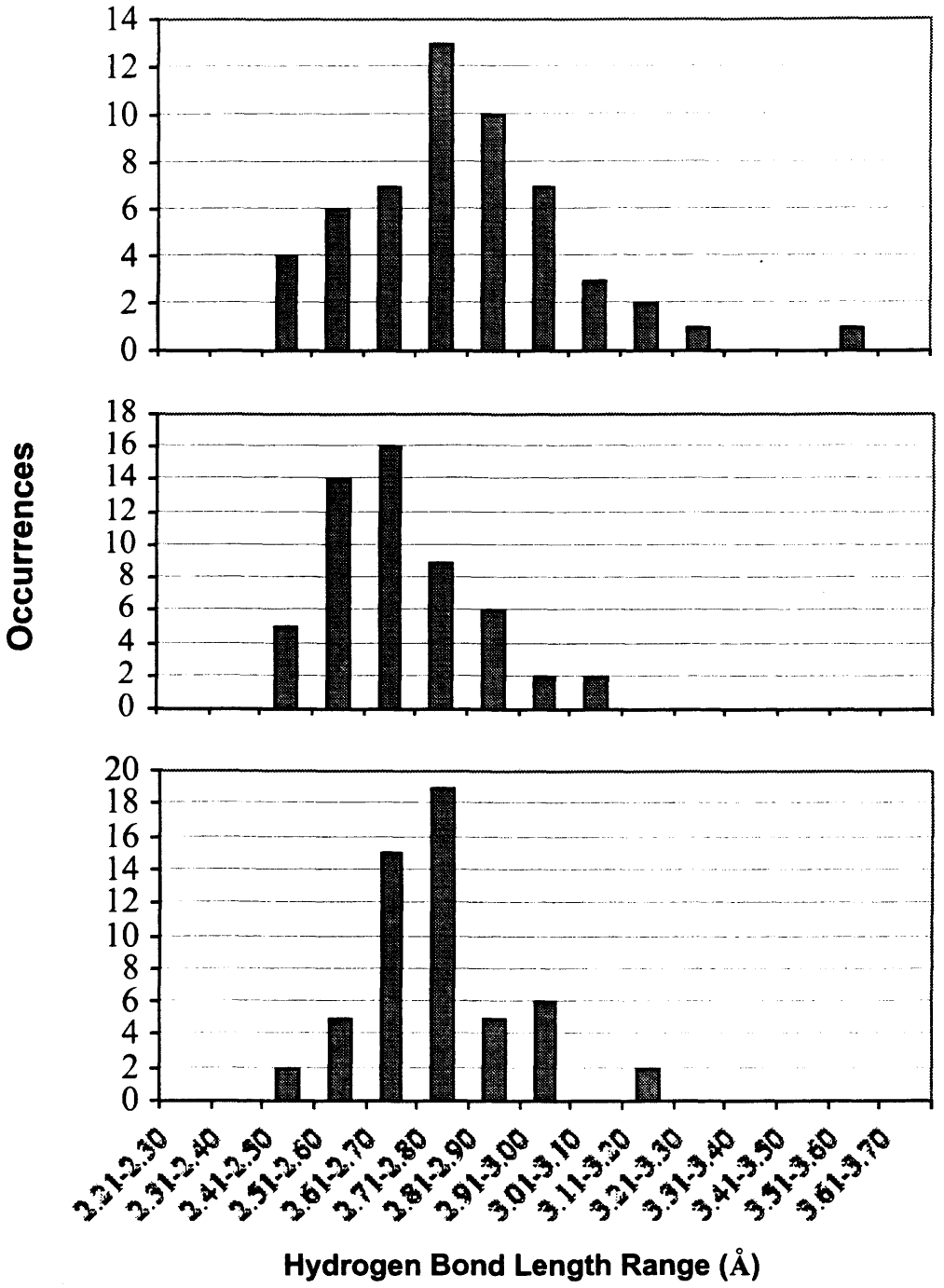

Figure 3.40. Distribution of base-pair hydrogen bond lengths. The top graph represents values for the Co^{2+} complex, the middle for Ni^{2+} and the bottom for Zn^{2+}.

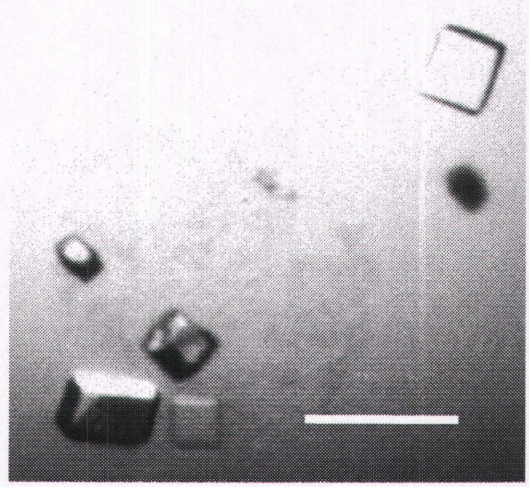

Figure 3.41. Crystals of d[GA(5FU)(5FU)AA(5FU)C] grown in the presence of Co^{2+}. The scale bar represents a distance of about 0.2 mm.

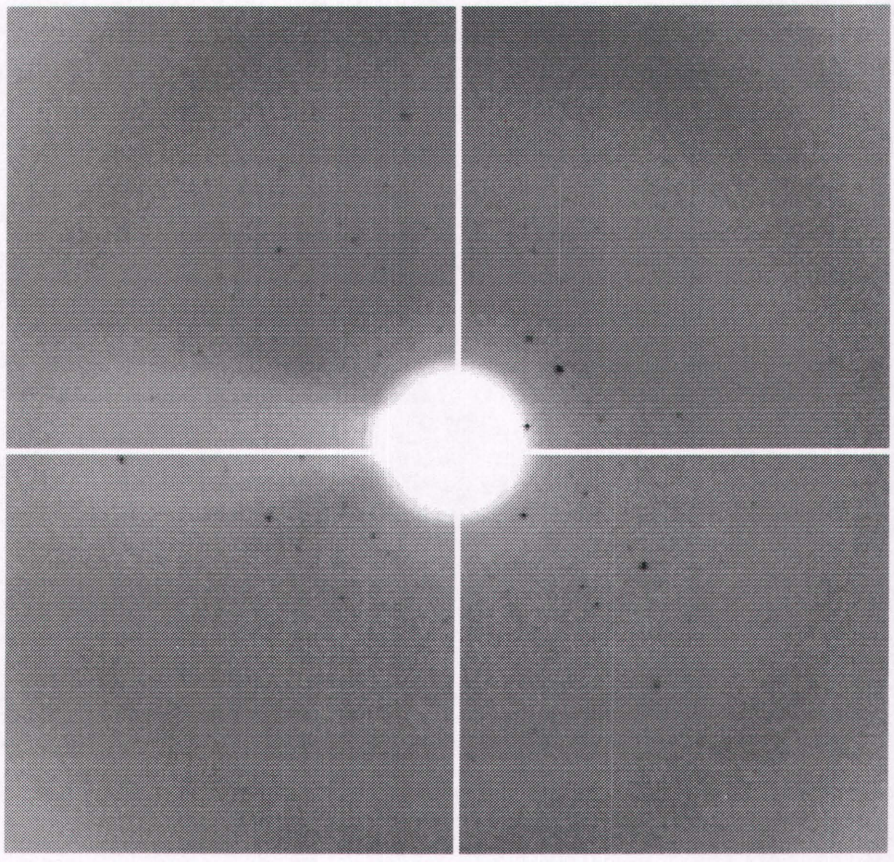

Figure 3.42. Diffraction observed for the d[GA(5FU)(5FU)AA(5FU)C] crystal grown in the presence of Co^{2+}. The maximum resolution is approximately 7 Å.

4.0 DISCUSSION

4.1 Ionizing Radiation-Induced Crosslinking of M-DNA

The ethidium fluorescence assay is a sensitive and convenient assay for assessing damage to DNA caused by radiation exposure. By using circular plasmid DNA as well as after-heat measurements with linear DNA, both nicking and crosslinking could be measured.

To summarize the results of this set of experiments, it can be said that there is more general damage at pH 9.0 than at pH 7.5. From the results with the plasmid DNA it can be concluded that considerable nicking occurs and that this too is enhanced at pH 9.0. The higher the ^{-}OH concentration becomes, the more favorable the mechanisms outlined in Section 1.4.1 are expected to be, thus partly explaining the increased strand breakage at high pH.

Additionally, it is possible that at high pH, reactions may occur such as:

$$H_2O^{\bullet+} + {}^{-}OH \rightarrow H_2O + {}^{\bullet}OH \qquad \text{(Equation 4.5).}$$

This would result in additional radical formation and an increased chance of hydrogen abstraction from the sugar residues on DNA.

Though these mechanisms adequately explain the increased rate of plasmid DNA nicking at pH 9.0, it is remarkable that the ethidium fluorescence assay was

unable to detect this nicking for the Co^{2+} sample based on after-heat fluorescence measurements. A hint at another explanation can be gained by examining the before-heat measurements that show an initial sharp increase in ethidium fluorescence similar to that observed with the other M^{2+}. This indicates that the plasmid DNA is indeed still being nicked but that the lack of decrease in the after-heat fluorescence must be attributable to some other mechanism. That the effect was due to interstrand crosslink formation was shown using linear DNA.

The mechanism of Co^{2+}-induced crosslinking involves a free radical mechanism since the addition of the free radical scavenger TRIS (Murphy *et al.*, 1974; Halliwell and Gutteridge, 1986; Grady *et al.*, 1988; Hodgkins *et al.*, 1996), nearly eliminates the effect completely. Since M-DNA can efficiently transport electrons up and down the helix, it is possible that free radicals produced near a particular base-pair could travel *via* the metal ions of M-DNA to a different base-pair where crosslink formation is more favorable. The degree of crosslinking was similar in three bacterial DNAs ranging in G•C content from 27% to 72%. As well, the synthetic DNAs poly(dA)•poly(dT), poly(dG)•poly(dC) and poly[d(TC)]• poly[d(GA)] all showed crosslinking although the effect was most pronounced with poly[d(TG)]•poly[d(CA)]. Therefore it can be concluded that the sequence or

structure of the DNA can affect the rate of crosslinking but that both A•T and G•C base-pairs can participate.

The structure of the crosslinked base-pair is unclear but Co cations are known to promote homolytic bond cleavage and formation in reactions catalyzed by coenzyme B_{12} (Halpern, 1985). One possibility is that the Co shuttles the electron from the $^{\bullet}OH$ to a base by switching between +2 and +3 oxidation states. Ni and Zn are less likely to participate in this type of reaction because the +3 oxidation state is less stable for Ni and unknown for Zn (Gerloch and Constable, 1994).

It is clear that the ionizing radiation-induced crosslinks are dependent on the M-DNA conformation. This conclusion is based on several observations. First, crosslink formation is not observed at pH 7.5 even in the presence of Co^{2+}. Second, crosslink formation is completely inhibited in the presence of EDTA. Both of these conditions cause reversion of M-DNA back to the B-DNA conformation. Third, the degree of crosslink formation is dependent on the concentration of Co^{2+} present in solution at pH 9.0, reaching a maximum when the ratio of [DNA] : $[Co^{2+}]$ is about 1 : 5. This is consistent with the original studies on M-DNA that generally used an approximate 10-fold excess of M^{2+} in order to demonstrate the new conformation. The results obtained here demonstrate that such an excess of M^{2+} may not be necessary for formation of the M-DNA conformation. In fact, this assay provides a

sensitive test for the M-DNA conformation although its usefulness is limited by the fact that the crosslinking reaction only occurs with Co^{2+} and not with Ni^{2+} or Zn^{2+}.

4.2 UV-Induced Crosslinking of M-DNA

In contrast to the effects of γ-radiation, the results show less nicking with UV radiation. As well, there is no pH-dependent effect on nicking in the case of UV radiation, indicating that a mechanism involving free radical formation outside of the DNA helix is unlikely.

Compared to γ-radiation, UV radiation caused less general damage to the DNA and fewer crosslinks at pH 9.0 compared to pH 7.5. In general, however, there was some crosslinking in the presence of all of the M^{2+} assayed even at pH 7.5. The major difference observed upon formation of M-DNA with either Co^{2+}, Ni^{2+} or Zn^{2+} is that while general damage, including nicking, increases slightly there is a large increase in the level of crosslinking.

Interstrand crosslinking of DNA exposed to UV radiation has also been observed by another group (Glisin and Doty, 1967). It was proposed that the mechanism involves the photochemical dimerization of pyrimidine moieties on opposite strands requiring changes in strand conformation. The structure of this type of crosslink remains unknown but is presumed to involve formation of a cyclobutyl dimer between double bonds in the bases on opposite strands. A mechanism

involving •OH formation from the aqueous solution is unlikely since the results presented in the present work show that the presence of a radical scavenger does not prevent crosslink formation.

As in the case with γ-irradiation, UV radiation caused some crosslinking with all of the synthetic DNAs assayed in the presence of Co^{2+} at high pH. Interstrand crosslinking was observed even between strands containing only purines and strands containing only pyrimidines as well as with mixed strands. Of considerable interest is the observation that poly(dA)•poly(dT) showed a high rate of crosslinking even at pH 7.5 or in the presence of Mg^{2+} suggesting that the UV radiation-induced crosslinks that were observed by Glisin and Doty (1967) may have resulted primarily from an interaction between an A residue on one strand with a T on the complementary strand.

It has been shown that tracts of poly(dA)•poly(dT) adopt a conformation which is significantly different from the usual form of B-DNA (Chandrasekaran *et al.*, 1995). This crystal structure shows a more compact structure having less pitch with a narrower minor groove compared to standard B-DNA. This altered structure may allow A on one strand and T on the complementary strand to adopt an orientation that is more favorable for the occurrence of a [2 + 2] photoaddition reaction. Similarly, it is hypothesized that the formation of M-DNA may distort the

helix such that similar crosslinks can form in sequences containing both A•T and G•C base-pairs.

As with γ-radiation, increased crosslink formation induced by UV radiation is dependent on the M-DNA conformation since it is inhibited by EDTA or a decrease in pH. In addition, the reaction occurs in the presence of Co^{2+}, Ni^{2+} or Zn^{2+} but not Mg^{2+} or Mn^{2+}.

4.3 Proton Release During M-DNA Formation

At pH 7.5 there was virtually no M-DNA formation and the ethidium fluorescence decreased very little during the course of the assay. There was a corresponding lack of proton release in the system.

At pH 8.5, there was approximately one proton released from the system for every Ni^{2+} added during the period when ethidium fluorescence was decreasing. This fits in well with the model for M-DNA that shows the imino proton of every base-pair replaced with M^{2+}. It is not clear why complete M-DNA formation was observed with a [DNA] : [Ni^{2+}] ratio of only approximately 1 : 1.5. In light of the γ-irradiation experiments with Co^{2+}, one would expect a requirement for a higher ratio of M^{2+}, although this could represent a difference imposed by the higher concentration of

DNA or simply a difference between Co^{2+} and Ni^{2+} in their respective kinetics of M-DNA formation.

Even though the experiment performed at pH 9.5 also revealed approximately one Ni^{2+} being incorporated into M-DNA per base-pair, there was a greater release of protons on the order of approximately four times. This is most likely due to a release of protons from the hydration sphere of Ni^{2+} as it is added to the basic DNA solution, this effect having been described in Section 1.2.1. This is especially likely when the lack of lag phase before commencement of M-DNA formation is considered. The presence of the lag phase in the pH 8.5 experiment acts as a control to demonstrate the lack of proton release from the hydration sphere of Ni^{2+}. If protons were being released from the hydration sphere, the effect would be expected at every addition step.

4.4 The d(GGCGCC)-M^{2+} B-DNA Crystal Structures

All three of the structures presented share a similar packing arrangement to that of the same sequence crystallized in the presence of spermine (Vargason *et al.*, 2000). Since packing interactions can affect the conformation of DNA in a crystal (Tereshko and Subirana, 1999), it might be argued that there may be some difficulty in overcoming the tendency of this sequence to adopt the B-DNA conformation, with the observed result that the M-DNA conformation has not been adopted. However,

the same sequence has also been crystallized as A-DNA (Urpí *et al.*, 2000) and in a number of different space groups (Vargason *et al.*, 2000). Therefore, it is seen as more likely that the determining factor has been an inability to crystallize the sequence at sufficiently high pH.

Whereas the Vargason *et al.* (2000) structure is stabilized by spermine, the structures with Co^{2+}, Ni^{2+} or Zn^{2+} show the stabilizing function of spermine being effectively replaced by the M^{2+} that bind to G residues G1, G7, G19 and G25 to stabilize the interaction between the major groove and the neighboring phosphate backbones. In the case of spermine, the molecule often lies along the entire length of the major groove where it stabilizes the interaction with neighboring phosphate backbones. It is interesting that the M^{2+} are able to stabilize the crystal lattice even though they only interact with the neighboring phosphate backbones at four distinct points. Whereas the structures with M^{2+} show hydrogen bonding interactions between the metals' hydration sphere at position G19 and oxygen atoms of the neighboring phosphate backbone, there is no spermine molecule bound in the major groove near this position in the corresponding structure (Vargason *et al.*, 2000).

A structure of the same sequence crystallized in the presence of $Co(NH_3)_6^{3+}$ was also recently reported (NDB entries BD0039 and BD0050) (Vargason *et al*, 2000; Vargason *et al.*, 2001). This structure showed several differences to the ones crystallized in the presence of the M^{2+}. One Co^{3+} was observed to crosslink two G

residues of neighboring helices by coordinating both N(7) positions. The near-octahedral coordination sphere of Co^{3+} was completed by four NH_3 molecules. Additional stabilization of the interaction between neighboring duplexes was *via* Mg^{2+} octahedrally coordinated to six water molecules which formed hydrogen bonds within the major groove of one duplex and phosphate oxygen atoms of neighboring duplexes. No Co^{3+} cations were reported bound to terminal G residues besides those involved in the crosslink.

The structures reported in this thesis are the result of data with relatively low resolution. This is not unusual with DNA that packs in a similar manner, such as that reported by Vargason *et al.*, (2000). The limitations in resolution are primarily caused by a highly disordered solvent content, which may actually have an advantage since the results might better approximate biological conditions. It is estimated that all three crystals have a solvent content of nearly 65%. This is of interest in itself because the few interactions with M^{2+} are sufficient to stabilize the crystal lattice even with such a high solvent content. It is noteworthy that, of the five M^{2+} present in each asymmetric unit, only four participate in interactions between neighboring helices and that this is sufficient to stabilize such a sparse crystal lattice. Even considering the limitations imposed by the low resolution data, the results are clear and unambiguous, supporting the claim that these transition metal cations do not bind B-type DNA except at terminal G positions.

To summarize the studies of M^{2+} binding to G within B-DNA sequences thus far: Co^{2+} does not bind within CGC sequences (Gao *et al.*, 1993), Ni^{2+} does not bind TGT (Abrescia *et al.*, 2002) and Zn^{2+} does not bind TGC (Soler-López *et al.*, 2002). The present results show that none of these M^{2+} coordinate the central G residues in GGC or CGC sequences either. These results are consistent with the proposal that it is a general phenomenon that M^{2+} such as these do not bind B-DNA in a stable manner (Gao *et al.*, 1993). This is also the reason that these metal cations can cause a decrease in the melting temperature of DNA (Eichorn and Shin, 1968; Lee *et al.*, 1993), fraying being observed in several structures involving these cations. It should be noted that in none of the studies involving these cations are there any A residues at terminal positions of a B-DNA region. One would expect that coordination would also occur in this case though the stability of the complex would be predicted to be lower because the N(7) atom of G is more basic than that of A (Sigel *et al.*, 1994).

The patterns observed with Co^{2+}, Ni^{2+} and Zn^{2+} appear at this point to be common for transition metal cations that have an octahedral coordination geometry. The nucleosome core particle, showing a histone protein octamer associated with a 146 base-pair DNA sequence in the B conformation, was crystallized in the presence of Mn^{2+} (Luger *et al.*, 1997). Of the six Mn^{2+} ions in the asymmetric unit, none are reported to be coordinated to G residues at N(7) positions. Rather, they seem to mediate interactions between phosphate backbones of neighboring DNA strands,

probably *via* coordinated water molecules. One Mn^{2+} was located within the minor groove, likely interacting through coordinated water molecules although water molecules were not located due to the relatively low resolution of the data.

An alternative model has also been proposed (Montrel *et al.*, 1998) suggesting that a single M^{2+} may be able to coordinate the N(7) positions of two G residues that occur next to each other on the same strand. This hypothesis is supported by nuclear magnetic resonance studies involving synthetic DNA sequences with Mn^{2+} and Zn^{2+} (Frøystein *et al.*, 1993; Steinkopf and Sletten, 1994). In these studies it was reported that M^{2+} interacts preferentially with G residues at the ends of oligonucleotide sequences and to 5' G residues in the middle of the helix if they are next to another G residue. X-ray crystallography studies with consecutive G residues within a B-DNA helix in the presence of similar transition metal cations have not yet been performed.

The structures described in this thesis contain two G residues at the 5'-end of the helix but M^{2+} is only coordinated to the terminal G. It interacts with the neighboring G residue only *via* coordinated water molecules. It is not clear whether this would be the case for two G residues in the context of a double helix, but it is clear that if two G residues occur at the 5'-end of a helix, coordination with the terminal G is preferred.

That M^{2+} binds B-DNA very selectively is consistent with the observation that the left-handed Z-DNA is stabilized by M^{2+}. The effect is partly due to the limited

interaction with G residues at the N(7) position which are more exposed to the solvent in Z-DNA than in B-DNA. In the appropriate sequence, these M^{2+} would thus favor the left-handed conformation and the equilibrium would be shifted toward Z-DNA.

4.5 Implications for the M-DNA Model

Aside from the knowledge gained regarding the response of DNA to ionizing and UV radiation in the presence of M^{2+}, these experiments have implications for the M-DNA model. The ability to measure renaturation of DNA due to crosslink formation using the ethidium assay proves that M-DNA, like B-DNA, is a duplex structure. It is impossible that the conformation is single-stranded because in this case, no renaturation would be observed with rapid cooling.

It is also apparent that the M^{2+} involved in M-DNA formation must be intimately connected with the bases of the base-pairs. In order for M^{2+} to be able to participate in crosslink formation, it must interact with at least one atom of the base. It is likely that the positions at which M^{2+} are bound involve both G N(1) and T N(3) positions since the titration experiment revealed proton release during M-DNA formation. This fits well with nuclear magnetic resonance data that showed loss of the imino proton peaks during formation of Zn^{2+} M-DNA (Lee *et al.*, 1993). As well, crosslink formation occurs with both G•C and A•T base-pairs so that it is unlikely that the M^{2+} interacts preferentially with either G N(1) or T N(3) atoms, the

interaction in all likelihood being more influenced by local helix conformational restraints.

When the crosslinking results are considered in conjunction with the x-ray crystallography results, the purine N(7) atom can virtually be eliminated as the site responsible for the unique characteristics of M-DNA. It would be expected that the M^{2+} would be bound to terminal N(7) positions on DNA at pH 7.5. Thus, especially with poly(dG)•poly(dC), poly[d(TC)]•poly[d(GA)] and poly[d(TG)]•poly[d(CA)], crosslinking would be expected to occur more rapidly as strand nicking proceeded even at pH 7.5, but this was not observed. M^{2+}-N(7) coordination is therefore not likely responsible for the induced crosslinking so that another site must be involved in M^{2+} binding. This also agrees with the proposed model for M-DNA in which it has a general conformation that is similar to B-DNA, which does not coordinate M^{2+} at N(7).

4.6 The Possibility of M-DNA in Biological Systems

Even though M-DNA forms only at relatively high pH in the presence of Co^{2+}, Ni^{2+} or Zn^{2+}, it may have biological implications. Of import is the observation that M-DNA exhibits hysteresis (Aich *et al.*, 2000; Wood *et al.*, 2002). That is, M-DNA requires a higher pH to form than to undergo the reverse process of reverting back to the B-DNA conformation. While for the Co^{2+} and Zn^{2+} forms of M-DNA reversion to

B-DNA is virtually complete at pH 7.5, the Ni^{2+} form is much more stable. It was shown to revert back to the B-DNA conformation only below pH 7.0, suggesting that, once formed, it might be stable under physiological pH conditions.

Co^{2+}, Ni^{2+} and Zn^{2+} are present in virtually all living systems in low concentrations. But there are known instances of biological entities containing high concentrations of these M^{2+} or living in environments that contain them. Co accumulating plants exist, for example *Astragalus* species that contain concentrations of Co up to 100 mg kg^{-1} of dried plant material (Young, 1979). If one were to consider a plant having a water content of 75%, this would translate into a Co concentration of approximately 0.4 mM, although it is not clear whether the Co is bound predominantly to components such as proteins or whether it is stored only in certain organelles.

Ni has long been associated with carcinogenicity and DNA lesions in living systems. If Ni^{2+} is injected into rats, it accumulates in kidney tissue resulting in the induction of single-strand breaks as well as crosslinks in DNA from kidney cell nuclei (Ciccarelli and Wetterhahn, 1982).

Bacterial communities have also been described that are adapted to ultramafic soils that are characterized by high levels of Ni (5 mg g^{-1} of soil compared to the normal level of about 0.02 mg g^{-1}) and low levels of nitrogen, carbon and phosphorus (Héry *et al.*, 2003). While studying bacterial populations, this same study saw M-

DNA as the culprit when difficulty was encountered in isolating bacterial DNA from $NiCl_2$-spiked soil samples. The usual extraction method involved grinding the samples in liquid nitrogen then mixing the powdered soil with buffer at pH 8.0 followed by ethanol precipitation. Although the extraction buffer contained EDTA, it was not in high enough concentration and no DNA could be recovered from soils that had been $NiCl_2$-spiked. Washing the soil with KCl, a procedure that extracts M^{2+} from soil, solved the problem.

In humans and other mammals, Zn^{2+} is required for normal development of sexual organs and is found in unusually high concentrations in semen and sperm (Millar *et al.*, 1958; Van Rij and Pories, 1980; Rennert and Chan, 1984; Henkel *et al.*, 1999). For example, average concentrations of Zn^{2+} are approximately 2000 $\mu g\ g^{-1}$ dry weight in human sperm (Mawson and Fischer, 1953). It is not certain how much of this Zn^{2+} is bound to proteins although the authors estimate that less than 1% of it can be accounted for by its association with carbonic anhydrase in human sperm.

Because semen and sperm cells contain unusually high concentrations of Zn^{2+}, it is most interesting that both of these also have alkaline pH values. Human semen, for example, has an approximate pH value near 8.2 but can range between 7.3 and 9.5 (Harraway *et al.*, 2000). Measurements of the internal pH of resting *Sicyonia ingentis* capacitated sperm reveal a pH of 8.29 ± 0.10 (Lindsay and Clark, 1992).

When considering the behavior of M-DNA under biological conditions, it is noteworthy that it displays nuclease resistance (Aich *et al.*, 2000). Because of the hysteresis, it was possible to perform an experiment in which DNA was exposed to DNase I in the presence of Ni^{2+} either having the B-DNA or the M-DNA conformation. It was observed that the M-DNA conformation was completely protected from digestion by the nuclease even though Ni^{2+} did not inhibit digestion of B-DNA. This observation also lends support to the proposal that, even though M-DNA has a double-helical conformation similar to B-DNA, it is significantly different from it. The structural differences such as the proposed wider minor groove and location of the M^{2+} apparently act to inhibit the binding and/or catalysis by the nuclease.

4.7 Summary

For the Co^{2+} form of M-DNA, γ-radiation caused the very efficient formation of interstrand crosslinks that was not observed with B-DNA, nor with the Ni^{2+} or Zn^{2+} forms of M-DNA. The crosslinks occurred in both A•T and G•C base-pairs but did not form in the presence of a free radical scavenger. Crosslinks induced by UV radiation also formed at a faster rate for the Co^{2+}, Ni^{2+} or Zn^{2+} forms of M-DNA

compared to B-DNA. In this case crosslinking occurred in all DNA but was more prominent in A•T base-pairs and was not inhibited by a free radical scavenger.

Some aspects of the proposed structural model for M-DNA are supported by these results. The double-stranded nature of the conformation is the only reasonable explanation for its ability to rapidly renature after crosslink formation. Further, the most likely location for M^{2+} coordination is at the T N(3) and G N(1) positions. The titration experiments thus show a release of protons during M-DNA formation when the pH is sufficiently high. Although model studies show that the binding of M^{2+} at this position allows the helix to maintain a B-like conformation, the differences in the crosslinking responses between B- and M-DNA require that there be some difference in the structural and/or electronic properties. Purine N(7) coordination is ruled out as being responsible for the unique characteristics of M-DNA. It is unlikely that the N(7) position, even of G residues, is occupied by M^{2+} except perhaps at terminal positions or where two or more G residues occur in a row.

The crystal structures of d(GGCGCC) complexed to Co^{2+}, Ni^{2+} or Zn^{2+} demonstrate the ability of these M^{2+} to replace other molecules such as spermine or $Co(NH_3)_6^{3+}$ for the purpose of stabilizing the crystal lattice. The effect is especially striking because of the very high solvent content of the crystals. Even though the sparse lattice was responsible for limitations in the resolution of the data, it was still possible to locate the positions of M^{2+} coordinated to the DNA. The M^{2+} coordinate

only to terminal G residues at N(7) positions probably due to potential clashes with the metals' hydration spheres and neighboring bases at internal G locations. The structures were isomorphous and had five B-DNA strands and five M^{2+} per asymmetric unit. The water molecules bound to the M^{2+} interacted with neighboring G residues 3' to the ones to which the cations were coordinated, affecting the propeller twist. As well as lending support to the proposal that these M^{2+} do not coordinate B-DNA in a stable manner, the results presented also extend the crystallographic evidence for this phenomenon to the GGC and CGC sequences for all three metal cations.

A DNA sequence containing 5FU has been crystallized at high pH and it is anticipated that this will provide a crystal structure that will improve the understanding of the M-DNA conformation.

4.8 Future Perspective

In light of the present discussion, it becomes ever more apparent that when cellular exposure to radiation is considered, it is important to take into account not only the type of radiation, but also the pH and which types of M^{2+} are interacting with DNA. It would be interesting to observe how the presence of other transition metal cations affect the response of DNA to radiation exposure.

Although it is not known whether M-DNA exists *in vivo*, the possibility exists. Regardless of this, it has been shown that differential damage may occur even with B-DNA in the presence of various M^{2+}. It should be possible to design an experiment wherein live cells or tissues that would be expected to contain M-DNA are exposed to radiation. Subsequent isolation of cellular DNA could be analyzed for the presence of interstrand crosslinks and this would indicate the presence of the M-DNA conformation *in vivo*.

It would also be interesting to further analyze sequence-dependent M^{2+} coordination to DNA. By now it is quite apparent that transition metals that have an octahedral coordination geometry preferentially bind to terminal G residues. However, considering other experimental results, it seems necessary to design a crystallographic experiment in which a B-DNA helix containing a non-terminal GG sequence is crystallized in the presence of various M^{2+}. It would also be of interest to crystallize a sequence containing a terminal A residue with M^{2+} to observe whether coordination also occurs in this case.

A critical step towards a more complete structural understanding of the M-DNA conformation is expected to be the solution of the d[GA(5FU)-(5FU)AA(5FU)C] crystal structure. This sequence is expected to form M-DNA very readily because of the presence of 5FU. Furthermore, crystals have been obtained at pH 8.5, a condition that is anticipated to be favorable for the M-DNA conformation.

Improvement of the crystallization conditions and cryoprotection protocol will be necessary steps toward this goal.

5.0 REFERENCES

Abrescia, N. G. A., Huynh-Dinh, T. and Subirana, J. A. (2002) Nickel-Guanine Interactions in DNA: Crystal Structure of Nickel-d[CGTGTACACG]$_2$. *J. Biol. Inorg. Chem.* 7: 195-199.

Abrescia, N. G. A., Malinina, L., Fernandez, L. G., Huynh-Dinh, T., Neidle, S. and Subirana, J. A. (1999a) Structure of the Oligonucleotide d(CGTATATACG) as a Site-Specific Complex with Nickel Ions. *Nucleic Acids Res.* 27: 1593-1599.

Abrescia, N. G. A., Malinina, L. and Subirana, J. A. (1999b) Stacking Interaction of Guanine with Netropsin in the Minor Groove of d(CGTATATACG)$_2$. *J. Mol. Biol.* 294: 657-666.

Adams, A., Guss, J. M., Collyer, C. A., Denny, W. A. and Wakelin, L. P. G. (2000) A Novel Form of Intercalation Involving Four DNA Duplexes in an Acridine-4-Carboxamide Complex of d(CGTACG)$_2$. *Nucleic Acids Res.* 28: 4244-4253.

Aich, P., Kraatz, H.-B. and Lee, J. S. (2000) M-DNA: pH Stability, Nuclease Resistance and Signal Transmission. *J. Biomol. Struct. Dyn.* Conversation 11: 297-301.

Aich, P., Labiuk, S. L., Tari, L. W., Delbaere, L. T. J., Roesler, W. J., Falk, K. J., Steer, R. P. and Lee, J. S. (1999) M-DNA: A Complex Between Divalent Metal Ions and DNA which Behaves as a Molecular Wire. *J. Mol. Biol.* 294: 477-485.

Ananthaswamy, H. N. and Pierceall, W. E. (1990) Molecular Mechanisms of Ultraviolet Radiation Carcinogenesis. *Photochem. Photobiol.* 52: 1119-1136.

Angelici, R. J. (1973) Stability of Coordination Compounds. In *Inorganic Biochemistry* 1 (Edited by Eichhorn, G. L.), Elsevier Scientific Publishing Company, New York, pp. 63-101.

Aoki, K. (1976) The Crystal and Molecular Structure of the Polymeric Complex of Zinc(II) with Cytosine 5'-Phosphate: Metal Bonding to Both N(3) and Phosphate. *Biochim. Biophys. Acta,* 447: 379-381.

Aoki, K. (1996) General Conclusions from Solid State Studies of Nucleotide-Metal Ion Complexes. In *Metal Ions in Biological Systems* 32 (Edited by Sigel, A. and Sigel, H.), Marcel Dekker, Inc., New York, pp. 91-134.

Arnott, S. (1970) The Geometry of Nucleic Acids. *Prog. Biophys. Mol. Biol.* 21: 265-319.

Avery, O. T., MacLeod, C. M. and McCarty, M. (1944) Studies on the Chemical Nature of the Substance Inducing Transformation of Pneumococcal Types. Induction of Transformation by a Desoxyribonucleic Acid Fraction Isolated from Pneumococcus Type III. *J. Exp. Med.* 79: 137-158.

Breen, A. P. and Murphy, J. A. (1995) Reactions of Oxyl Radicals with DNA. *Free Radical Biol. Med.* 18: 1033-1077.

Brown, T. and Brown, D. J. S. (1992) Purification of Synthetic DNA. *Methods Enzymol.* 211: 20-35.

Brünger, A. T. (1992) *X-PLOR Manual, Version 3.1*, Yale University Press, New Haven, CT.

Calladine, C. R. and Drew, H. R. (1992) *Understanding DNA: The Molecule and How it Works*, Academic Press, San Diego.

Cartwright, B. A., Goodgame, D. M. L., Jeeves, I. and Skapski, A. C. (1977) X-Ray Structure of a Compound of Cobalt with Uridine 5'-Monophosphate. Evidence for Metal-Phosphate Bonding Only. *Biochim. Biophys. Acta* 477: 195-198.

Caruthers, M. H., Beaton, G., Wu, J. V. and Wiesler, W. (1992) Chemical Synthesis of Deoxyoligonucleotides and Deoxyoligonucleotide Analogs. *Methods Enzymol.* 211: 3-20.

CCP4 (1994) Collaborative Computational Project, Number 4, The CCP4 Suite: Programs for Protein Crystallography. *Acta Crystallogr.* D50: 760-763.

Chandrasekaran, R., Radha, A. and Park, H.-S. (1995) Sodium Ions and Water Molecules in the Structure of Poly(dA)•Poly(dT). *Acta Crystallogr.* D51: 1025-1035.

Chargaff, E., Lipschitz, R., Green, C. and Hodes, M. E. (1951) The Composition of the Deoxyribonucleic Acid of Salmon Sperm. *J. Biol. Chem.* 192: 223-230.

Ciccarelli, R. B. and Wetterhahn, K. E. (1982) Nickel Distribution and DNA Lesions Induced in Rat Tissues by the Carcinogen Nickel Carbonate. *Cancer Res.* 42: 3544-3549.

Clark, G. R. and Orbell, J. D. (1974) Transition-metal-Nucleotide Complexes. X-Ray Crystal and Molecular Structure of the Complex Between Nickel(II) and Inosine 5'-Monophosphate [Ni(imp)$(H_2O)_5$,$2H_2O$]. *J. Chem. Soc., Chem. Commun.* 139-140.

Clark, G. R. and Orbell, J. D. (1975) Transition-metal-Nucleotide Complexes. X-Ray Crystal and Molecular Structures of the Cobalt(II) and Cadmium(II) Complexes of Cytosine 5'-Monophosphate, [Co(CMP)(H_2O)] and [Cd(CMP)(H_2O)]•H_2O. *J. Chem. Soc. Chem. Commun.* 697-698.

Clark, G. R., Orbell, J. D. and Aoki, K. (1978) Crystallographic Studies of Interactions between Nucleotides and Metal Ions. III. Two Independent Structural Investigations of the Polymeric Complex of Copper(II) with Guanosine 5'-Phosphate. *Acta Crystallogr.* B34: 2119-2128.

Collins, A. D., De Meester, P., Goodgame, D. M. L. and Skapski, A. C. (1975) The Site of Metal Ion Binding in a Nickel Derivative of Adenosine 5'-Monophosphate: an X-Ray Study. *Biochim. Biophys. Acta* 402: 1-6.

Cotton, F. A., Wilkinson, G., Murillo, C. A. and Bochmann, M. (1999) *Advanced Inorganic Chemistry*. 6th edition, John Wiley and Sons, New York.

Dekker, C. A., Michelson, A. M. and Todd, A. R. (1953) Nucleotides. Part XIX. Pyrimidine Deoxyribonucleoside Diphosphates. *J. Chem. Soc.* 947-951.

De Meester, P., Goodgame, D. M. L., Jones, T. J. and Skapski, A. C. (1974a) Mise en évidence par diffraction X de la liaison métal-N (7) dans deux complexes hydratés du cobalt avec la guanosine 5'-monophosphate et l'inosine 5'-monophosphate. *C. R. Acad Sc. Paris, série C* 279: 667-669.

De Meester, P., Goodgame, D. M. L., Jones, T. J. and Skapski, A. C. (1974b) The Polymeric Structure of Zinc Inosine 5'-Monophosphate: X-Ray Evidence for Metal Bonding to Both N(7) and Phosphate. *Biochim. Biophys. Acta* 353: 392-394.

De Meester, P., Goodgame, D. M. L., Skapski, A. C. and Smith, B. T. (1974c) X-Ray Structure of a hydrated Nickel Salt of Guanosine 5'-Monophosphate; Evidence for the Absence of Direct Metal-Phosphate Bonding. *Biochim. Biophys. Acta* 340: 113-115.

Dickerson, R. E. (1992) DNA Structures From A to Z. *Methods Enzymol.* 211: 67-111.

Dickerson, R. E. (1998) DNA Bending: The Prevalence of Kinkiness and the Virtues of Normality. *Nucleic Acids Res.* 26: 1906-1926.

Dickerson, R. E., Bansal, M., Calladine, C. R., Diekmann, S., Hunter, W. N., Kennard, O., von Kitzing, E., Lavery, R., Nelson, H. C. M., Olson, W. K., Saenger, W., Shakked, Z., Sklenar, H. and Soumpasis, D. M. (1989) Definitions and Nomenclature of Nucleic Acid Structure Parameters. *EMBO J.* 8: 1-4.

Dickerson, R. E., Drew, H. R., Conner, B. N., Wing, R. M., Fratini, A. V. and Kopka, M. L. (1982) The Anatomy of A-, B-, and Z-DNA. *Science* 216: 475-485.

Dizdaroglu, M., Schulte-Frohlinde, D. and von Sontag, C. (1977) Isolation of 2-Deoxy-D-*erythro*-Pentonic Acid from an Alkali-Labile Site in γ-Irradiated DNA. *Int. J. Radiat. Biol.* 32: 481-483.

Dock-Bregeon, A.-C., Moras, D., Giegé, R. (1999) Nucleic Acids and their Complexes. In *Crystallization of Nucleic Acids and Proteins*, 2nd edition (Edited by Ducruix, A. and Giegé, R.), Oxford University Press, New York.

Douki, T. and Cadet, J. (1995) UV and Nucleic Acids. In *Interface Between Chemistry and Biochemistry*, (Edited by Jollès, P. and Jörnvall, H.), Birkhäuser, Basel.

Douki, T., Zalizniak, T. and Cadet, J. (1997) Far-UV-Induced Dimeric Photoproducts in Short Oligonucleotides: Sequence Effects. *Photochem. Photobiol.* 66: 171-179.

Drew, H. R. and McCall, M. J. (1988) Recent Studies of DNA in the Crystal. *Ann. Rev. Cell Biol.* 4: 1-20.

Eichorn, G. L. and Shin, Y. A. (1968) Interaction of Metal Ions with Polynucleotides and Related Compounds XII. *J. Am. Chem. Soc.* 90: 7323-7328.

Ennifar, E., Walter, P. and Dumas, P. (2003) A Crystallographic Study of the Binding of 13 Metal Ions to Two Related RNA Duplexes. *Nucleic Acids Res.* 31: 2671-2682.

Evans, S. V. (1993) Setor: Hardware-Lighted Three-Dimensional Solid Model Representation of Macromolecules. *J. Mol. Graph.* 11: 134-138.

Felsenfeld, G., Davies, D. R. and Rich, A. (1957) Formation of a Three-Stranded Polynucleotide Molecule. *J. Am. Chem. Soc.* 79: 2023-2024.

Felsenfeld, G and Rich, A. (1957) Studies on the Formation of Two- and Three-Stranded Polyribonucleotides. *Biochim. Biophys. Acta* 26: 457-468.

Franklin, R. E. and Gosling, R. G. (1953) Molecular Configuration in Sodium Thymonucleate. *Nature* 171: 740-741.

Frøystein, N. Å., Davis, J. T., Reid, B. R. and Sletten, E. (1993) Sequence-Selective Metal Ion Binding to DNA Oligonucleotides. *Acta Chem. Scand.* 47: 649-657.

Gao, Y. G., Sriram, M. and Wang, H. J. (1993). Crystallographic Studies of Metal Ion-DNA Interactions: Different Binding Modes of Cobalt(II), Copper(II) and Barium(II) to N^7 of Guanines in Z-DNA and a Drug-DNA Complex. *Nucleic Acids Res.* 21: 4093-4101.

Gellert, R. W. and Bau, R. (1979) X-Ray Structural Studies of Metal-Nucleoside and Metal-Nucleotide Complexes. In *Metal Ions in Biological Systems* 8 (Edited by Sigel, H.), Marcel Dekker, Inc., New York, pp. 1-55.

Gellert, R. W., Shiba, J. K. and Bau, R. (1979) X-Ray Crystal and Molecular Structures of the Ni(II) and Co(II) Complexes of 2'-Deoxyguanosine-5'-Monophosphate. *Biochem. Biophys. Res. Commun.* 88: 1449-1453.

Gerloch, M. and Constable, E. C. (1994) *Transition Metal Chemistry*, VCH Publishers, New York.

Glisin, V. R. and Doty, P. (1967) The Cross-Linking of DNA by Ultraviolet Radiation. *Biochim. Biophys. Acta* 142: 314-322.

Grady, J. K., Chasteen, N. D. and Harris, D. C. (1988) Radicals from "Good's" Buffers. *Anal. Biochem.* 173: 111-115.

Guay, F. and Beauchamp, A. L. (1979) Model Compounds for the Interactin of Silver I with Polyuridine. *J. Am. Chem. Soc.* 101: 6260-6263.

Halliwell, B. and Gutteridge, J. M. (1986) Oxygen Free Radicals and Iron in Relation to Biology and Medicine: Some Problems and Concepts. *Arch. Biochem. Biophys.* 246: 501-514.

Halpern, J. (1985) Mechanism of Coenzyme B_{12}-Dependent Rearrangements. *Science* 227: 869-875.

Hampel, K. J., Burkholder, G. D. and Lee, J. S. (1993) Plasmid Dimerization Mediated by Triplex Formation Between Polypyrimidine-Polypurine Repeats. *Biochemistry* 32: 1072-1077.

Harraway, C., Berger, N. G. and Dubin, N. H. (2000) Semen pH in Patients with Normal Versus Abnormal Sperm Characteristics. *Am. J. Obstet. Gynecol.* 182: 1045-1047.

Henkel, R. Bittner, J, Weber, R, Hüther, F. and Miska, W. (1999) Relevance of Zinc in Human Sperm Flagella and its Relation to Motility. *Fertil. Steril.* 71: 1138-1143.

Herbert, A. and Rich, A. (1996) The Biology of Left-Handed Z-DNA. *J. Biol. Chem.* 271: 11595-11598.

Héry, M., Nazaret, S., Jaffré, T., Normand, P. and Navarro, E. (2003) Adaptation to Nickel Spiking of Bacterial Communities in Neocaledonian Soils. *Environ. Microbiol.* 5: 3-12.

Hodgkins, P. S., Fairman, M. P. and O'Neill, P. (1996) Rejoining of Gamma-Radiation-Induced Single-Strand Breaks in Plasmid DNA by Human Cell Extracts: Dependence on the Concentration of the Hydroxyl Radical Scavenger, Tris. *Radiat. Res.* 145: 24-30.

Hoogsteen, K. (1959) The Structure of Crystals Containing a Hydrogen-Bonded Complex of 1-Methylthymine and 9-Methyladenine. *Acta Crystallogr.* 12: 822-823.

Hoogsteen, K. (1963) The Crystal and Molecular Structure of a Hydrogen-Bonded Complex Between 1-Methylthymine and 9-Methyladenine. *Acta Crystallogr.* 16: 907-916.

Hunter, C. A. (1993) Sequence-Dependent DNA Structure. The Role of Base Stacking Interactions. *J. Mol. Biol.* 230: 1025-1054.

Hunter, C. A. and Sanders, J. K. M. (1990) The Nature of π- π Interactions. *J. Am. Chem. Soc.* 112: 5525-5534.

Itakura, K., Katagiri, N., Bahl, C. P., Wightman, R. H. and Narang, S. A. (1975) Improved Triester Approach for the Synthesis of Pentadecathymidylic Acid. *J. Am. Chem. Soc.* 97: 7327-7332.

Jaworski, A., Hsieh, W.-T., Blaho, J. A., Larson, J. E. and Wells, R. D. (1987) Left-Handed DNA in Vivo. *Science* 238: 773-777.

Kagawa, T. F., Geierstanger, B. H., Wang, A. H.-J. and Ho, P. S. (1991) Covalent Modification of Guanine Bases in Double-Stranded DNA. *J. Biol. Chem.* 266: 20175-20184.

Kang, C., Zhang, X., Ratliff, R., Moyzis, R. and Rich, A. (1992) Crystal Structure of Four-Stranded *Oxytricha* Telomeric DNA. *Nature* 356: 126-131.

Kazakov, S. A. (1996) Nucleic Acid Binding and Catalysis by Metal Ions. In *Bioorganic Chemistry: Nucleic Acids* (Edited by Hecht, S. M.), Oxford University Press, New York, pp. 244-260.

Kosturko, L. D., Folzer, C. and Stewart, R. F. (1974) The Crystal and Molecular Structure of a 2:1 Complex of 1-Methylthymine-Mercury(II). *Biochemistry* 13: 3949-3952.

Laughlan, G., Murchie, A. I. H., Norman, D. G., Moore, M. H., Moody, P. C. E., Lilley, D. M. J. and Luisi, B. (1994) The High-Resolution Crystal Structure of a Parallel-Stranded Guanine Tetraplex. *Science* 265: 520-524.

Lee, J. S. (1990) The Stability of Polypurine Tetraplexes in the Presence of Mono- and Divalent Cations. *Nucleic Acids Res.* 18: 6057-6060.

Lee, J. S., Burkholder, G. D, Latimer, L. J. P., Haug, B. L. and Braun, R. P. (1987) A Monoclonal Antibody to Triplex DNA Binds to Eucaryotic Chromosomes. *Nucleic Acids Res.* 15: 1047-1061.

Lee, J. S., Johnson, D. A. and Morgan, A. R. (1979) Complexes Formed by $(Pyrimidine)_n \bullet (Purine)_n$ DNAs on Lowering the pH are Three-Stranded. *Nucleic Acids Res.* 6: 3073-3091.

Lee, J. S., Latimer, L. J. P. and Reid, R. S. (1993) A Cooperative Conformational Change in Duplex DNA Induced by Zn^{2+} and Other Divalent Metal Ions. *Biochem. Cell Biol.* 71: 162-168.

Lee, J. S., Woodsworth, M. L., Latimer, L. J. P. and Morgan, A. R. (1984) Poly(pyrimidine)•poly(purine) Synthetic DNAs Containing 5-Methylcytosine Form Stable Triplexes at Neutral pH. *Nucleic Acids Res.* 12: 6603-6614.

LePecq, J.-B. and Paoletti, C. (1967) A Fluorescent Complex Between Ethidium Bromide and Nucleic Acids. *J. Mol. Biol.* 27: 87-106.

Levene, P. A. and Tipson, R. S. (1935) The Ring Structure of Thymidine. *J. Biol. Chem.* 109: 623-630.

Lindsay, L. and Clark, W. Jr. (1992) Preloading of Micromolar Intracellular Ca^{2+} During Capacitation of *Sicyonia ingentis* Sperm, and the Role of the pH_i Decrease During the Acrosome Reaction. *The Journal of Experimental Zoology* 262: 219-229.

Lu, X.-J. (2002) 3DNA Homepage at http://rutchem.rutgers.edu/~xiangjun/3DNA/.

Luger, K., Mäder, A. W., Richmond, R. K., Sargent, D. F. and Richmond, T. J. (1997) Crystal Structure of the Nucleosome Core Particle at 2.8 Å Resolution. *Nature* 389: 251-260.

Mamula, O., von Zelewsky, A., Bark, T., Stoeckli-Evans, H., Neels, A. and Bernardinelli, G. (2000) Predetermined Chirality at Metal Centers of Various Coordination Geometries: A Chiral Cleft Ligand for Tetrahedral (T-4), Square-Planar (SP-4), Trigonal-Bipyramidal (TB-5), Square-Pyramidal (SPY-5), and Octahedral (OC-6) Complexes. *Chem. Eur. J.* 6: 3575-3585.

Marmur, J. and Doty, P. (1962) Determinatin of the Base Composition of Deoxyribonucleic Acid from its Thermal Denaturation Temperature. *J. Mol. Biol.* 5: 109-118.

Martin, R. B. and Mariam, Y. H. (1979) Interactions Between Metal Ions and Nucleic Bases, Nucleosides, and Nucleotides in Solution. In *Metal Ions in Biological Systems* 8 Edited by Sigel, H.), Marcel Dekker, Inc., New York, pp. 57-124.

Mawson, C. A. and Fischer, M. I. (1953) Zinc and Carbonic Anhydrase in Human Semen. *Biochem. J.* 55: 696-700.

McCarty, M. and Avery, O. T. (1946) Studies on the Chemical Nature of the Substance Inducing Transformation of Pneumococcal Types. II. Effect of Desoxyribonuclease on the Biological Activity of the Transforming Substance. *J. Exp. Med.* 83: 89-96.

Mergny, J.-L. and Hélène, C. (1998) G-Quadruplex DNA: A Target for Drug Design. *Nat. Med.* 4: 1366-1367.

Millar, M. J., Fischer, M. I., Elcoate, P. V. and Mawson, C. A. (1958) The Effects of Dietary Zinc Deficiency on the Reproductive System of Male Rats. *Can. J. Biochem. Physiol.* 36: 557-569.

Montrel, M., Chuprina, V. P., Poltev, V. I., Nerdal, W. and Sletten, E. (1998) Sequence-Dependent Binding of Metal Ion to DNA Oligomers. A Comparison of Molecular Electrostatic Potentials with NMR Data. *J. Biomol. Struct. Dyn.* 16: 631-637.

Morgan, A. R., Evans, D. H., Lee, J. S. and Pulleyblank, D. E. (1979a) Review: Ethidium Fluorescence Assays. Part II. Enzymatic Studies and DNA-Protein Interactions. *Nucleic Acids Res.* 7: 571-594.

Morgan, A. R., Lee, J. S., Pulleyblank, D. E., Murray, N. L. and Evans, D. H. (1979b) Review: Ethidium Fluorescence Assays. Part I. Physiochemical Studies. *Nucleic Acids Res.* 7: 547-569.

Morgan, A. R. and Wells, R. D. (1968) Specificity of the Three-Stranded Complex Formation Between Double-Stranded DNA and Single-Stranded RNA Containing Repeating Nucleotide Sequences. *J. Mol. Biol.* 37: 63-80.

Murphy, P. A., Lin, J. S. and Olcott, H. S. (1974) Peroxide Oxidation of Tris to a Free Radical. *Arch. Biochem. Biophys.* 164: 776-777.

Nilsson, L. and Karplus, M. (1986) Empirical Energy Functions for Energy Minimization and Dynamics of Nucleic Acids. *J. Comput. Chem.* 7: 591-616.

Olson, W. K., Bansal, M., Burley, S. K., Dickerson, R. E., Gerstein, M., Harvey, S. C., Heinemann, U., Lu, X.-J., Neidle, S., Shakked, Z., Sklenar, H., Suzuki, M., Tung, C.-S., Westhof, E., Wolberger, C. and Berman, H. M. (2001) A Standard Reference Frame for the Description of Nucleic Acid Base-Pair Geometry. *J. Mol. Biol.* 313: 229-237.

Otwinowski, Z. and Minor, W. (1997) Processing of X-Ray Diffraction Data Collected in Oscillation Mode. *Methods Enzymol.* 276: 307-326.

Phan, A. T. and Mergny, J.-L. (2002) Human Telomeric DNA: G-Quadruplex, I-Motif and Watson-Crick Double Helix. *Nucleic Acids Res.* 30: 4618-4625.

Pohl, F. M. and Jovin, T. M. (1972) Salt-Induced Co-operative Conformational Change of a Synthetic DNA: Equilibrium and Kinetic Studies with Poly(dG-dC). *J. Mol. Biol.* 67: 375-396.

Poojary, M. D. and Manohar, H. (1986) Interaction of Metal Ions with 2'-Deoxyribonucleotides. Crystal and Molecular Structure of a Cobalt(II) Complex with 2'-Deoxyinosine 5'-Monophosphate. *J. Chem. Soc., Dalton Trans.* 309-312.

Portugal, F. H. and Cohen, J. S. (1977) *A Century of DNA*, MIT Press, Cambridge, Massachusetts, and London, England.

Prütz, W. A. (1996) Measurement of Copper-Dependent Oxidative DNA Damage by HOCl and H_2O_2 with the Ethidium-Binding Assay. *J. Biochem. Bioph. Methods* 32: 125-135.

Pyeritz, R. E., Schlegel, R. A. and Thomas C. A. Jr. (1972) Hydrodynamic Shear Breakage of DNA May Produce Single-Chained Terminals. *Biochim. Biophys. Acta* 272: 504-509.

Rakitin, A., Aich, P., Papadopulos, C., Kobzar, Y., Vedeneev, A. S., Lee, J. S. and Xu, J. M. (2001) Metallic Conduction Through Engineered DNA: DNA Nanoelectronic Building Blocks. *Phys. Rev. Lett.* 86: 3670-3673.

Rennert, O. M. and Chan, W.-Y. (1984) Genetic Diseases: Models for the Study of Trace Metals. In *Metabolism of Trace Metals in Man*, Volume 2 (Edited by Rennert, O. M. and Chan, W.-Y.), CRC Press, Boca Raton, pp. 133-140.

Rich, A. (1958) The Molecular Structure of Polyinosinic Acid. *Biochim. Biophys. Acta* 29: 502-509.

Rich, A., Nordheim, A. and Wang, A. H.-J. (1984) The Chemistry and Biology of Left-Handed Z-DNA. *Ann. Rev. Biochem.* 53: 791-846.

Richter, J. (2003) Metallization of DNA, *Physica E* 16: 157-173.

Roussel, A. and Cambillau, C. (1992) TURBO-FRODO, Biographics, Marseilles, France.

Saenger, W. (1984) *Principles of Nucleic Acid Structure*. Springer Verlag, New York.

Sambrook, J., Fritsch, E. F. and Maniatis, T. (1989) Concentrating Nucleic Acids. In *Molecular Cloning, A Laboratory Manual*, Second Edition, Cold Spring Harbor Laboratory Press, Plainview, NY.

Schaffitzel, C., Berger, I., Postberg, J., Hanes, J., Lipps, H. J. and Plückthun, A. (2001) *In Vitro* Generated Antibodies Specific for Telomeric Guanine-Quadruplex DNA React with *Stylonychia lemnae* Macronuclei. *Proc. Natl. Acad. Sci. USA* 98: 8572-8577.

Seeman, N. C., Rosenberg, J. M., Suddath, F. L., Kim, J. J. P. and Rich, A. (1976) RNA Double-helical Fragments at Atomic Resolution: I. The Crystal and Molecular Structure of Sodium Adenylyl-3',5'-Uridine Hexahydrate. *J. Mol. Biol.* 104: 109-144.

Sigel, H., Massoud, S. S. and Corfù, N. A. (1994) Comparison of the Extent of Macrochelate Formation in Complexes of Divalent Metal Ions with Guanosine (GMP^{2-}), Inosine (IMP^{2-}), and Adenosine 5'-Monophosphate (AMP^{2-}). The Crucial Role of N-7 Basicity in Metal Ion-Nucleic Base Recognition. *J. Am. Chem. Soc.* 116: 2958-2971.

Sletten, E. and Lie, B. (1976) Copper Complex of Guanosine-5'-Monophosphate. *Acta Crystallogr.* B32: 3301-3304.

Soler-López, M., Malinina, L., Tereshko, V., Zarytova, V. and Subirana, J. A. (2002) Interaction of Zinc Ions with d(CGCAATTGCG) in a 2.9 Å Resolution X-ray Structure. *J. Biol. Inorg. Chem.* 7: 533-538.

Soyfer, V. N. and Potaman, V. N. (1996) *Triple-Helical Nucleic Acids*, Springer-Verlag, New York.

Steinkopf, S. and Sletten, E. (1994) Sequence-Selective Metal Ion Binding to DNA Hexamers. *Acta Chem. Scand.* 48: 388-392.

Swaminathan, V. and Sundaralingam, M. (1979) The Crystal Structures of Metal Complexes of Nucleic Acids and their Constituents. *CRC Crit. Rev. Biochem.* 6, 245-336.

Taboury, J. A., Bourtayre, P., Liquier, J. and Taillandier, E. (1984) Interaction of Z Form Poly(dG-dC)•Poly(dG-dC) with Divalent Metal Ions: Localization of the Binding Sites by I. R. Spectroscopy. *Nucleic Acids Res.* 12: 4247-4258.

Tereshko, V. and Subirana, J. S. (1999) Influence of Packing Interactions on the Average Conformation of B-DNA in Crystalline Structures. *Acta Crystallogr.* D55: 810-819.

The International Union of Crystallography (1968) International Tables for X-Ray Crystallography, Volume III, Physical and Chemical Tables (Edited by C. H. Macgillavry, G. D. Rieck and K. Lonsdale), The Kynoch Press, Birmingham, England.

Thomas, R. (1954) Recherches sur la dénaturation des acides desoxyribonucléiques. *Biochim. Biophys. Acta* 14: 231-240.

Thorpe, J. H., Hobbs, J. R., Todd, A. K., Denny, W. A., Charlton, P. and Cardin, C. J. (2000) Guanine Specific Binding at a DNA Junction Formed by d[CG(5-BrU)ACG]$_2$ with a Topoisomerase Poison in the Presence of Co^{2+} Ions. *Biochemistry* 39: 15055-15061.

Tsai, C.-C., Jain, S. C. and Sobell, H. M. (1975) X-Ray Crystallographic Visualization of Drug-Nucleic Acid Intercalative Binding: Structure of an Ethidium-Dinucleoside Monophosphate Crystalline Complex, Ethidium: 5-Iodouridylyl(3'-5')Adenosine. *Proc. Natl. Acad. Sci. USA* 72: 628-632.

Urpí, L., Navaza, J. and Subirana, J. A. (2000) Alternation of DNA and Solvent Layers in the A Form of d(GGCGCC) Obtained by Ethanol Crystallization. *J. Biomol. Struct. Dyn.* 18: 363-369.

Van de Sande, J. H., McIntosh, L. P. and Jovin, T. M. (1982) Mn^{2+} and Other Transition Metals at Low Concentrations Induce the Right-to-Left Helical Transformation of Poly[d(G-C)]. *EMBO J.* 1: 777-782.

Van Rij, A. M. and Pories, W. J. (1980) Zinc and Copper in Surgery. In *Zinc and Copper in Medicine* (Edited by Karcioglu, Z. A. and Sarper, R. M.), Charles C. Thomas, Springfield, p. 550.

Vargason, J. M., Eichman, B. F. and Ho, P. S. (2000) The Extended and Eccentric E-DNA Structure Induced by Cytosine Methylation or Bromination. *Nat. Struct. Biol.* 7: 758-761.

Vargason, J. M., Henderson, K. and Ho, P. S. (2001) A Crystallographic Map of the Transition From B-DNA to A-DNA. *Proc. Natl. Acad. Sci. USA* 98: 7265-7270.

Wang, A. H.-J., Quigley, G. J., Kolpak, F. J., Crawford, J. L., van Boom, J. H., van der Marel, G. and Rich, A. (1979) Molecular Structure of a Left-Handed Double Helical DNA Fragment at Atomic Resolution. *Nature* 282: 680-686.

Wang, A. H.-J., Gessner, R. V., van der Marel, G. A., van Boom, J. H. and Rich, A. (1985) Crystal Structure of Z-DNA Without an Alternating Purine-Pyrimidine Sequence. *Proc. Natl. Acad. Sci. USA* 82: 3611-3615.

Wang, J. (2002) Electrochemical Nucleic Acid Biosensors. *Anal. Chim. Acta* 469: 63-71.

Ward, M. D. (2001) Chemistry and Molecular Electronics: New Molecules as Wires, Switches and Logic Gates. *J. Chem. Educ.* 78: 321-328.

Watson, J. D. and Crick, F. H. C. (1953a) A Structure for Deoxyribose Nucleic Acid. *Nature* 171: 737-738.

Watson, J. D. and Crick, F. H. C. (1953b) Genetical Implications of the Structure of Deoxyribonucleic Acid. *Nature* 171: 964-967.

Wilkins, M. H. F., Stokes, A. R. and Wilson, H. R. (1953) Molecular Structure of Deoxypentose Nucleic Acids. *Nature* 171: 738-740.

Wood, D. O., Dinsmore, M. J., Bare, G. A. and Lee, J. S. (2002) M-DNA is Stabilised in G•C Tracts or by Incorporation of 5-Fluorouracil. *Nucleic Acids Res.* 30: 2244-2250.

Wyatt, G. R. (1952) The Nucleic Acids of Some Insect Viruses. *J. Gen. Physiol.* 36: 201-205.

Yang, X., Robinson, H., Gao, Y.-G. and Wang, A. H.-J. (2000) Binding of a Macrocyclic Bisacridine and Ametantrone to CGTACG Involves Similar Unusual Intercalation Platforms. *Biochemistry* 39: 10950-10957.

Young, R. S. (1979) *Cobalt in Biology and Biochemistry*, Academic Press, London.

Zahler, A. M., Williamson, J. R., Cech, T. R. and Prescott, D. M. (1991) Inhibition of Telomerase by G-Quartet DNA Structures. *Nature* 350: 718-720.